12-2012

DEVELOP NOVEL FRAP TECHNIQUES FOR DETERMINING ANISOTROPIC SOLUTE DIFFUSION IN CARTILAGINOUS TISSUES

Changcheng Shi
Clemson University, changcheng.shi@gmail.com

DEVELOP NOVEL FRAP TECHNIQUES FOR DETERMINING ANISOTROPIC SOLUTE DIFFUSION IN CARTILAGINOUS TISSUES

A Dissertation
Presented to
the Graduate School of
Clemson University

In Partial Fulfillment
of the Requirements for the Degree
Doctor of Philosophy
Bioengineering

---

by
Changcheng Shi
December 2012

Accepted by:
Dr. Hai Yao, Committee Chair
Dr. Martine LaBerge,
Dr. Michael Kern,
Dr. Zhi Gao

ABSTRACT

Cartilaginous tissue is a connective tissue composed of specialized cells (*e.g.,* chondrocytes and fibroblasts) that produce a large amount of extracellular matrix (ECM), which is comprised mostly of collagen fibers, abundant ground substance rich in proteoglycan, and elastic fibers. It is characterized by its avascular structures within the tissue, implying that nutrition for normal tissue cells and maintaining a healthy ECM, is mainly supplied through diffusion from nearby vascularized tissues and synovial fluid. Poor nutritional supply to the cartilaginous tissue is believed to be an important factor leading to tissue degeneration. Moreover, due to the complex collagen fiber structures, the solute diffusion properties in cartilaginous tissues are mainly anisotropic (*i.e.*, orientation dependent) in three-dimensional (3D) space. Thus, the determination of nutrient solute anisotropic diffusion properties is crucial for understanding the mechanism of nutrient transport in cartilaginous tissues. Furthermore, characterization of the solute diffusive transport properties in cartilaginous tissues will delineate the relationship between solute diffusion and tissue morphology for further understanding the pathophysiology and etiology of tissue dysfunction and degeneration.

Fluorescence recovery after photobleaching (FRAP) is a versatile and widely used tool for the determination of local diffusion properties within solutions, cells, and tissues due to its high spatial resolution offering the possibility to microscopically examine a specific region of a sample. However, there is a lack of FRAP techniques which can determine the two-dimensional (2D) and 3D anisotropic solute diffusion properties in cartilaginous tissues. Therefore, the objective of this project is to develop novel FRAP

techniques for determining 2D and 3D anisotropic solute diffusion properties in cartilaginous tissues.

First, a new 2D FRAP technique solely based on the spatial Fourier analysis (SFA) was developed to determine the 2D anisotropic diffusion tensor in cartilaginous tissues. The major innovations of this study included the derivation of a close-form solution for the 2D diffusion equation by solely using Fourier transform and the complete determination of three independent components of the 2D diffusion tensor. The new theory was validated by computer simulated FRAP experiments indicating the high accuracy and robustness. The new method was applied to determine the 2D diffusion tensor of 4kDa FITC-Dextran in porcine TMJ discs. It was found that the diffusion of this solute in TMJ discs was inhomogeneous and anisotropic. This study has provided a new method to quantitatively investigate the relationship between transport properties and tissue composition and structure. The obtained transport properties are crucial for future development of numerical models studying nutritional supply within the TMJ disc.

Next, the relationship between solute diffusion properties and tissue morphology was investigated by using the new FRAP technique and scanning electron microscopy (SEM). The SEM results demonstrated that the collagen fibers in the TMJ disc aligned anteroposteriorly in the medial, intermediate and lateral regions while aligning mediolaterally in the posterior region. Interestingly, fibers aligned in both the anteroposterior and mediolateral directions were found in the anterior region of the TMJ disc. The diffusion properties were highly correlated with tissue morphology. It was found again that the solute diffusion in the TMJ disc was anisotropic and inhomogeneous,

which suggested that tissue structure (*i.e.*, the collagen fiber alignment) and composition (*e.g.*, water content) could be key factors that affect the solute diffusion properties within TMJ discs.

Lastly, a new 3D MP-FRAP technique was fully developed for determining 3D anisotropic solute diffusion in cartilaginous tissues. A closed-form solution for the 3D anisotropic diffusion equation was derived by using SFA and all the components of the 3D diffusion tensor were obtained by averaging the diffusivities over a shell of a spherical surface in the frequency domain. The new method was well validated by analyzing computer simulated MP-FRAP data as well as measuring the diffusivities of FITC-Dextran (FD) molecules in the glycerol/PBS solutions. Quantitative analysis of 3D MP-FRAP experiments in the ligament tissues was demonstrated as an *in vitro* application of our new technique. The results demonstrated that the 3D diffusion properties of two types of FD solutes (FD70 and FD150) in the ligament tissue slices were anisotropic and the diffusion along the fiber orientation was always faster than the other two directions.

The advantages of the new 2D and 3D FRAP techniques includes (1) the boundary and initial conditions for these analyses are flexible, so bleaching volume could be any 2D or 3D geometries, (2) the real first recovery image frame or stack right after photobleaching is not required for the diffusion tensor calculation, and (3) the diffusion tensor can be calculated without measuring the point spread function or optical transfer function of the microscope. Due to these features, our techniques can be conveniently carried out on a commercial confocal or multiphoton laser scanning microscope for the

2D or 3D anisotropic diffusion measurements. Future work for this project involves incorporating high-speed fluorescence imaging techniques into our FRAP methods in order to enhance the capabilities and broaden the applications of our method. In addition, investigating diffusion properties in cartilaginous tissues by using other imaging modalities [*e.g.,* magnetic resonance imaging (MRI) and computed tomography (CT)] may lead to translational applications for the FRAP techniques developed in this dissertation.

ACKNOWLEDGEMENTS

There are many people I would like to thank for helping me grow as a scientific researcher and individual over my years of study. Firstly, I would like to deeply thank my advisor, Dr. Hai Yao, for constantly guiding me during every stage of my dissertation. He has been an extraordinary mentor and friend in providing countless resources and opportunities in my training. I was so lucky to become one of his students and travel halfway around the world to study in his lab. I can still remember how excited I was when receiving his offer letter because, right before then, I was quite frustrated having received eleven rejection letters from other universities in the U.S. I really want to thank Dr. Yao for making my dream of studying in U.S. finally come true. I would also like to thank my committee members, Drs. Martine LaBerge, Michael Kern, Zhi Gao, and Michael Rosol, for their thoughtful advice and encouragement in unique ways that have significantly improved my research and broadened my understanding of science and engineering. Next, I would like to thank all the students in the Clemson-MUSC Bioengineering program. They have not only contributed scientific and technical support and creative input, but have also been great friends as well. I really appreciate all of their support over the years. Finally, I'd like to thank my parents, Zhengding and Renzhen Shi, back in China for always being extremely supportive to my academic career even when they have been struggling with illness. I strongly believe that I will pay a debt of gratitude to them in the near future. I also would like to thank my wife, Hao, for standing with me during all the difficult times and cooking me the most delicious dinners which have given me tremendous energy and strength to finish this dissertation. I love you.

TABLE OF CONTENTS

Page

Table of Contents (Continued)

Page

LIST OF TABLES

LIST OF FIGURES

List of Figures (Continued)

Figure Page

List of Figures (Continued)

Figure Page

List of Figures (Continued)

Figure Page

CHAPTER 1 GENERAL INTRODUCTION

1.1 Introduction

Diffusion of solutes plays a crucial role in maintaining cell and tissue function and is also essential to many disease diagnostics and therapies that deliver drugs and genes to the human body.[1, 2] For instance, investigations on solute diffusion in aqueous cellular compartments are important for understanding metabolism, second messenger signaling, and protein-protein interactions.[3] Moreover, magnetic resonance (MR) based diffusion measurements have become the most successful and applicable diffusion techniques in clinics. As a result, the related diagnostic approaches have been utilized in detecting the tissue structure changes related to the anatomic pathological information in brain diseases.[4] Finally, diffusion is a dominant mechanism for the transport of nutrient solutes through the extracellular matrix (ECM) of cartilaginous tissues with an avascular nature, while the dysfunctional diffusion of nutrient solutes is believed to contribute to the degeneration of these tissues over time.[5-7] Therefore, determination of solute diffusion properties in cells, tissues or other biological systems does not only measure specific solute diffusion coefficients and mobilities, but also becomes a means for exploring the function and structure of these systems. The overall goal for my Ph.D. research is to develop the fluorescence-based diffusion measurement techniques for determining anisotropic solute diffusion properties in cartilaginous tissues.

1.1.1 Degeneration of Cartilaginous Tissues

Cartilaginous tissue is a connective tissue composed of specialized cells (*e.g.,* chondrocytes and fibroblasts) that produce a large amount of extracellular matrix (ECM),

which is comprised mostly of collagen fibers, abundant ground substance rich in proteoglycan, and elastic fibers. It is characterized by its avascular structures within the tissue, implying that nutrition for normal tissue cells, for maintaining a healthy ECM, is mainly supplied through diffusion from nearby vascularized tissues and synovial fluid. Poor nutritional supply to the cartilaginous tissue is believed to be an important factor leading to tissue degeneration.[6] Urban, J.P. *et al.* have studied the nutrition of the intervertebral disc (IVD), the largest avascular tissue in the human body, and found the dysfunctional diffusion of nutrients in IVD tissue can lead to cell death, loss of matrix production, an increase in matrix degradation, and hence disc degeneration [8]. Recently, water diffusion measured by the diffusion tensor imaging (DTI) technique has been reported to have the potential to become a valuable bioindicator for detecting articular cartilage degeneration.[9] Thus, my research focused on developing novel two-dimensional (2D) and three-dimensional (3D) diffusion measurement techniques to determine the anisotropic solute diffusion properties in the cartilaginous tissues.

1.1.2 Fluorescence Recovery after Photobleaching (FRAP) Technique

FRAP is a versatile and widely used tool for the determination of local solute diffusion properties within solutions, tissues, cells, and membranes.[10] Due to the high spatial resolution, FRAP offers the possibility to microscopically examine a specific region of a sample using confocal or multiphoton laser scanning microscopy (CLSM or MP-LSM).[11, 12] The basic principle of FRAP is based on photobleaching the fluorescence of molecular probes using a high intensity laser and analyzing the recovery of the photobleached area to obtain solute diffusivities, as shown in Figure 1.1.

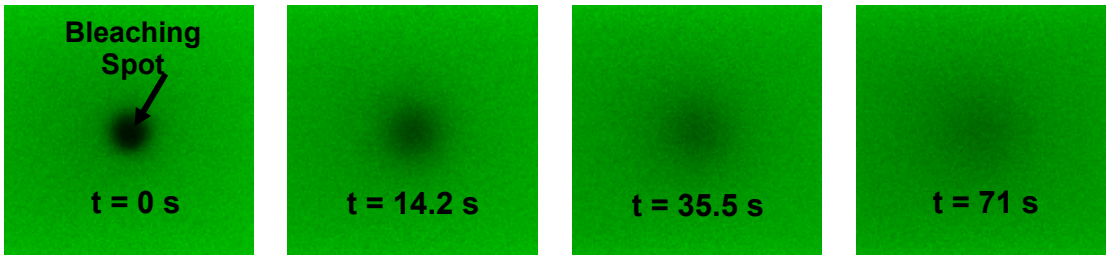

(a) (b) (c) (d)

Figure 1.1 Postbleaching process of FRAP experiments.
(a) The first confocal microscopy image after photobleaching using sufficiently high intensity laser. (b)-(d) Fluorescence recovery process after photobleaching at different time period. Due to the diffusion of fluorescently-labeled solutes, the dark bleaching spot gradually becomes brighter during the recovery course.

To date, most FRAP analyses are based on the method proposed by Axelrod et al. [13] more than 30 years ago for isotropic diffusion. FRAP has become the gold standard for measuring protein mobility on cell membranes. In the past decade, the FRAP technique has been developed and applied to study diffusion properties from the cellular level to the tissue level, especially, in cartilaginous tissues.[5, 7, 14] Because of the complex collagen fibers and ECM structure, the solute diffusion in cartilaginous tissue is commonly anisotropic. A successful approach for FRAP analysis is based on the spatial Fourier analysis (SFA) of the recovery images and has the advantage of detecting the anisotropic solute diffusion properties.[15, 16] This method has been used to characterize 2D anisotropic diffusion in knee meniscus and IVD tissue.[17] **Based on the previous studies, we will further develop a new FRAP method solely based on the SFA to completely determine 2D anisotropic diffusion tensor.** Additionally, the dramatic development of MP-LSM during the last decade has provided an essential pathway to the realization of 3D FRAP techniques.[12] Due to the nonlinear optical process, the multiphoton excitation can really generate a 3D spatially well-defined geometry of the bleaching profile (Figure 1.2). Thus, MP-LSM is perfect to study the 3D FRAP model. However, to our knowledge, there are no 3D models for anisotropic diffusion measurements by using SFA and multiphoton bleaching experiments. **Therefore, another major goal of this study is to develop the mathematical theory and techniques of 3D FRAP with SFA and multiphoton technique to determine the anisotropic solute diffusion properties in solutions and ligament tissues.**

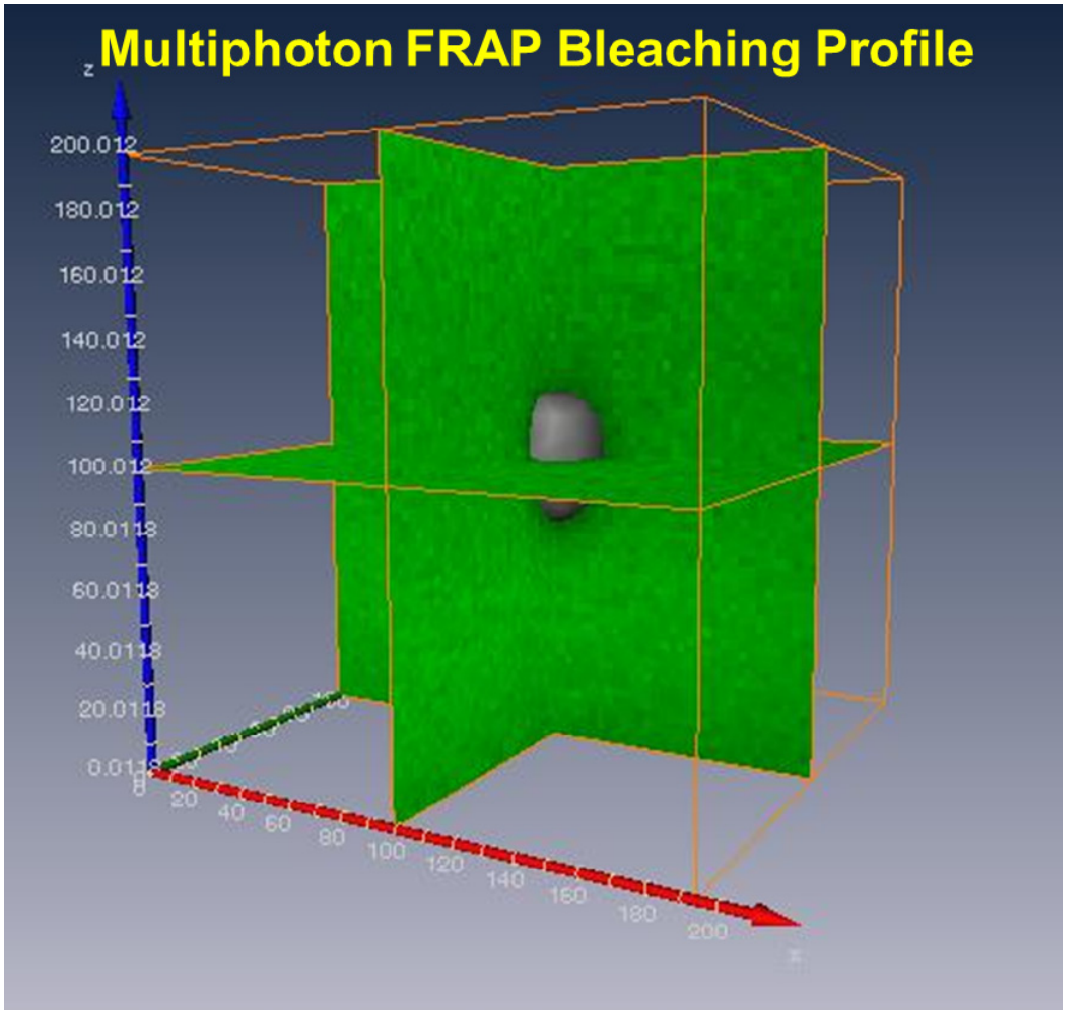

Figure 1.2 The 3D well-defined bleaching profile induced by multiphoton laser scanning.

1.1.3 Innovation

- ***Implication for the Solute Diffusion Measurements***

Based upon the successful accomplishment of this study, the 2D and 3D anisotropic solute diffusion properties in cartilaginous tissue will be fully characterized for the first time. The novel FRAP techniques can also be applied to investigate the complex 2D and 3D solute diffusion properties in the intracellular space by incorporating super-resolution imaging techniques. Furthermore, the 2D and 3D diffusion of important drugs in tumor or brain tissues can be quantified by our new techniques as well.

- ***Implication for the Diagnosis and Treatment of Cartilaginous Tissue Degeneration***

There are few useful diagnostic procedures for degenerating cartilaginous tissues and treatments are also limited. With the development of modern medical imaging technology, this proposed study can be translated to in vivo studies using non-invasive imaging techniques, which can be further developed to diagnose the patients who have cartilaginous tissue degeneration. New treatments for the degeneration of cartilaginous tissues may be initialized if the nutritional supply process could be comprehensively understood.

- ***Guidance for Engineered Cartilaginous Tissues***

Many designs of tissue-engineered cartilaginous tissues fail due to inappropriate biochemical and biomechanical composition and structure. Abnormal nutrient solute diffusion is also an aspect of unsuccessful design of the engineered cartilage because the

cells inside the artificial tissues cannot acquire the nutrient supply functionally. Tissue engineering studies may benefit from this proposed study because mimicking normal nutrient solute diffusion is a key factor in designing appropriate cartilaginous tissue engineered constructs.

1.2 Research Goals and Specific Aims

Diffusion of solutes plays a crucial role in maintaining cell and tissue function and is also essential to many therapies that deliver drugs and genes to the human body. Determination of diffusion properties in cells, tissues, or other biological systems could not only measure specific solute diffusion coefficients, but also becomes a means for exploring the function and structure of these systems. For instance, investigations on molecular diffusion in cell membranes are important for understanding the dynamics of diverse proteins. Moreover, diffusive transport of nutrient solutes through the ECM plays a key role in maintaining the normal function of avascular cartilaginous tissues, while the dysfunctional diffusion of those solutes is believed to contribute to the degeneration of the tissues over time. The most current 2D and 3D diffusion studies have concentrated on isotropic solute diffusion measurements at cell level. However, to our knowledge, there are very few studies examining the 2D and 3D anisotropic solute diffusion properties at tissue level by using FRAP techniques. Therefore, our research goal is to develop the novel FRAP techniques for 2D and 3D anisotropic solute diffusion measurements in cartilaginous tissues.

Hypothesis: We hypothesize that the novel 2D and 3D FRAP techniques can completely determine the anisotropic solute diffusion properties at tissue level and

therefore, further characterize the relationship between solute diffusion and tissue morphology of cartilaginous tissues.

Aim 1. Develop and validate the mathematical theory and technique of SFA-based 2D FRAP method for determining the anisotropic solute diffusion tensor and apply this novel technique to investigate the 2D anisotropic solute diffusion properties in the TMJ disc. The mathematical theory for the most current 2D FRAP techniques is mainly based on the analysis in the spatial domain and the assumption of isotropic diffusion in the samples. However, the solute diffusion in various cartilaginous tissues (*e.g.*, IVD and TMJ disc) with complex structures is believed to be anisotropic (*i.e.*, orientation dependent). Therefore, in this specific aim, we will derive a close-form solution of the 2D diffusion equation in the frequency domain by using SFA and develop a new mathematical theory for data analysis of the 2D FRAP technique. Validation of the new FRAP method will be accomplished by diverse computer simulated diffusion tests with pre-defined diffusion tensors. Finally, this novel technique will be applied to investigate the 2D anisotropic solute (FITC-Dextran with molecular weight of 4KDa) diffusion properties in porcine TMJ discs.

Aim 2. Determine the relationship between anisotropic solute diffusion properties and tissue morphology in porcine TMJ discs. Based on the accomplishment of Aim 1, the novel 2D FRAP technique (developed and validated in Aim 1) will be utilized to determine the solute (Fluorescein with molecular weight of 332Da) diffusion processes in the porcine TMJ disc tissue. Tissue morphology of porcine TMJ discs will be examined by scanning electron microscopy (SEM). The

relationship between solute diffusion properties and tissue morphology will be investigated to explore the impact of tissue structure on the solute diffusion properties and for further understanding the pathways of nutritional supply into the TMJ disc.

Aim 3. Develop the mathematical theory and technique of a novel 3D FRAP method with SFA and multiphoton microscopy for determining the 3D anisotropic solute diffusion tensor in the porcine ligament tissue. The dramatic development of multiphoton laser scanning microscopy (MP-LSM) during the last decade has provided an essential pathway to the realization of 3D FRAP techniques. However, to our knowledge, there are no 3D FRAP methods for anisotropic diffusion measurements by using SFA and multiphoton technique. Therefore, based on the accomplishment of Aim 1 and 2, we will also derive a close-form solution of the 3D diffusion equation in the frequency domain by using SFA and develop the new mathematical theory for data analysis of the 3D FRAP technique. Validation of the new methods will be firstly accomplished by diverse computer simulated FRAP experiments. Additionally, the solute diffusivities in different glycerol solutions will be determined to further validate the new 3D FRAP technique by comparing the results with the diffusivity values reported in other literatures under similar testing conditions. Finally, in order to demonstrate that the new 3D FRAP method is capable to investigate the 3D solute diffusion in the biological tissues, this technique will be utilized to determine 3D solute diffusion properties in the porcine ligament tissue, which is a typical soft collagenous tissue with well-organized collagen fibers,

Impact on the Field: Based upon the successful accomplishment of the proposed

study, novel FRAP techniques will be fully developed for determining the 2D and 3D anisotropic diffusion in cartilaginous tissue. Moreover, characterization of the 2D and 3D solute diffusive transport properties in cartilaginous tissues will delineate the relationship between solute diffusion and tissue morphology for further understanding the pathophysiology and etiology of tissue dysfunction and degeneration. These new techniques could also be translated to study the diffusion of anti-tumor drugs and genes to tumor cells as well as the diffusion properties in the brain. Finally, mimicking the normal solute diffusion properties in cartilage will be a key factor for developing successful tissue engineered constructs.

1.3 Organization of Dissertation

The following manuscript is organized in chapters of related studies that combine to form the overall aims of this project. In Chapter 2 we firstly presented a brief introduction on solute diffusion in various biological systems to demonstrate the significance of this project, and then summarized five different types of diffusion measurement techniques including diffusion cell method, optical fluorescence methods, electrical conductivity approach for ion diffusion, radiotracer methods, and MR-based diffusion imaging methods. In Chapter 3, we presented a comprehensive overview of 2D and 3D FRAP techniques and applications. Both spatial and frequency analysis based 2D FRAP techniques were discussed and the developments and typical mathematical theories for both techniques were demonstrated in this chapter. We also introduced the applications of FRAP in various biological researches including molecular diffusion in cell membranes, protein dynamic studies in living cells, and solute diffusion in the ECM.

FRAP techniques for 3D diffusion measurements were introduced in the last section, which mainly include confocal and multiphoton based 3D FRAP methods. In Chapter 4, a novel 2D FRAP technique solely based on the SFA was developed to determine the anisotropic solute diffusion tensor in porcine TMJ disc. We found the new FRAP technique can accurately determine the anisotropic 2D diffusion tensor of 4KDa FTIC-Dextran in porcine TMJ disc. These findings indicated that the diffusion of this solute in TMJ discs was inhomogeneous and anisotropic. In Chapter 5, we investigated the relationship between solute diffusion properties and tissue morphology in porcine TMJ discs by utilizing the FRAP technique we developed in the chapter 4 as well as SEM. It was found that the diffusion of fluorescein in the TMJ disc was anisotropic and inhomogeneous, which indicated that tissue structures (*i.e.*, the collagen fiber alignment) and composition (*e.g.*, water content) could be the key factors that mainly affect the solute diffusion properties in the TMJ disc. In Chapter 6, the SFA based FRAP technique was further developed to determine the solute anisotropic diffusion in 3D tissue samples. Multiphoton photobleaching technique was applied to create a cubic bleached block in the central region of the samples and the 3D fluorescence recovery process was recorded by taking the Z-stack image series over time. All the components of 3D diffusion tensor were calculated by our new 3D MP-FRAP methods. Finally, quantitative analysis of 3D MP-FRAP experiments in porcine ligament tissues was demonstrated as an in-vitro application of our technique. Chapter 7 outlines the overall conclusions of this project and identifies future directions of this work.

CHAPTER 2 METHODS OF DIFFUSION MEASUREMENTS

2.1 Introduction

Diffusion is the process by which molecules spread from regions of high concentration to regions of low concentration. It results from the thermal and random movement of molecules and is driven by concentration gradients. The mathematical framework to describe the phenomena of diffusion was developed by Adolf Eugen Fick (1829–1901).[18] His vital contribution to the research of diffusion was to define the diffusion coefficient and to measure the diffusion of salt in water. John Crank published a well-known book providing a collection of solutions of the diffusion equations described how these solutions may be obtained.[19] Biomedical and biophysical scientists have been using those equations and solutions to determine the molecular diffusion in the biological systems.[7, 15, 20-24]

2.1.1 Molecular Diffusion in Cell Membranes

Cell membranes, consisting of a phospholipid bilayer [25] with embedded proteins, separate the intracellular components from the extracellular environment. The lateral diffusion of molecules is very important in the functional activities of cell membranes, such as membrane-bound enzymes, regulatory proteins and the transmission of hormone signals.[26, 27] These diffusion properties have been measured by a variety of methods, for example, fluorescence recovery after photobleaching (FRAP) and single particle tracking (SPT).[28] Investigations of molecular diffusion in cell membranes are crucial for understanding the dynamics of diverse proteins and the metabolism of cells.

2.1.2 Solute Diffusion inside the Living Cells

Various intracellular processes including second messenger signaling, metabolism and protein-protein interactions are related to the diffusion of solutes. The intracellular diffusion of solutes could be affected by solute properties, and by the composition and structure of the intracellular compartments. Studies have shown that small solute diffusion is relevant for metabolite uptake and second messenger signaling, the diffusion of enzymes is important for metabolism, and the diffusion of DNA is important in antisense and gene therapy.[3] Experimental approaches to measure solute diffusion inside living cells include FRAP, fluorescence correlation spectroscopy (FCS), [29] time-resolved anisotropy methods [30] and magnetic resonance methods.[31] Determination of solute diffusion inside the living cells could be useful not only in understanding the diffusive properties, but also in improving the efficiency of strategies in drug delivery.

2.1.3 Diffusion in the ECM: Applications in the Brain

Diffusion plays a crucial role in brain function and is also essential to many therapies that deliver drugs to the brain.[32] Based on the appropriate measurement methods, the diffusion concentration distributions of well-chosen molecules could unveil the structure of brain ECM space under normal or pathological condition. Numerous techniques [1] have been developed to determine the diffusion in brain tissue, which include radiotracer technique, real-time iontophoresis (RTI) and real-time pressure (RTP) ejection, integrative optical imaging (IOI), FRAP , light scattering and transmission, magnetic resonance (MR) based imaging [*i.e.*, diffusion weighted imaging (DWI), diffusion tensor imaging (DTI), diffusional kurtosis imaging (DKI)] , microdialysis and

impedance. The most successful and applicable technique of diffusion measurement to clinics could be MR based imaging techniques which have been validated as indispensable clinical diagnostic approaches that provide trustworthy anatomic pathological information for brain-related diseases.[4]

2.1.4 Diffusion in the ECM: Applications in the Cartilaginous Tissues

Diffusive transport of nutrient solutes through the ECM plays a key role in maintaining the normal function of cartilaginous tissues while the dysfunctional transport of those solutes is believed to contribute to the degeneration of the tissues over time. Solute diffusivities in articular cartilage, intervertebral disc (IVD) and temporomandibular joint (TMJ) discs have been determined using a variety of techniques including FRAP, [5] Magnetic Resonance Imaging (MRI), [33, 34] tracking the net movement of radiolabeled solutes, [20, 35] and fluorescence [36] or radiotracer desorption.[37, 38] These findings suggested that diffusive transport in cartilaginous tissues is dependent upon tissue composition (*e.g.*, water content) and structure (*e.g.*, collagen orientation). Tissue engineering studies may benefit from the diffusion studies because mimicking the normal nutrient solute transport in real tissues should be a key factor for successful tissue engineering of cartilaginous tissues.

In conclusion, the solute diffusion is significantly important in the biological systems. Therefore, this chapter summarizes the experimental approaches for quantifying the molecular diffusion in cells, tissues and biomaterials. A wide variety of methods have been created and developed to measure solute diffusion in cells, tissues and biomaterials. These methods will be generally divided into five categories: diffusion cell

method, optical fluorescence methods, electrical conductivity approach for ion diffusion, radiotracer methods, and MR-based methods (*i.e.*, DWI, DTI and DKI). The typical techniques in each category will be introduced in the following sections.

2.2 Diffusion Cell Method

Diffusion cell method is a one-dimensional steady-state diffusion experiment which has been used to directly yield values of apparent solute diffusivities in the intervertebral disc (IVD) tissues.[39-41] The principle of the diffusion measurement is straightforward and governed by Fick's law. The solute is introduced into the upstream chamber, then which gradually diffuses across the specimen into the downstream chamber. (Figure 2.1) The solute concentrations in downstream are measured at different time points and the diffusion equation is used to curve-fit the experiment data to yield the diffusivity. Jackson et al. investigated the effect of static compression and anisotropy on the apparent diffusivity of glucose in bovine annulus fibrosus (AF) and found the diffusion of glucose in bovine AF is anisotropic and significantly dependent on strain.[30] This method only can determine the diffusion in a large scale (*e.g.*, mm), the diffusion rate at the micron-level is difficult to be measured using diffusion cell method. The diffusion cell method is also time-consuming.

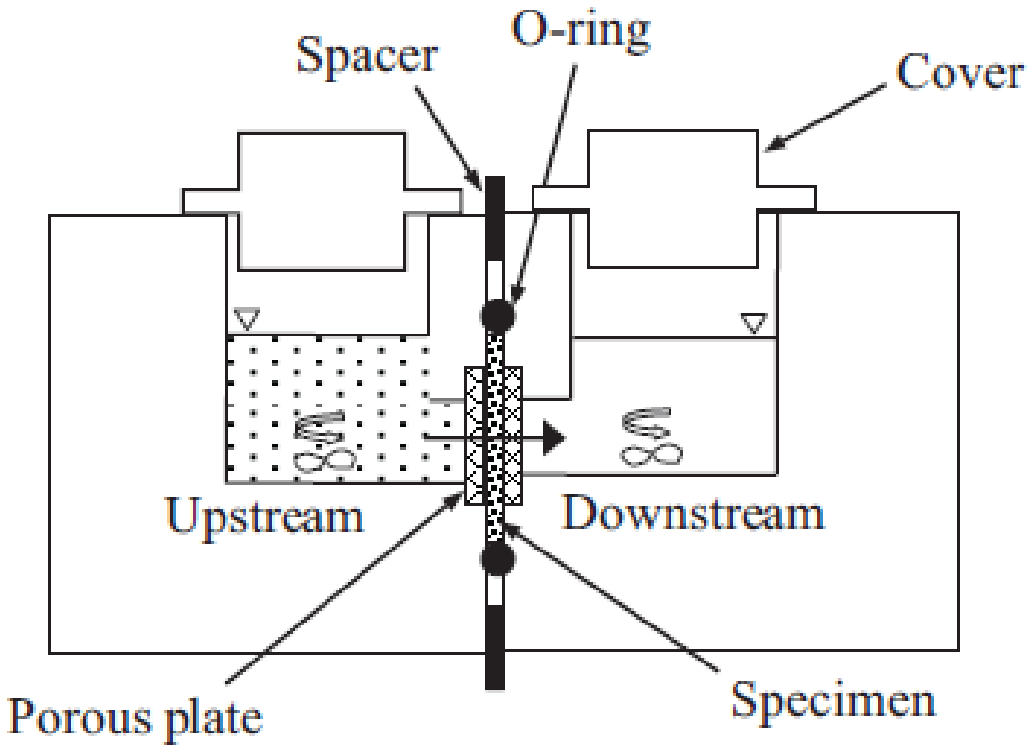

Figure 2.1 Schematic of a custom diffusion cell. [41]

2.3 Optical Fluorescence Methods

Optical fluorescence method is the most popular approach which is mainly used in the cell biology field to quantify the diffusion properties of fluorescent molecules in cell membranes and intracellular components. Thousands of studies have been done on the solute diffusion determination using this type of methods since the 1970's. The applications of optical fluorescence methods started from *in vitro* cell membrane studies, with the tremendous progress of the researches on fluorescent dye and microscopy, they've been applied to study the intracellular diffusion and the solute mobility at tissue level *in vivo*. Four major optical fluorescence methods for diffusion measurements will be presented in the following sections.

2.3.1 Single Particle Tracking (SPT)

The basic principle (Figure 2.2) of SPT is using video microscopy to record the motion of an individual particle within a medium and processing the images to obtain the trajectory of the particle motion. The trajectory can be analyzed using an appropriate statistical distribution function to provide a diffusion coefficient. The first SPT experiment was implemented by Barak and Webb [42] who tracked a fluorescent-labeled low density lipoprotein receptor on human fibroblast.

Many SPT studies [43-47] have been conducted to explore the detailed modes of protein diffusion and motion (*i.e.*, normal diffusion, anomalous diffusion, directed motion with diffusion and corralled motion) in cell membranes. Due to the high spatial (tens of nanometers) and temporal (tens of milliseconds) resolution, the SPT technique has become a powerful tool to study the molecular dynamics in heterogeneous cell

membranes and intracellular compartments. However, the limitation of SPT technique is that the solute concentration is always low, so this method cannot be applied to the medium with high concentration.

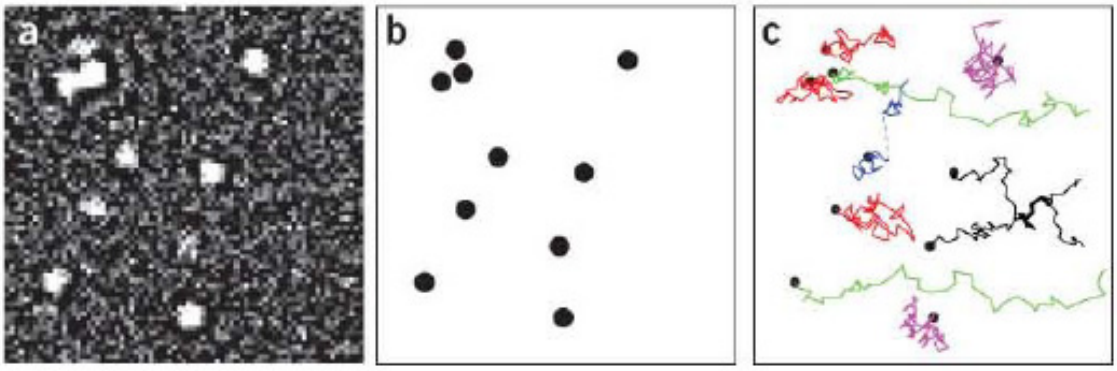

Figure 2.2 Schematic drawing of a SPT experiment.
(a, b) In the localization step, the fluorescence image at a given time (a) is analyzed to give the positions of the particles at that time (b). (c) After repeating the localization step on a time series of images, the positions at each time point are linked into trajectories in the connection step. The trajectories are then interpreted. Shown here are pure random walks (red), directed motion (green), confined motion (purple), a random walk with blinking (blue) and a trajectory with merging and splitting (black). [48]

2.3.2 Fluorescence Correlation Spectroscopy (FCS)

The FCS technique was first proposed by Dr. Webb's lab in 1972 at *Physical Review Letters*.[49] His group established the theoretical basis and experimental realization of FCS.[50-52]

Figure 2.3 shows the schematic of a typical FCS experiment. The basic principle of FCS is to measure the spontaneous molecular concentration fluctuation driven by thermodynamics as a function of time in a well-defined open microscopic volume without disturbing the macroscopic equilibrium of the system. Fluorescent intensity corresponding to the fluorescence concentration could be detected in the practical FCS setup and autocorrelation analysis on fluorescent intensity fluctuation yields diffusion coefficients.

One early successful application of FCS was the measurement of lateral diffusion of fluorescent lipid in planar bilayer membranes.[53] In the last two decades, the FCS technique has been successfully applied to study molecular diffusion in the biomedical field. Due to the advances in signal detectors, fluorescent markers, autocorrelation electronics and confocal and multiphoton microscopy, FCS has been improved in many aspects, such as detection limits, measurement times and signal-to-noise ratio.[29, 54-57] Potential problem with using FCS for measuring translational mobilities within a cell membrane is that the depth of the observation volume (~μm) is significantly larger than the thickness of biological membranes (~10nm) which can lead to mixed sampling of the mobility in the membrane and adjacent aqueous surrounds.

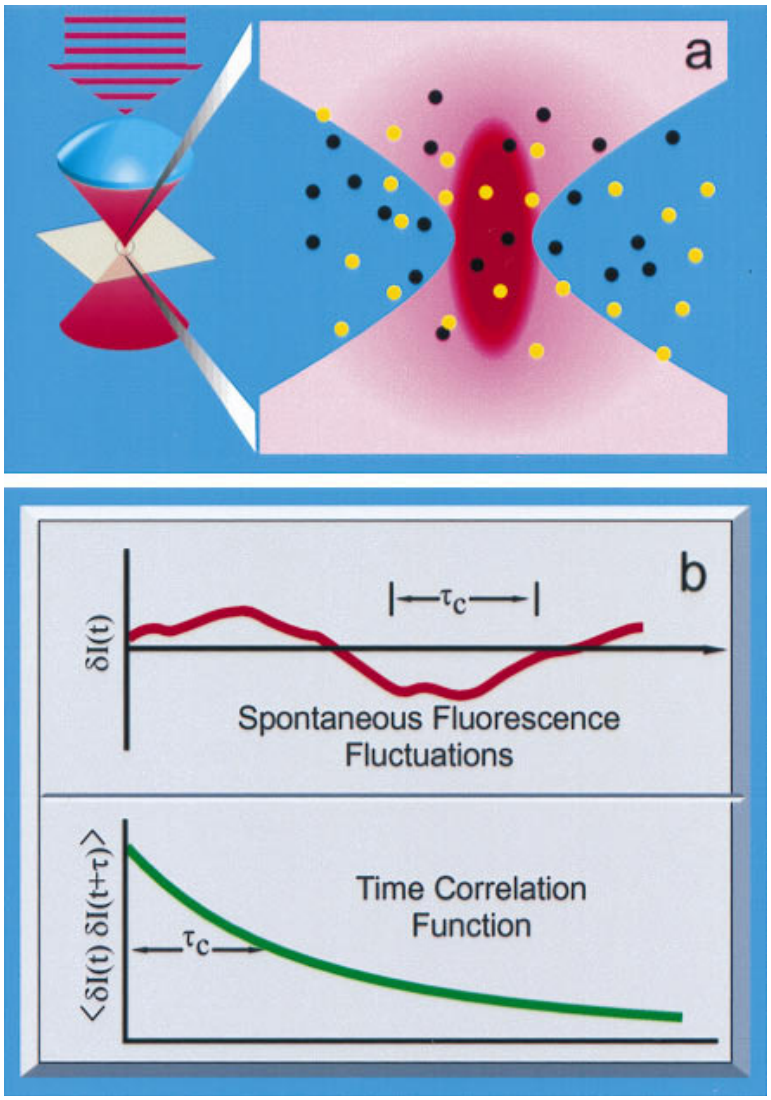

Figure 2.3 Schematic drawing of a FCS experiment.
(a) Fluorescence is collected from the molecules (circles) in a small well defined volume (red) near the focus of a laser beam (pink) within an equilibrated solution. The number of fluorescent molecules (yellow) in this volume fluctuates due to diffusion/flow in and out of this volume. The fluorescence fluctuates (b Upper) in proportion to the number of fluorescent molecules in the volume, and its autocorrelation (b Lower) yields the dynamic parameters. [29]

2.3.3 Fluorescence Recovery after Photobleaching (FRAP)

FRAP is a versatile and widely used tool for the determination of local solute diffusion properties within solutions, tissues, cells, and membranes.[3, 10, 58-61] Due to the high spatial resolution, FRAP offers the possibility to microscopically examine a specific region of a sample using confocal or multiphoton laser scanning microscopy. For instance, the site-specific (*i.e.*, inhomogeneous) solute diffusion in articular cartilage has been previously studied using FRAP. [5] The typical principle of FRAP is based on photobleaching the fluorescence of molecular probes using a high intensity laser and analyzing the recovery of the bleached area to obtain solute diffusivities, see Figure 1.1.

To date, most FRAP analyses are based on the method proposed by Axelrod et al. for isotropic diffusion.[13] Another approach for FRAP analysis is based on the SFA of the recovery images and has the advantage of potential detection of anisotropic diffusion. [7, 14-16, 62, 63] The major limitation of FRAP technique is the photobleaching laser could damage the living cells. The details of FRAP related techniques and applications will be further discussed in the following sections.

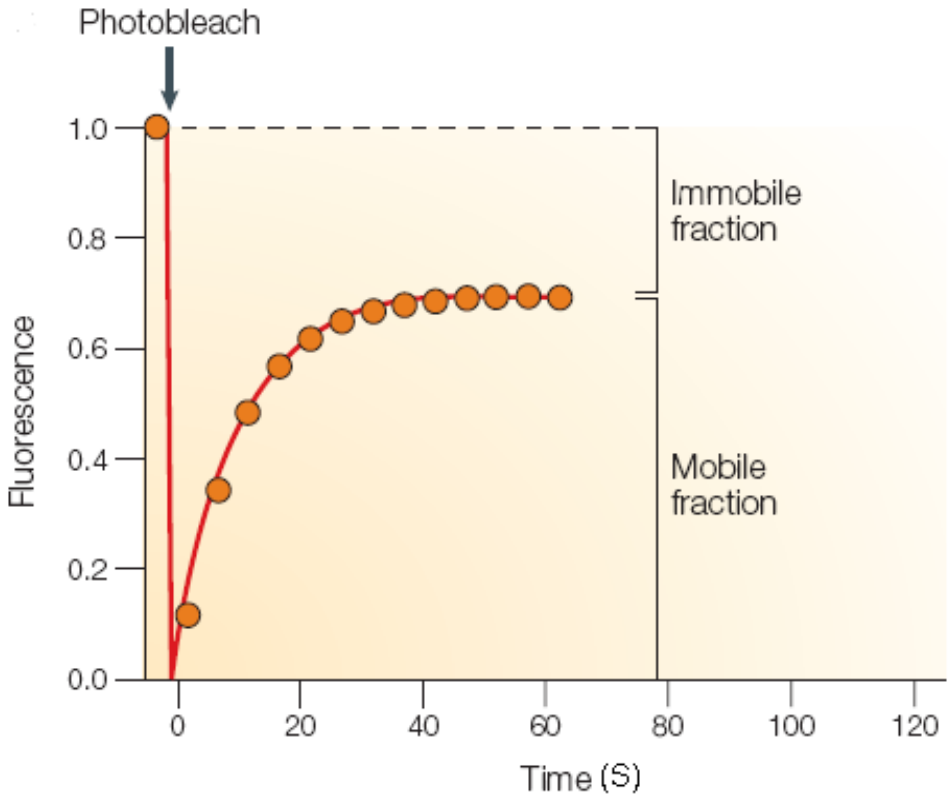

Figure 2.4 A typical relative fluorescence intensity VS. time curve in FRAP experiment. Immobile fraction and diffusivity could be calculated by analyzing this curve.[64]

2.3.4 Integrative Optical Imaging (IOI)

IOI technique is a special optical method first presented by Nicholson and Tao in 1993 [65] in order to determine the macromolecular diffusion in brain tissue. Figure 2.5 shows an example of IOI technique. In hydrogel or brain tissue samples, the diffusion of fluorescently labeled macromolecules released from a micropipette is monitored and measured by fluorescence microscopy. One-dimensional (1D) fluorescence intensity profile is combined with the theoretical analysis of diffusion and imaging model to yield the diffusivities.[1] This technique was improved by Xiao *et al.* and successfully used to determine the anisotropic diffusion of dextran polymers in brain ECM space.[66] However, one limitation of this method is that the measurement is restricted to optically thin slices of brain tissue and the characterization of diffusion properties in deep brain tissue requires an alternative approach.

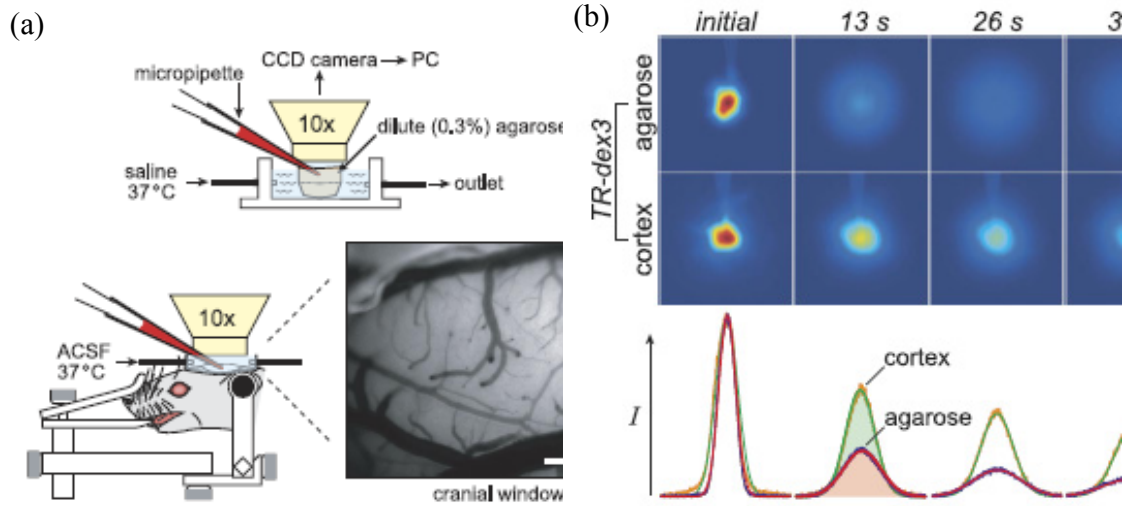

Figure 2.5 IOI measurements *in vivo* using 3kDa dextran.
(a) Experimental setup for IOI diffusion measurements *in vivo*. Successive images of fluorescent probe diffusion were captured by a cooled charge-coupled device (CCD) camera and fluorescent microscope with a 10X water-immersion objective after pressure ejection from a micropipette into either dilute agarose or somatosensory cortex, accessed through an open cranial window in rat (scale bar = 500μm). (b) Dextran diffusion in neocortex. Representative images after fluorescent dex3 ejection into agarose or cortex. Fluorescence intensity profiles and theoretical fits for the images shown below images, yielding D $=2.3\times10^{-6}$cm^2/s (agarose) and D*$= 4.5\times10^{-7}$cm^2/s (cortex). Scale bars = 200μm. [67]

2.4 Electrical Conductivity Approach for Ion Diffusion

Electrical conductivity approach for ion diffusion is mainly applied to measure the diffusivity of ions in hydrated soft tissue (i.e., articular cartilage and lumbar annulus fibrosus). Under zero fluid flow condition, the linear relationship between electrical conductivity and ion diffusivity provides a simple way to calculate diffusion according to the results of conductivity tests in soft tissue samples. The electrical conductivity of ion in human articular cartilage was first reported by Maroudas.[68] Afterwards, Hasegawa used a four-wire method which became a standard setup (Figure 2.6). The four-wire method uses two current sensing electrodes inserted in the center of larger two source supplying stainless steel electrodes. The sensing electrodes measures the voltage drop across the tissue resulting. From the voltage drop or resistance, conductivity is directly calculated. Gu's group started to employ this method to study the conductivity in IVD tissue [69, 70] and built the mathematical model of ion diffusivity and conductivity, they also extended the study to successfully obtain the anisotropic ion diffusivity in bovine IVD tissue by testing the samples in three orthogonal orientations.[71] Sadleir improved the method to acquire 2D anisotropic conductivity and diffusivity with a solo test in a gel phantom.[72] Compressive loading could be easily applied to the specimens in this method which allows investigation of the effect of mechanical loading on the ion transport in soft tissues. Kuo *et al.* examined the impact of mechanical loading on solute transport in porcine temporomandibular joint (TMJ) discs using the electrical conductivity method and found that compressive strain impeded solute transport in the TMJ disc.[73]

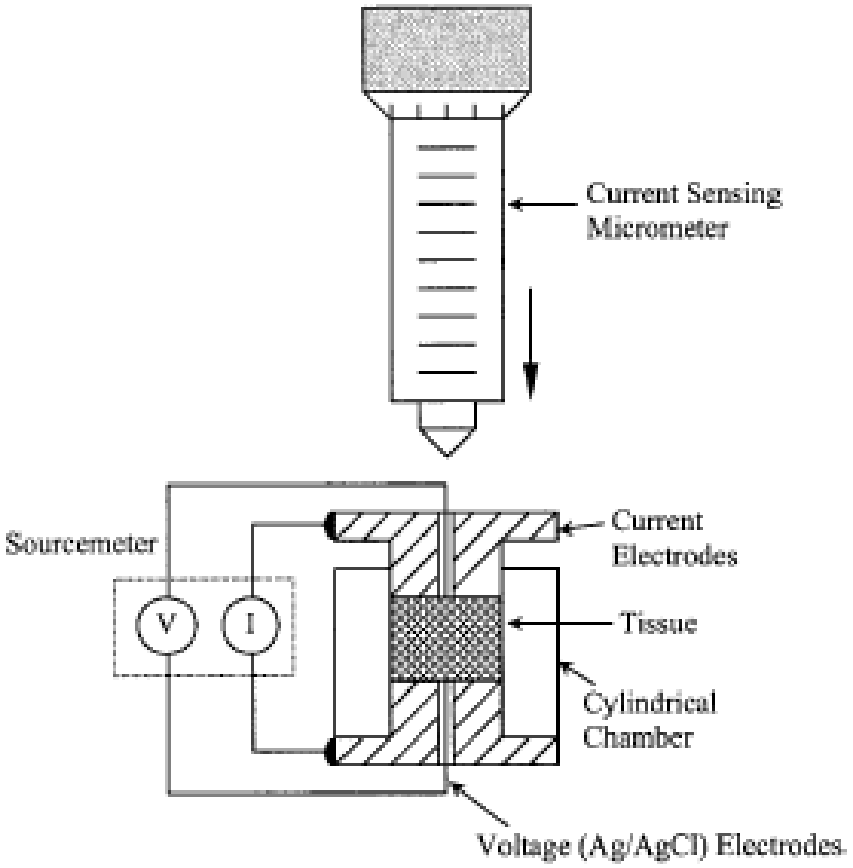

Figure 2.6 Schematic of apparatus for measuring electrical conductivity.
The devise consists of two stainless steel current electrodes, two Ag/AgCl voltage-sensing electrodes, a nonconductive plexiglass chamber, a current sensing micrometer, and a Keithley Sourcemeter.[70]

2.5 The Radiotracer Technique

The radiotracer method is usually a 1D and macroscopic diffusion experiment performed by tracking radioactive (i.e., ^{3}H, ^{14}C and ^{35}S) tagged solutes diffusing into the specimens.[20] This method was first presented by Urban who studied the diffusion of (^{35}S) sulphate and (^{3}H) methyl glucose into IVD *in vivo* and *in vitro*. The tracer concentration profile inside the tissue was used to characterize the diffusion properties of solutes.[21] Torzilli developed a radiotracer method measuring the solute diffusion in articular cartilage harvested from adult bovine knees.[20] In this study, the distribution of concentration profile was obtained by solving the 1D diffusion equation analytically with some certain boundary and initial conditions. The diffusion coefficient was calculated by curve-fitting the measurements of tracer concentrations at different positions within the specimens and time points using the analytical solution of the diffusion equation. The advantages are that a wide variety of solutes can be tested and macroscopic diffusion properties can be investigated. However, the disadvantages are that the spatial and temporal resolution of it is not high and the use of radioactive material is required.

2.6 MRI-based Measurements on Water Diffusion

The effects of diffusion on the nuclear magnetic resonance (NMR) signal were first reported theoretically [74] and experimentally [75] by the physicists in the 1950s. Most diffusion NMR studies have begun after Stejskal and Tanner [76] developed the bipolar pulse field gradient method to better control the signal measurements and

simplify the understanding of the encoding of the diffusion process in the NMR signal. The basic principles of diffusion MRI were outlined in the mid-1980s. Three main MRI-based diffusion techniques will be briefly reviewed: diffusion-weighted imaging (DWI), diffusion tensor imaging (DTI), and diffusional kurtosis imaging (DKI).

2.6.1 Diffusion-Weighted Imaging (DWI)

DWI is most applicable when the water movement within the specimens is primarily isotropic, such as grey matter in the cerebral cortex and major brain nuclei. The water diffusion rate appears to be the same when measured along any orientations in these tissues. In DWI technique, the magnetic field with linear and pulsed gradient is used to measure the apparent diffusion coefficient (ADC) which can be mapped as an image, using diffusion as the contrast.

$$\frac{S}{S_0} = e^{-\gamma^2 G^2 \delta^2 (\Delta - \delta/3) D} = e^{-bD} \tag{2.1}$$

Where S_0 is the signal intensity without the diffusion weighting, S is the signal with the gradient, γ is the gyromagnetic ratio, G is the strength of the gradient pulse, δ is the duration of the pulse, Δ is the time between the two pulses, and finally, D is the diffusion coefficient. The most successful clinical application of DWI was in imaging the brain following stroke in adults.[77, 78] The injured areas of brain during a stroke was present a "darker" on an ADC map when compared to the normal tissues. (Figure 2.7)

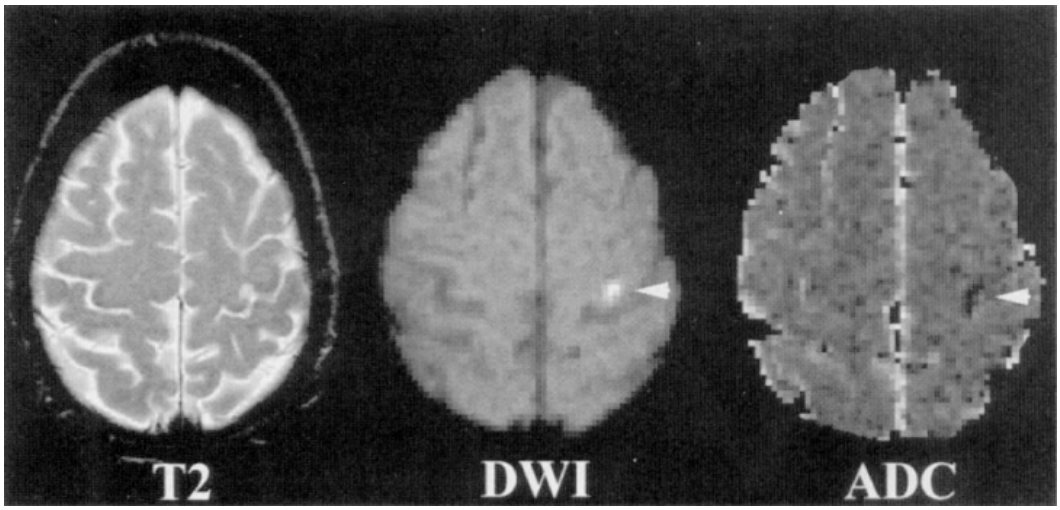

Figure 2.7 Regular MR image and DWI images.
This patient presented with right arm weakness and unsteady gait and was considered clinically to have a posterior circulation stroke. The T2 image is normal at 24 hours; however, a small lesion is present in the left hemisphere on diffusion-weighted imaging (DWI) (arrowhead). This lesion is demonstrated to be acute because it is dark on the apparent diffusion coefficient (ADC) map (arrowhead). [78]

2.6.2 Diffusion Tensor Imaging (DTI)

When the researcher measured the water diffusion in the brain tissue with complex structure using DWI technique, they noticed that ADC values varied depending on which direction the pulse gradient was applied. This orientation dependent contrast is generated by diffusion anisotropy. Therefore, it's necessary to use a mathematical operator, called a diffusion tensor [79], to fully characterize the water diffusion in all orientations.

$$\vec{D} = \begin{bmatrix} D_{xx} & D_{xy} & D_{xz} \\ D_{yx} & D_{yy} & D_{yz} \\ D_{zx} & D_{zy} & D_{zz} \end{bmatrix} \tag{2.2}$$

The equation (2.1) could be rewritten using diffusion tensor in equation (2.2) (symmetric tensor assumed) as below:

$$\frac{S}{S_0} = e^{(-b_{xx}D_{xx} - b_{yy}D_{yy} - b_{zz}D_{zz} - 2b_{xy}D_{xy} - 2b_{xz}D_{xz} - 2b_{yz}D_{yz})} \tag{2.3}$$

Multiple DWI measurements along the different gradient directions have to be done to determine all the components of diffusion tensor and three eigenvalues, λ_1, λ_2, and λ_3, could be calculated. Mean diffusivity (MD) and fractional anisotropy (FA) which can be calculated by equation (2.4) and (2.5) are mainly used as imaging contrasts in DTI technique.

$$\text{Mean Diffusvity} = (\lambda_1 + \lambda_2 + \lambda_3)/3 \tag{2.4}$$

$$\text{Fractional Anisotropy} = \frac{\sqrt{(\lambda_1 - \lambda_2)^2 + (\lambda_1 - \lambda_3)^2 + (\lambda_2 - \lambda_3)^2}}{\sqrt{2(\lambda_1{}^2 + \lambda_2{}^2 + \lambda_3{}^2)}} \quad (2.5)$$

The principal application of DTI is in the imaging of white matter where the location, orientation, and anisotropy of the tracts can be detected. Clinically, the DTI technique has been widely used to diagnose multiple sclerosis, chronic ischaemia, and Alzheimer's disease and to perform tractography which is a useful tool for measuring deficits in white matter, such as in aging. (Figure 2.8)

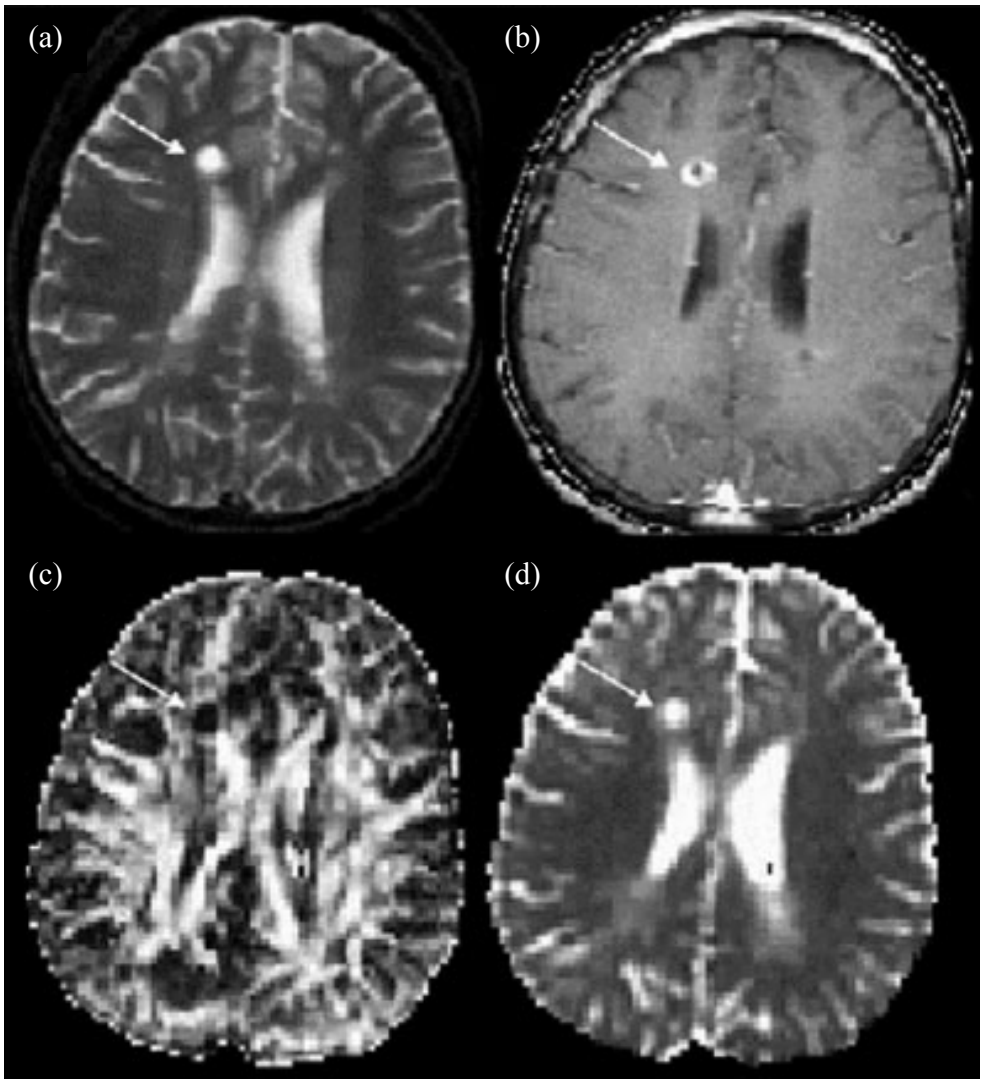

Figure 2.8 MR images of a Multiple Sclerosis (MS) lesion in axial section.
(a) T2-weighted image in which the lesion appears hyperintense. (b) Post-contrast T1-weighted scan in which a rim of hyperintensity surrounds the core of the lesion. (c) Fractional anisotropy image, in which the intensity of the image is directly proportional to the anisotropy. Note the marked loss of structure/anisotropy within the lesion. (d) Mean diffusivity image. The lesion exhibits high signal intensity suggesting little hindrance of diffusion due to breakdown of tissue structure.[78]

2.6.3 Diffusional Kurtosis Imaging (DKI)

In 2005, Jensen et al. first reported Diffusional Kurtosis Imaging (DKI) technique based on DWI.[80] Instead of using Gaussian possibility distribution function (PDF) of the movements of water molecules in DWI, The basic principle of DKI technique was to use non-Gaussian PDF and the equation below to curve fit the experimental data to obtain apparent diffusivity D_{app} and apparent kurtosis K_{app}.

$$S_{exp}=\left\{ \eta^2+\left[S_0 \exp\left(-bD_{app}+\frac{1}{6}b^2D_{app}^2K_{app}\right)\right]^2\right\}^{1/2} \tag{2.6}$$

They mentioned both D_{app} and K_{app} could be used as image contrast to map the tissue microstructure, but K_{app} may be more sensitive to the anisotropic microstructure.

DKI is a diffusion-weighted MRI technique that allows the diffusional kurtosis to be estimated with clinical scanners using standard diffusion-weighted pulse sequences and relatively modest acquisition times. DKI is an extension of the widely used DTI method, but requires the use of at least 3 b-values and 15 diffusion directions. It is reported that the diffusional kurtosis is sensitive to diffusive heterogeneity (Figure 2.9) and suggested that DKI may be useful for investigating ischemic stroke and Alzheimer's disease.[81, 82]

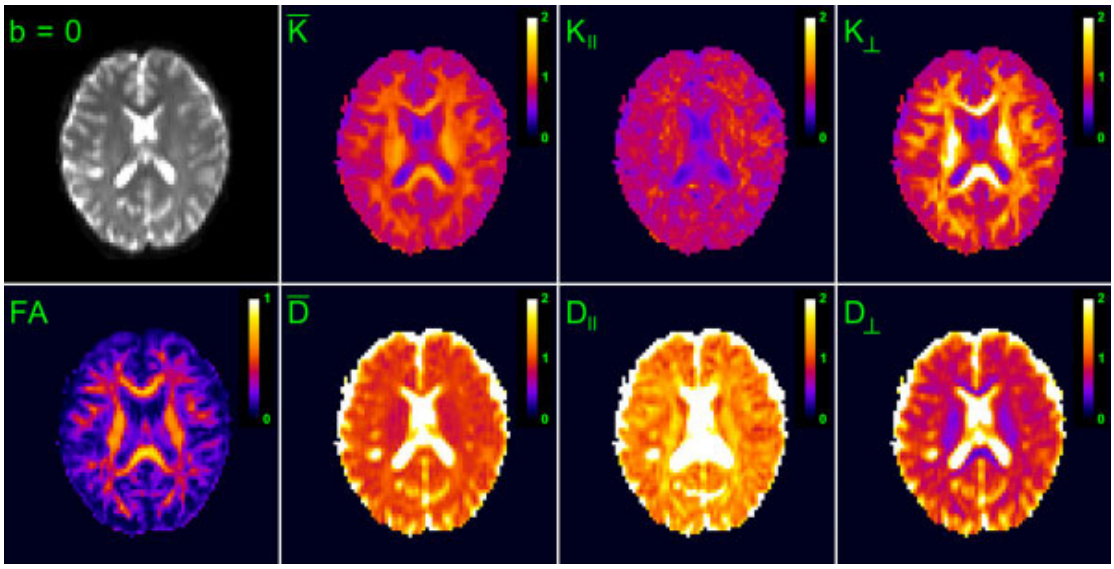

Figure 2.9 DKI diffusion metric maps for a single axial slice together with a T2-weighted (b=0) image from one normal subject.
The diffusion-weighted data were acquired at 3T with b-values of 0, 1000, and 2000 s/mm2. The maps for kurtoses provide additional information that quantify diffusional non-Gaussianity. The calibration bars for the diffusivities are in units of μm2/ms, while those for the FA and kurtoses are dimensionless.[80]

CHAPTER 3 FRAP TECHNIQUES AND APPLICATIONS FOR SOLUTE DIFFUSION MEASUREMENTS

3.1 Measurement Techniques for 2D Solute diffusion by FRAP

The diffusion properties of fluorescently labeled solutes can be assessed using a specific type of photobleaching technique called fluorescence recovery after photobleaching (FRAP). In this technique, fluorescent molecules in a small region of the samples are irreversibly photobleached using a high intensity laser beam shortly and subsequent movement of surrounding nonbleached fluorescent molecules into the photobleached area is recorded at low laser power. (Figure 1.1) The series images are analyzed to determine the molecular mobility parameters, for example, the mobile fraction, M_f ,which is the fraction of fluorescent solutes that can diffuse into the bleached region during the time course of the experiment, and the diffusion coefficient, D, which is a measure of the rate of solute movement in the absence of flow or active transport.[59]

3.1.1 Factors Affecting the FRAP Analyses

Since Axelrod *et al.* first proposed FRAP technique in 1976, [13] thousands of publications related the FRPA techniques and applications have been reported in various biological research fields. Most FRAP analyses start from solving the diffusion equations and then either analytical or numerical solutions will be used to calculate diffusion parameters. Many factors could affect the analyses of FRAP data, including:

1) The solute diffusion domain could affect the selection of forms of diffusion equations between 2D (*e.g.*, the protein diffusion in cell membrane) and 3D (*e.g.,* the molecular diffusion in the intracellular matrix).

2) The bleaching geometries (*e.g.*, circular spot with Gaussian or uniform intensity profile, lines, [83] stripes, and elliptical spot [84]) could bring in the different initial and boundary conditions to the diffusion equations.
3) The diffusion in the samples with few structures, such as the grey matter in the brain, could be considered as isotropic diffusion, on the other hand, the complex and organized structures in the samples (*e.g.*, intervertebral disc with well-organized fiber structure) will results in the anisotropic solute diffusion.[85]
4) The instrumentation setup also could affect the FRAP data analyses. The different mathematical analysis methods have been reported because of the development of the hardware of microscopes ranging from the traditional fluorescent microscope to the confocal [86] and multiphoton [12] scanning laser microscope.

The approaches for solving diffusion equations in FRAP analysis are generally divided into two categories: the first approach is the classic Axelrod method which will be reviewed in this section, and the second approach based on Fourier transform will be introduced in the section 3.2. FRAP techniques for 3D diffusion measurements will be continually discussed in the chapter 6.

3.1.2 The Conventional FRAP Analysis

From late the 1970s through the mid-1980s, the basic and conventional FRAP analysis was well established by researchers.[13, 87-92] The first systemic FRAP technique paper was published by Axelrod *et al.* in Dr. Webb's lab at Cornell University in 1976.[13] They used a conventional fluorescent non-scanning microscope with a stationary laser beam and large cone of out-of-focus light bleaching the molecules above

and below the focal plane so that the fluorescence recovery could be assumed as a pure 2D diffusion in an infinite plane. They also assumed there is no diffusion in or out of the bleached area during bleaching. The shape of bleached spot was a circle and both Gaussian and uniform fluorescence bleaching intensity profiles were considered in their work. The axial symmetric diffusive transport is governed by Fick's second law in 2D, the partial differential equation becomes:

$$\partial C(r,t)/\partial t = D\nabla^2 C(r,t) \tag{3.1}$$

where r is the spatial coordinate of the imaging system, t is the time, and D is the diffusion coefficient. The fluorescence recovery with Gaussian bleaching profile can be described by the fractional fluorescence recovery curve f(*t*) :

$$f(t) = \sum_{n=0}^{n=\infty} \frac{-\kappa^n}{n!} \cdot \frac{1}{1+n\left[1+\left(\frac{2t}{\tau_D}\right)\right]} \tag{3.2}$$

$$\tau_D = \frac{\omega^2}{4D} \tag{3.3}$$

where κ is the bleach constant, τ_D is the characteristic diffusion time that is related to the diffusion coefficient in equation (3.3), ω is defined as half the width of the Gaussian intensity profile of the laser spot determined at e^{-2} times the height of the profile. The mobile fraction, M_f, is defined by equation (3.4) to characterize the partial fluorescence recovery after photobleaching due to the immobilized molecules.

$$M_f = \frac{F(\infty) - F(0)}{F(-) - F(0)} \tag{3.4}$$

where $F(\infty)$ is the fluorescence intensity of the bleached spot at the equilibrium status, $F(0)$ is the intensity of the bleached spot just after bleaching and $F(-)$ is the intensity before the photobleaching. D and M_f could be determined by curve-fitting the fluorescence recovery data.

3.1.3 The Improvements to FRAP Technique

In Axelrod's original theory of "spot" FRAP, the membrane was assumed to be approximated by an infinite 2D plane. A number of studies have extended the applicability of FRAP measurements by treating specific geometric corrections to this planar geometry and the assumption of infinite source.

Koppel, for example, proposed a new multipoint FRAP analysis.[93] The fluorescence recovery was monitored by a focused laser beam sequentially positioned at each of several locations in and adjacent to the bleached area. The additional spatial information thus obtained provided a sensitivity to systematic flow and a direct mean of distance calibration.

- ***The development of curve-fitting model***

Yguerabide *et al.*[90] developed a method for precise analysis of FRAP data based on the Gaussian bleaching profile and zero membrane flow. This method used a linear fit to reciprocal function $R(t) = F(\infty)/[F(\infty) - F(t)]$ to calculate the recovery time constant $\tau_{1/2}$ and also detect flow or multiple diffusion coefficients. Von Zoelen et al. [92] continued Yguerabide's study to report a linearization procedure that permits unequivocal determination of all diffusion parameters and the validation was done by simulating recovery curves and other conditions on a regular mini-computer.

Soumpasis[91] derived an exact closed formula for the fluorescence recovery curve measured in FRAP experiments employing uniform circular laser beams. This new expression was simple and free of mathematical drawbacks, thus facilitating the quantitative analysis of FRAP data. Lopez *et al.*[94] developed a numerical method based on the scheme of finite differentiate in combination with statistical analysis of the data to calculate diffusion coefficients, which can be used for any conditions of illumination, beam profile, and relative dimensions of bleached and diffusion areas.

- ***Lateral diffusion on the curved biological surfaces***

Wolf *et al.* [95] studied the effect of surface microvilli on measurements of lateral diffusion by FRAP and found only slight differences in diffusion in the two regions which are the villated main body and unvillated budding polar body of unfertilized mouse eggs. Ten years after that, Wolf [96] reported another study about the FRAP measurements of isotropic diffusion on cylindrical surface with Gaussian laser beam illumination. A mathematical theory was proposed in this study to describe a general analytical solution which is a function of the ratio of the cylindrical radius (r) to the Gaussian laser beam width ω.(Figure 3.1) Numerical analysis of this solution demonstrated that there are significant deviations when the values of r/ ω vary. Sbalzarini *et al.*[97] presented a computational method for the simulation of isotropic and anisotropic diffusion on curved biological surfaces that have been reconstructed from the endoplasmic reticulum (ER) in live cells. (Figure 3.2) This method could process surfaces of high curvature and complex shape, which are often encountered in biology.

The simulation results indicated that the specific shape of the membrane affects the molecular diffusion properties.

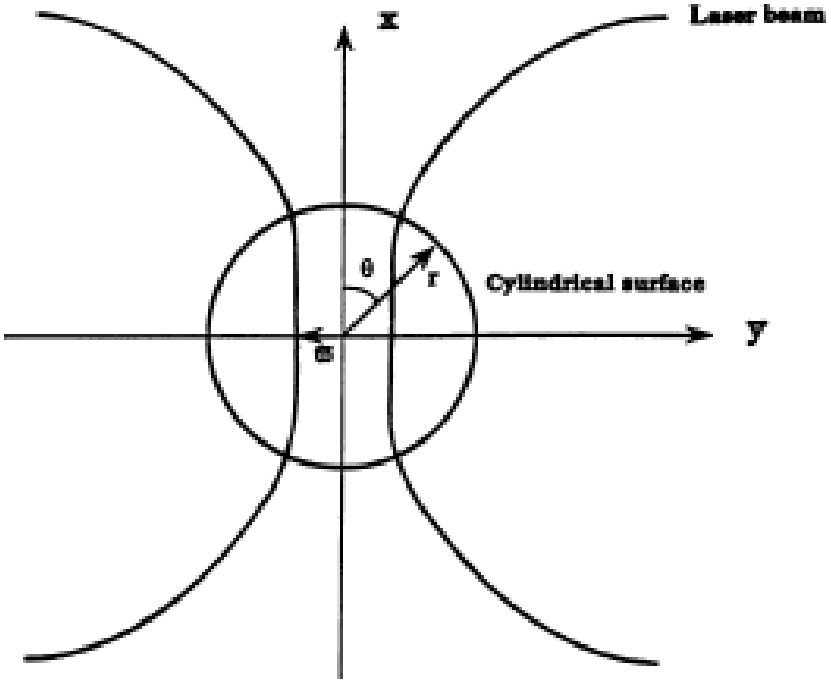

Figure 3.1 Schematic diagram of laser beam and cell.
It shows, in cross section in the x-y plane, bleaching of a cylindrical surface of radius r, which lies along the z-axis with a Gaussian Laser beam of e^{-2} radius ω along the x-axis.[96]

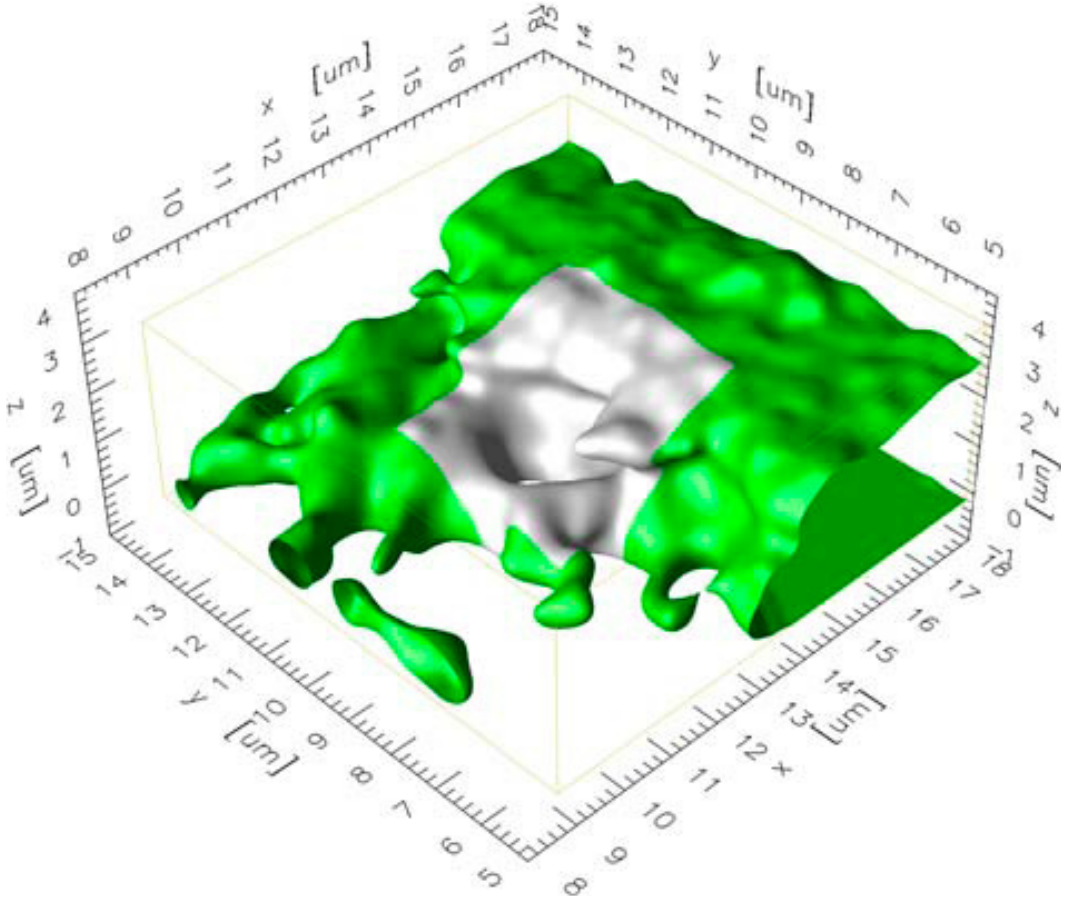

Figure 3.2 Visualization of an endoplasmic reticula (ER) piece with overhanging regions. The visualization is done in the computer from the reconstructed ER membrane surface.[97]

- ***Analysis of nonsimple diffusion by FRAP: Multicomponent and anomalous diffusion***

Solute diffusion is described as “normal” or “simple” in a homogeneous medium. Periasamy and Verkman [98] described the nonsimple diffusion which was usually found in many environments and situations as anomalous diffusion and diffusion of two or more diffusing species.

The possibility of two distinct diffusing components was considered in Gordon et al.’s study. They developed the approach of fitting FRAP curves by the full series solution using a Marquardt algorithm. Their method was validated by simulation program and experiments on artificial liposomes and fibroblast membranes. They showed the feasibility to analyzing one-component diffusion and extracting two-component diffusional parameters from biological membranes.

In anomalous diffusion system, the diffusion coefficient is not constant, but is time and/or space-dependent. This kind of diffusion has been observed for a variety of lipids and proteins in the plasma membranes of a variety of cells. Saxton used a Monte Carlo simulation to study the anomalous diffusion caused by the presence of moderate concentrations of obstacles.[99] He also investigated the FRAP experiments with anomalous diffusion and recommended the simplest approximate treatment of anomalous diffusion usually gave favorable results.[100]

Periasamy and Verkman [98] included the analyses of both multi-diffusing component and anomalous diffusion in their study. They introduced the idea that FRAP data can be resolved in terms of a continuous distribution of diffusion coefficients $\alpha(D)$

and also proposed an independent method to analyze FRAP data for anomalous diffusive processes in terms of time-dependent diffusion coefficients *D(t).* Their results indicated that determination of α(D) and *D(t*) from photobleaching data provides a systematic approach to identify and quantify simple and anomalous diffusive phenomena.

- ***Fluorescence imaging of continuous point photobleaching (FICOPP)***

In order to determine the anisotropic solute diffusivity in avascular cartilaginous tissues, Leddy *et al.* [85] presented a novel fluorescence imaging of continuous point photobleaching technique with a theoretical model and experimental protocol. Significant anisotropy was observed in highly ordered cartilaginous tissues such as ligament tissue (Figure 3.3) and they found higher rates of diffusion are along the primary orientation of collagen fibers. The absolute value of diffusivity was not reported in this study, thus the mathematical theory may need to be further developed to determine the components of anisotropic diffusion tensor.

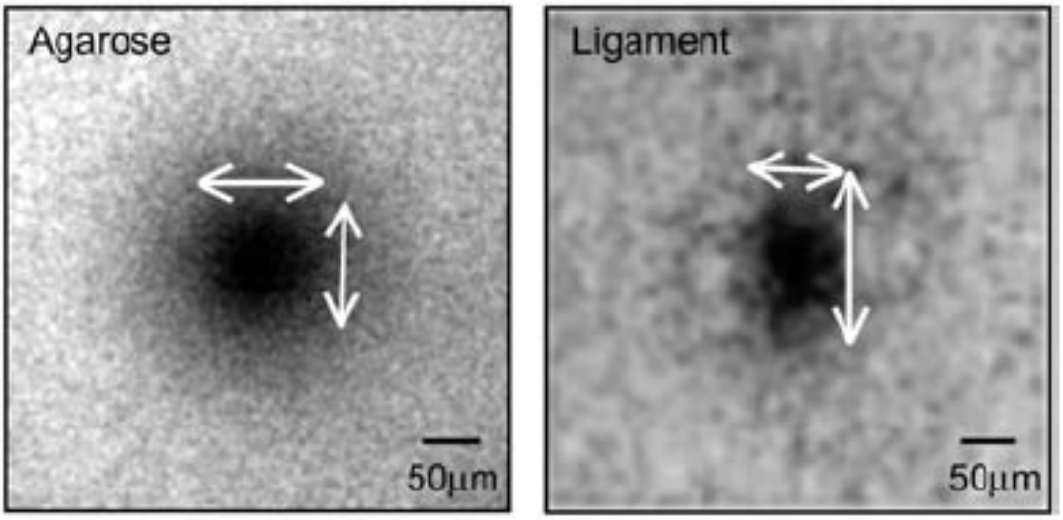

Figure 3.3 Images of photobleaching spots from agarose and ligament after 170 s of bleaching.
Fiber direction in ligament is vertical. The point photobleaching image of agarose shows the isotropic diffusion (left picture) and anisotropic diffusion (right picture) is found in the bleaching image of ligament.[85]

3.2 2D FRAP Techniques with Spatial Fourier Analysis (SFA)

FRAP is a widely used technique for measuring surface diffusion of solutes in biological membranes. The most common setup of FRAP instrumentation, so-called "spot" FRAP, makes use of the Gaussian laser beam. In his original development of the theory of "spot" FRAP, Axelrod assumed that the membrane could be approximated by an infinite two-dimensional plane. Diffusion equations were solved spatially with some strict boundary and initial conditions. Based on the solutions in spatial domain, the fluorescent intensity recovery curves were used to calculate the half time which was related to the diffusivity. Another approach based on Fourier transforms will also be reviewed in this section, since it is becoming increasingly important in FRAP analysis and is less stringent concerning the experimental conditions. This method can determine the anisotropic solute diffusion and has potential to be developed as 3D FRAP technique. (Chapter 6)

3.2.1 Periodic Pattern Photobleaching

SFA-based FRAP analysis was first proposed by Smith *et al.* [101] in 1979, but one year before that, they published another paper [62] about periodic pattern photobleaching, which probably initiated the idea of using Fourier transform in FRAP analysis.

The periodic pattern photobleaching was generated by directing a laser beam through a Ronchi ruling into the microscope. (Figure 3.4) The initial conditions after photobleaching are:

$$C(x,0) = A + B\sin ax + E\sin 3ax + F\sin 5ax + \cdots \tag{3.5}$$

The parameters A, B, E …etc. are determined by the concentration of the probe prior to the bleaching burst of light, the duration and intensity of the bleaching burst, and the contrast and resolution of the stripe image in the sample. The parameter a is the spatial frequency of the pattern and is equal to 2π/P in which P is the period of the pattern. They simplified the diffusion in 1D and solved the diffusion equation spatially.

$$C(x,t) = A + Be^{-Da^2t}\sin ax + Ee^{-9Da^2t}\sin 3ax + Fe^{-25Da^2t}\sin 5ax \tag{3.6}$$

The diffusion coefficient D can be then be calculated from the measured time constant of the amplitude of the pattern decays,

$$D = 1/a^2\tau\,. \tag{3.7}$$

They used this method to successfully measure the lateral diffusion of a fluorescent phospholipid probe in oriented multibilayers of dimyristoylphosphatidylcholine as well as the motion of fluorescent antibodies to murine EL-4 tumor cells.[62]

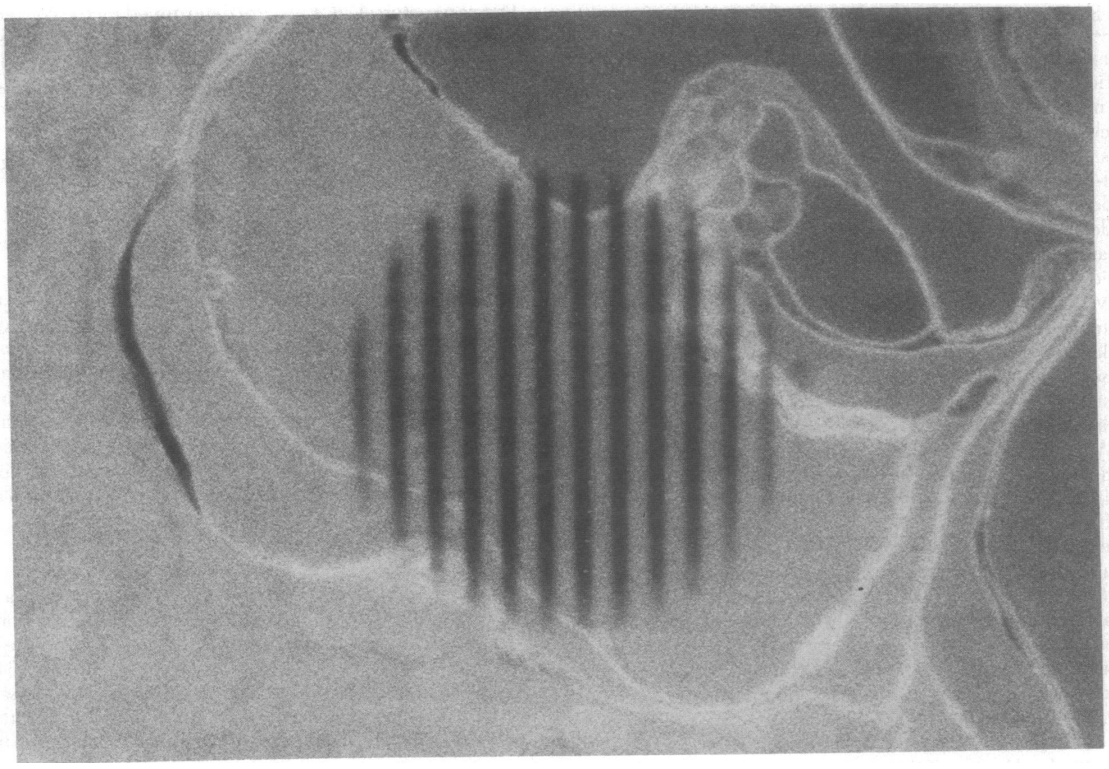

Figure 3.4 FRAP image with periodic pattern photobleaching generated by a laser beam through a Ronchi ruling into the microscope. The period of the striped pattern was 13μm.[62]

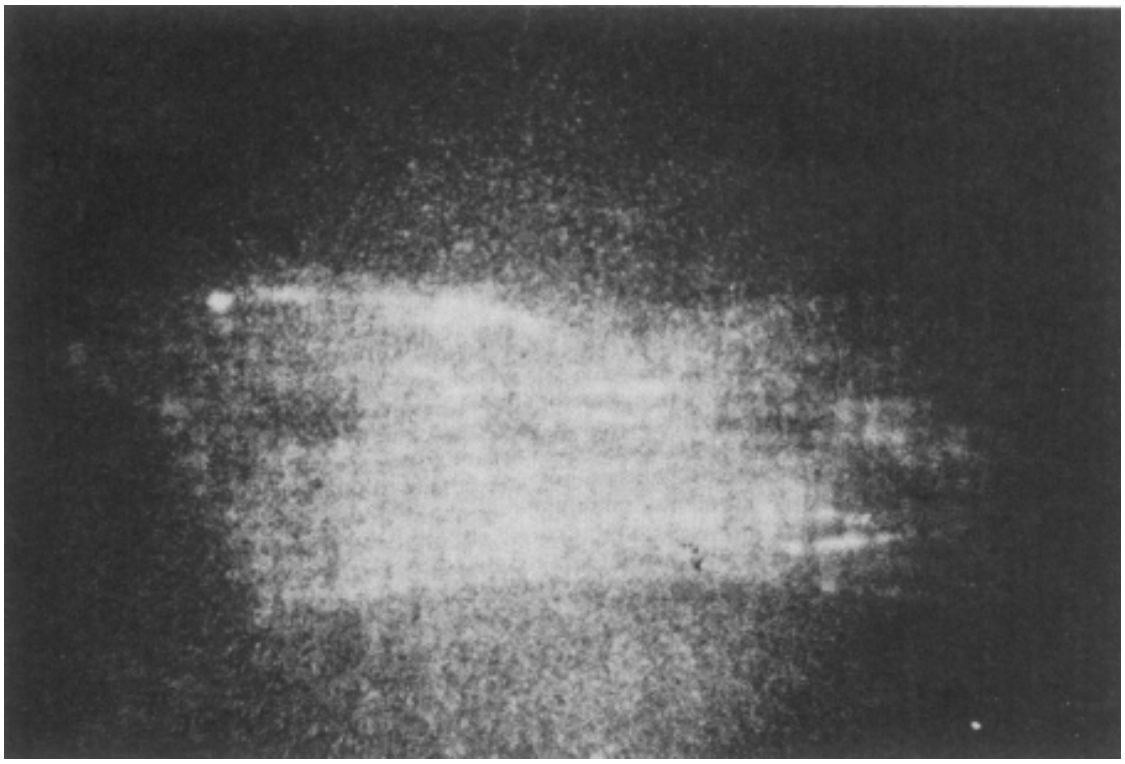

Figure 3.5 FRAP image taken 7 seconds after the 2D pattern of squares was bleached onto the cell surfaces.[101]

3.2.2 The Fundamental Studies of FRAP Analysis with SFA

Smith *et al.* first developed FRAP technique to determine the anisotropic diffusion using a 2D Fourier analysis in 1979.[101] Tsay and Jacobson further completed the systematic study of this FRAP technique.[15, 63] Jain's group [16] compared the SFA-based FRAP with the conventional FRAP analysis and demonstrated the advantage of the SFA for obtaining an accurate measure of the local diffusion coefficient in microscopic samples that are thick and scatter light. They also detected the simultaneous convection and anisotropic diffusion. Based on their outstanding studies, the foundation of FRAP analysis with SFA has been established in the early 1990s.

Smith *et al.* [101] extended the photobleaching to the 2D periodic pattern according to their previous study.[62] Instead of using the parallel stripes in only one direction, they started to setup the bleaching stripes in two perpendicular directions with square symmetry.(Figure 3.5) Fourier image analysis is an easy way to extract diffusivity from the FRAP data because of the simplicity of the solution to the transformed diffusion equation and the manner in which the periodic pattern is reflected as frequency in the Fourier transform. Diffusional anisotropic transport is described by Fick's second law; in two dimensions, the partial differential equation becomes:

$$\frac{\partial}{\partial t}C(x,y,t) = \nabla \bullet \{\mathbf{D}[\nabla C(x,y,t)]\} \tag{3.8}$$

Equation (3.8) could be rewritten as component form:

$$\frac{\partial}{\partial t}C(x,y,t) = D_{xx}\frac{\partial^2 C(x,y,t)}{\partial x^2} + 2D_{xy}\frac{\partial^2 C(x,y,t)}{\partial x \partial y} + D_{yy}\frac{\partial^2 C(x,y,t)}{\partial y^2} \tag{3.9}$$

Fourier transform is performed on (3.9) to obtain the diffusion equation in frequency domain as:

$$\frac{\partial}{\partial t}\widetilde{C}(u,v,t) = -4\pi^2(u^2 D_{xx} + 2uvD_{xy} + v^2 D_{yy})\widetilde{C}(u,v,t) \tag{3.10}$$

where u,v are the coordinates and $\widetilde{C}(u,v,t)$ is the solute concentration function in the frequency domain. Equation (3.10) has a simple solution which is:

$$\frac{\widetilde{C}(u,v,t)}{\widetilde{C}(u,v,0)} = e^{-4\pi^2(u^2 D_{xx}+2uvD_{xy}+v^2 D_{yy})t} \tag{3.11}$$

let $D(u,v) = \dfrac{u^2 D_{xx} + 2uvD_{xy} + v^2 D_{yy}}{u^2 + v^2}$, which could be considered as the diffusivity in frequency domain, equation (3.11) can be rewritten as:

$$\frac{\widetilde{C}(u,v,t)}{\widetilde{C}(u,v,0)} = e^{-4\pi^2(u^2+v^2)D(u,v)t} \tag{3.12}$$

The diffusivities in the different orientations could be calculated by curve-fitting Fourier amplitude decay data with equation (3.12) in the specific u,v frequency. Smith *et al.* found the anisotropy ratio of the diffusivities ranged from a factor of 2 to nearly a factor of 10 on the surface of fibroblast due to the stress fibers. The diffusion along the stress fiber orientation was faster than the diffusion perpendicularly to the fiber orientation.

Tsay and Jacobson [63] further developed the SFA-based FRAP analysis and examined the effects of different parameters (*e.g.*, size of bleaching spot, timing of the recovery process, and image noise) in this method. They concluded that this method does not require a specific initial condition (*e.g.*, the shape of bleaching pattern) created by

laser photobleaching. The feasibility of Fourier analysis to obtain the diffusion coefficient from a video FRAP measurement was fully demonstrated by using computer-simulated and experimental data. They also pointed out the high signal to noise ratio (SNR) is essential for successful FRAP analysis.

3.2.3 The Recent Improvements of FRAP Techniques with SFA

Wirth [102] evaluated Fourier transform as a means of improving precision in the analysis of FRAP data by using simulated experiments.

Travascio and Gu [6, 14, 17, 103] made many contributions to the improvement of FRAP method with SFA. They mainly applied FRAP technique to detect the anisotropic diffusive transport in annulus fibrosus (AF) with well-organized fiber structures. Several mathematical methods have been adopted in their studies to determine the full components of the diffusion tensor.

First of all, they used the integral of multiple diffusivities in the frequency domain to the mean diffusivity which was related to the trace of the diffusion tensor. [14]

$$\pi^{-1}\int_0^{\pi} D(\xi)d\xi = D_{av} = \frac{D_{xx}+D_{yy}}{2} \tag{3.13}$$

In equation (3.13), the angle ξ is defined by the wave vector specified by u and v, $D(\xi)$ is the diffusivity in each u,v frequency, and D_{av} is the mean diffusivity. From three independent FRAP tests performed in the three orthogonal planes of the samples, they extracted the three principal components of the 3D anisotropic solute diffusion tensor in AF tissues. The diffusion properties were correlated to the anisotropic fiber structure of AF tissue. (Figure 3.6) The components of the diffusion tensor only can be acquired

when testing one sample in three planes using this method, which will increase the amount of work.

Next, they added one more integral of the diffusivities in frequency domain (3.14) and combined SFA with Karhunnen-Loeve transform (KLT) which could detect the orientation of the diffusion tensor to completely determine the 2D anisotropic diffusion tensor. [17]

$$D_{av}^{+} = \left(\frac{\pi}{2}\right)^{-1} \int_{0}^{\frac{\pi}{2}} D(\xi) d\xi = \frac{D_{xx} + D_{yy}}{2} + \frac{2D_{xy}}{\pi} \tag{3.14}$$

Using numerically simulated FRAP images, the accuracy of this method was investigated for different sizes of bleached spots and for different "frequency rings". The effect of noise level on the data analysis was also investigated. The method was also validated using real FRAP experiments on bovine AF as well as meniscus and human AF tissues.[6] The major limitation of this method is the lack of robustness to deal with the imaging noise which is unavoidable in real experiments.

Furthermore, Travascio and Gu [103] considered the effects of both diffusion and binding on the mobility of solutes in biological tissues. The solution of the diffusion-reaction equations was obtained in the Fourier space and the components of the diffusion tensor (i.e., D_{xx}, D_{yy}, and D_{xy}) were calculated by curve-fitting the experimental values of $D(\xi)$ with the equation (3.15). In contrast, this new method was solely based on Fourier analysis avoiding the limitations imposed by the use of KLT in FRAP experiments.

$$D(\xi) = D_{xx}\cos^2\xi + 2D_{xy}\cos\xi\sin\xi + D_{yy}\sin^2\xi \tag{3.15}$$

Based on Travascio's studies, Shi and Yao [7] proposed the third integral (3.16) of the diffusivities in frequency domain and utilized three integrals to fully calculate all the components of 2D diffusion tensor.

$$D_{0,\frac{\pi}{4}} = \left(\frac{\pi}{4}\right)^{-1}\int_0^{\frac{\pi}{4}} D(\xi)d\xi = \frac{D_{xx}+D_{yy}}{2} + \frac{D_{xx}-D_{yy}}{\pi} + \frac{2D_{xy}}{\pi} \tag{3.16}$$

The accuracy and robustness of this method was validated by using computer-simulated FRAP experiments. The new method was applied to determine the 2D diffusion tensor of 4kDa FITC-dextran in the TMJ discs. It was determined that the diffusion of this solute in TMJ discs was inhomogeneous and anisotropic. This method was also solely based on the SFA to completely determine the anisotropic diffusion tensor.

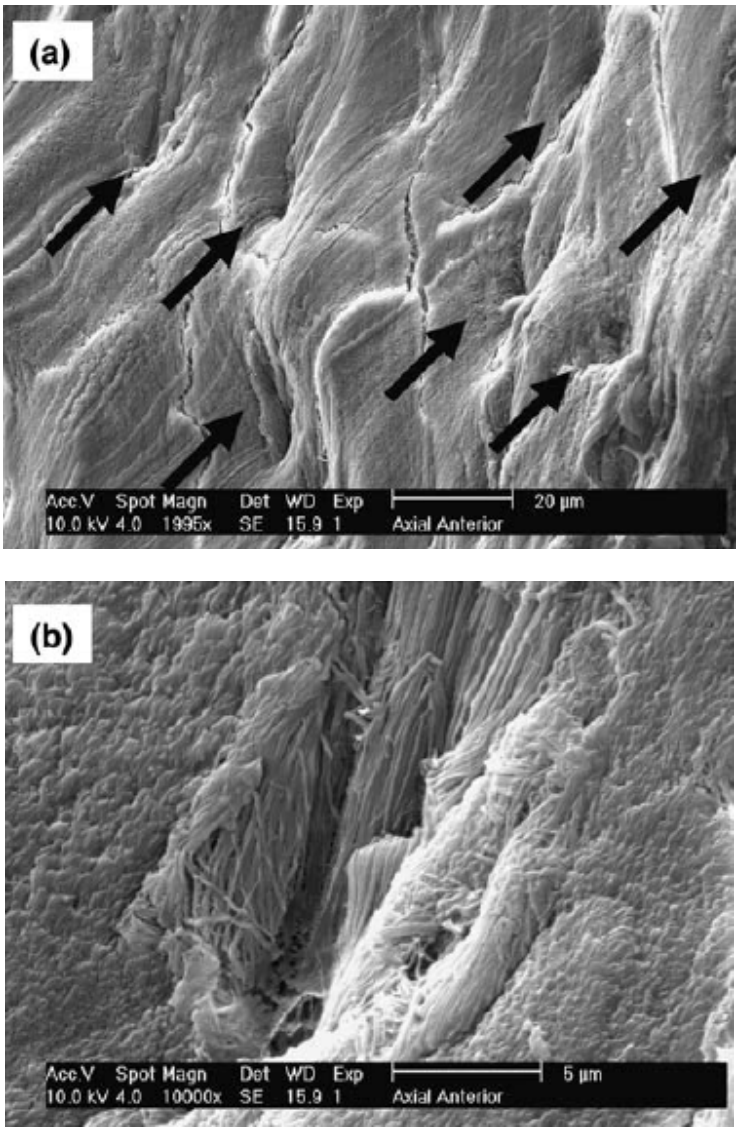

Figure 3.6 Scanning electron microscopy images of anterior axial section of AF.

(a) Microtubules are shown; (b) Magnification of a microtubule in picture (a).[14]

3.3 Applications of FRAP in Biological Research

FRAP has received increasing attention ever since it was first introduced into cell biological research. The method was developed in the 1970s, when its biological application mainly focused on the mobility of fluorescently labeled constituents in the cell membranes. The development of confocal or multiphoton laser scanning microscopy extended accurate investigation of the behavior of molecules in the inside of cells, (*e.g.*, intracellular space and nucleus) moreover, researchers also applied it to diffusion measurements of extracellular matrix at a larger scale level, such as the solute diffusion in the human brain or tumor tissues and nutrient solutes diffusion through the ECM of cartilaginous tissues. Figure 3.7 shows the statistics of FRAP applications in the different biological research areas according to 145 FRAP related scientific articles. In this section, the diverse applications of FRAP in different areas will be summarized to further understand the meaning of FRAP techniques.

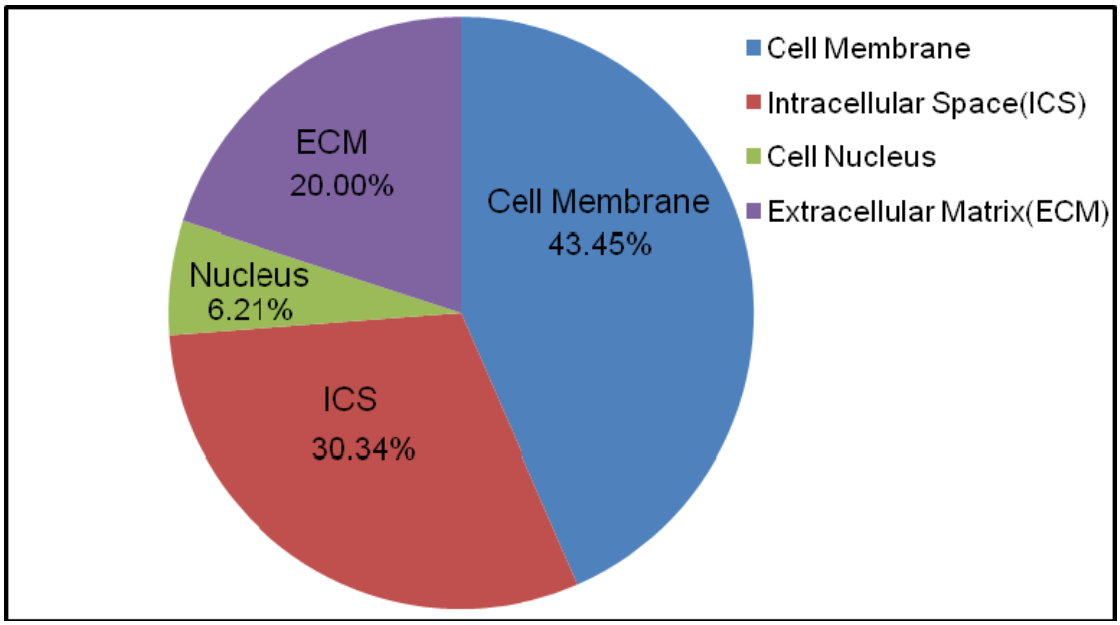

Figure 3.7 The statistics of FRAP applications in the different biological research areas.

3.3.1 Lateral Diffusion of Solutes in Cell Membranes

- ***Protein diffusion in real cell membranes***

The most common application of FRAP study is in the cell membranes. Jacobson *et al.* [87] monitored the lateral mobility of plant lectin-receptor complexes on the surface of human embryo fibroblasts and found over 75% of those complexes are mobile and with a diffusion coefficient in the range of 2×10^{-3} to 2×10^{-2} $\mu m^2/s$. They [104] also used FRAP technique to measure the lateral mobility of Concanavalin A (Con A) in the different types of cell surfaces. They reported a considerable fraction of the Con A molecules bound to the cell surface that were immobilized, with a lower diffusivity when compared to the plant lectin-receptor complexes.[87] Schlessinger *et al.* [105] presented a major cell surface glycoprotein (CSP) bindings to the cell surface in a fibrillar pattern and is immobile. They concluded that immobile fibrils of CSP on a cell's surface are suitable for binding it to the substratum and to other cells; however, they do not impede the lateral diffusion of various kinds of membrane components. (*e.g.,* lipid probe and surface antigen) The lateral mobility of band 3 which is a transport protein in the human erythrocyte membrane was studied by Golan and Veatch.[106] They demonstrated the strong but distinct dependencies of band 3 diffusion coefficient and fractional recovery on ionic strength and temperature. Sheetz *et al.* [107] reported the glycoprotein diffusivity increased about 50 times in mouse spherocytic erythrocytes probably due to the lack of the major components which could be found in the normal erythrocyte membrane matrix.

- ***Solute diffusion in artificial phospholipid multibilayers***

Besides the diffusion studies on the real cell membranes, many researchers have been working on the determination of diffusion properties in artificial phospholipid multibilayers [108-113] which could be a suitable model of the cell membrane. Wu *et al.* [114] applied FRAP technique to detect the diffusion rates of two fluorescent lipid analogues (*i.e.,* NBD-PE and diO-C_{18}(3)) in phospholipid multibilayers. They found cholesterol reduced diffusivity for NBD-PE in these multibilayers by a factor of 2 as well as abolished the gel-to-liquid-crystalline transition temperature. Gaub *et al.* [110] reported the lateral diffusion coefficient in butadiene-lipid bilayers decreased by a factor of 4 upon polymerization. FRAP was used with planar lipid bilayers as a model membrane system to examine how nisin might interact with the surface of bacterial cells by Giffard *et al.* [115] and they demonstrated nisin associates with planar lipid bilayers inhibited the lateral diffusion of lipid probe and reduced the capacitance of the bilayer. Guo *et al.* [116] considered that molecular diffusion in biological membranes is a determining factor in cell signaling and cell function. They compared the different fluorescence spectroscopy techniques and concluded the FRAP can determine absolute diffusion coefficients in lipid bilayers at high concentrations.

3.3.2 Studying Protein Dynamics in Living Cells

- ***Molecular diffusion in the intracellular space***

The two-dimensional movement of proteins in biological membranes has been demonstrated to be a central feature of many membrane-mediated events. However, the application of FRAP to the study of intracellular membrane proteins has been hampered

by the lack of specific probes and their physical inaccessibility in the cytoplasm.[117] In the 1980s, Hochman *et al.* [118] began to use FRAP to measure the lateral mobility of cytochrome c on the membrane of giant mitochondria and reported a diffusion coefficient of 1.6×10^{-2} $\mu m^2/s$. Rhodamine-labeled actin (rh-actin) were microinjected in living embryonic chicken gizzard cells and associated with its characteristic cytoskeletal structures by Kreis *et al*.[119] They found the diffusion properties of rh-actin exhibited a region-dependency. Salmon *et al.* [120] measured the diffusion rate of fluorescein-labeled tubulin in the cytoplasm of embryonic cells of a sea urchin using FRAP method. The results of their studies indicated that the viscosity of sea urchin cytoplasm for protein is about eight times that of water and most of the tubulin of the sea urchin cytoplasm exists as a dimer or small oligomer, which is mobile and unbound to structures.

In late 1990s and early 2000s, the popularity of FRAP technique in living cells increased when non-invasive fluorescent tagging became possible with the green fluorescent protein (GFP) and confocal laser scanning microscope which was commercially developed. There are several excellent review papers presenting the applications and future directions of diffusion studies by FRAP.[3, 59, 64, 121, 122] Storrie *et al.* [117] described a FRAP analysis of the intracellular mobility of organellar proteins using confocal microscopy. They showed that, in contrast to the plasma membrane, the temperature-sensitive vesicular stomatitis viral membrane glycoprotein (ts-O45-G) is highly mobile in intracellular membranes. Seksek *et al.* [123] used FRAP to quantify the translational diffusion of microinjected FITC-dextran in the cytoplasm of MDCK epithelial cells and Swiss 3T3 fibroblasts. They mentioned their results of the

independence of diffusivities on FITC-dextran size (4-2000kDa) did not support the concept of solute “sieving” (size-dependent diffusion) in cytoplasm. MP-FRAP technique was adopted to map the diffusion rate of the small heat shock protein sHSP27 throughout the cytoplasm.[124] Figure 3.8 shows at least two diffusive transport rates within a living cell potentially corresponding to the large and small oligomers of sHSP27.

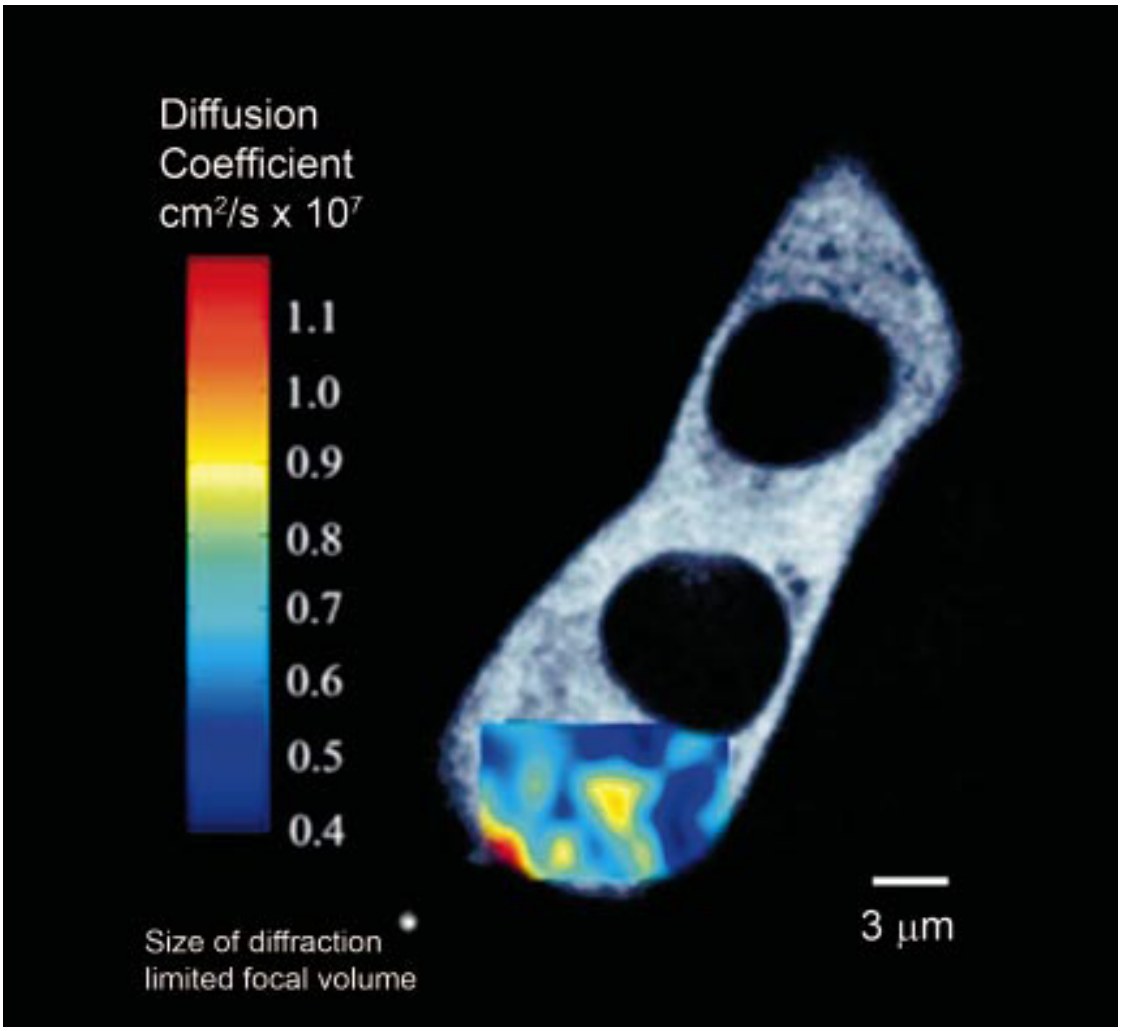

Figure 3.8 Intracellular diffusion map of EGFP-sHsp27 in an L929 cell.
A grid sampling protocol (right inset) was used to generate a diffusion map. The map reveals localizations of fast and slow rates of transport. Independent MP-FRAP measurements were used to generate the map.[124]

- ***Translational diffusion of solutes in the cell nucleus***

The measurements of solute diffusion in the cell nucleus by FRAP methods are relatively difficult because they only take place in very tiny regions.[60] Therefore, people started to investigate the protein mobility in the suspension of nuclei. Nandi and Wahl [125] incubated fluorescent-labeled clathrin with isolated mouse liver nuclei and measured the mobility of clathrin solutes by FRAP. They found that 78% clathrin was immobilized on the nuclear surface and concluded that this immobile fraction might correspond to aggregates of molecules. Phair and Misteli [126] published their outstanding study about the mobility properties of protein in the nucleus of living mammalian cells using photobleaching techniques.(Figure 3.9) They found that proteins involved in diverse nuclear processes (*e.g.*, transcription and splicing) move rapidly throughout the entire nucleus and rapidly associate and dissociate with nuclear compartments. Their observations have conceptual implications for understanding nuclear architecture and how nuclear processes are organized *in vivo*.

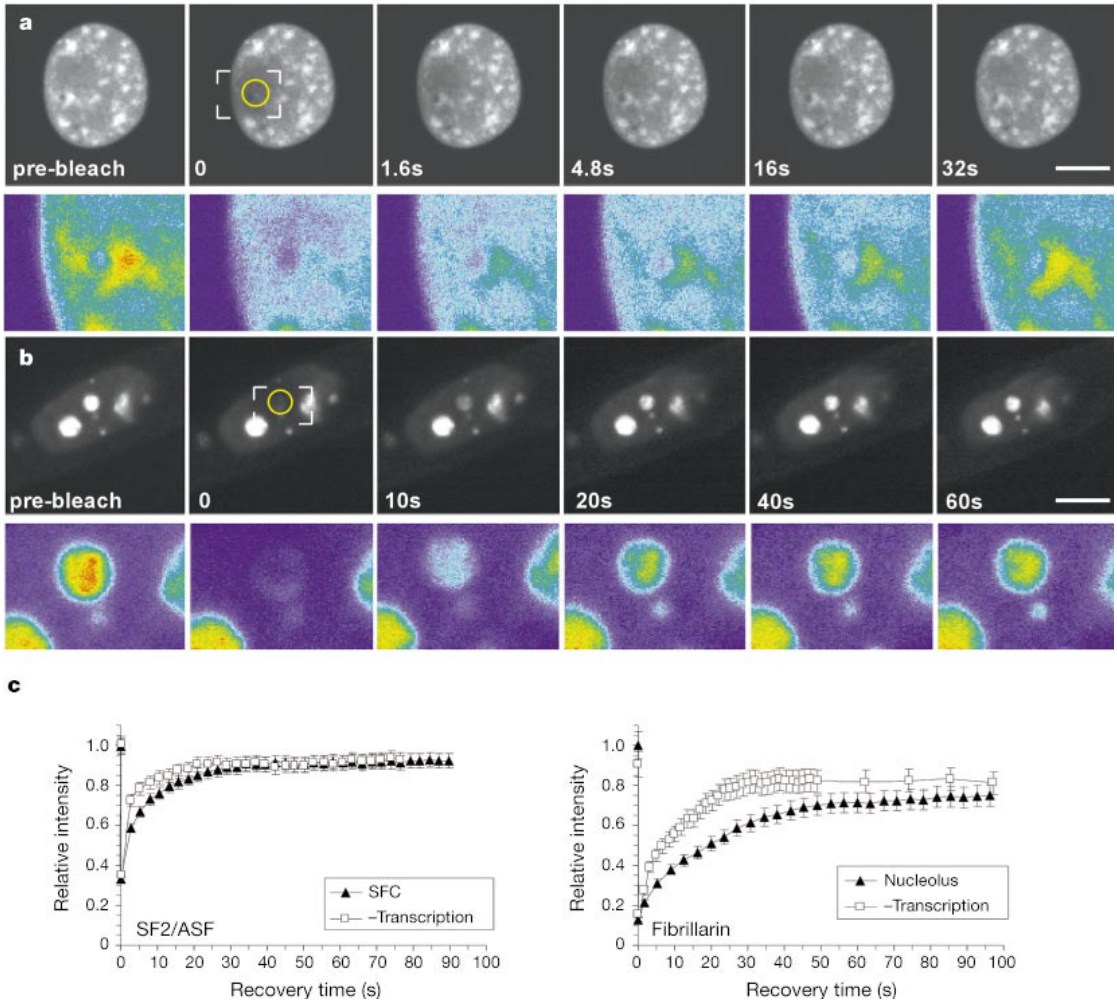

Figure 3.9 FRAP images and curves of nuclear compartments.
Cells expressing GFP-SF2/ASF (a) or GFP-fibrillarin (b) were imaged before and during recovery after bleaching of a splicing factor compartment (a) or an entire nucleolus (b). Reassociation of both proteins with their respective nuclear compartments was rapid. Scale bar, 5µm. (c) Kinetics of recovery after bleaching of nuclear compartments. Recovery of GFP-SF2/ASF was complete after 32 s, recovery of GFP-fibrillarin reached a plateau after 60 s. Inhibition of transcription by either α-amanitin or actinomycin D accelerated the reassociation of GFP-SF2/ASF as well as reassociation of GFP-fibrillarin.[126]

3.3.3 Diffusion in the ECM

- ***Diffusive transport in the brain extracellular space***

Nicholson and Tao [1, 32, 65, 66, 127, 128] developed an integrative optical imaging (IOI) system which is a variant of FRAP technique to analyze the diffusion of the fluorescent solutes in brain extracellular microenvironment. This technique has been introduced in section 2.3.4 and is designed for the *in vivo* diffusion measurement. They used a micropipette to inject the fluorescent dye in the hydrogel or the mouse brain and observed the spread of the fluorescent dye at the different time points, and then analyzed the concentration profile to calculate the diffusivity. They found that the brain extracellular space may have local constrictions that hinder the diffusion of molecules above a critical size that lies in the range of many neurotrophic compounds.[65] They also concluded diffusion is essential to many therapies that deliver drugs to the brain and the diffusion-generated concentration distributions of well-chosen molecules also reveal the structure of brain tissue. This structure is represented by the volume fraction (void space) and the tortuosity (hindrance to diffusion imposed by local boundaries or local viscosity). Analysis of these parameters also reveals how the local geometry of the brain changes with time or under pathological conditions.[1]

- ***Measurement of macromolecular diffusion coefficients in the tumors***

FRAP technique was used by Jain's group to detect the immobilization of fluorescently labeled ligand caused by binding to receptors in xenograft tumor tissues.[129] They presented that not only is receptor density likely to vary depending on the microenvironment, but the presentation and accessibility of receptors may also be

modulated by effects on cell metabolism or by indirect effects of the extracellular matrix. Their *in vivo* method revealed binding parameters relevant to tissue function such as the accessible receptor concentration, effective binding affinity, and the interstitial diffusion rate, and may be particularly useful for studies of physiology or drug delivery. The diffusive transport of macromolecules in tumors is an important determinant of the delivery of many anticancer therapeutics. Brown *et al.* [130] measured the diffusion coefficients of bovine serum albumin (BSA) and immunoglobulin M (IgM) in human tumor biopsies using FRAP. Their results showed the diffusion coefficients of BSA and IgM are higher in human tumor samples than in colon adenocarcinnoma xenografts. These data have important implications for the modeling of the distribution of large therapeutics in human colon adenocarcinoma. For the first time, the quantitative prediction of diffusive transport properties of these macromolecules in human tumors is possible. Stylianopoulos *et al.* [131] considered spatial alignment of matrix components within the tissue can affect diffusion patterns of drugs. They developed a methodology for the determination of diffusion properties of macromolecules and nanoparticles in collagenous tissues. They utilized a mathematical model and simulation experiments to find the overall diffusion coefficient is not affected by the orientation of the fiber network. However, structural anisotropy results in diffusion anisotropy, which becomes more significant with increase in the degree of alignment, the size of the diffusing particle, and the fiber volume fraction. The results of diffusion measurements in tumor xenografts showed for the first time in tumors that the structure and orientation of collagen fibers in the extracellular space leads to diffusion anisotropy.

- ***Applications of FRAP in the cartilage tissues***

Diffusive transport of nutrient solutes is crucial to the normal function of cartilage tissues, while poor nutritional supply is believed to be one of mechanisms for the tissue degeneration. Therefore, many researchers [5, 14, 17, 132, 133] have applied FRAP techniques to measure the diffusivities of various solutes in the cartilage tissues for understanding the pathways of nutritional supply into soft tissues. Leddy and Guilak [5] used FRAP to measure site-specific diffusion coefficients of fluorescent dextran molecules in porcine articular cartilage and found an inverse size dependence of diffusion coefficients. The diffusion rates also varied significantly with depth of tissue, indicating variations in the structure and composition of collagen, proteoglycans, and other macromolecules among the regions. (Figure 3.10) Fetter *et al.* [132] compared the diffusion coefficients of 70 KDa dextran in human ankle and knee cartilage but no differences in diffusivity were observed.

Travascio *et al.* [6, 14, 17, 103] developed a series of novel FRAP techniques to study the anisotropic solute diffusion properties in the intervertebral disc (IVD) tissues. They concluded that, in both anterior and posterior regions of bovine AF, the diffusion coefficient in the radial direction was found to be the lowest, and circumferential and axial diffusion coefficient were not significantly different.[14] Diffusivities in human AF were also inhomogeneous anisotropic, with higher values in the axial direction than in the radial direction.[6] They demonstrated that a relationship exists between anisotropic, inhomogeneous diffusion and the structure and composition of the human AF tissue.

Shi *et al.* [7] studied the solute diffusion in porcine temporomandibular joint (TMJ) disc and found the ratio of the two principal diffusivities ranged between 0.45 and 0.51 (1.0 = isotropic). Their results indicated that the solute diffusion in TMJ discs is inhomogenous and anisotropic. These findings suggested that diffusive transport in the TMJ disc is dependent on tissue composition (*e.g.*, water content) and structure (*e.g.*, collagen fiber orientation).

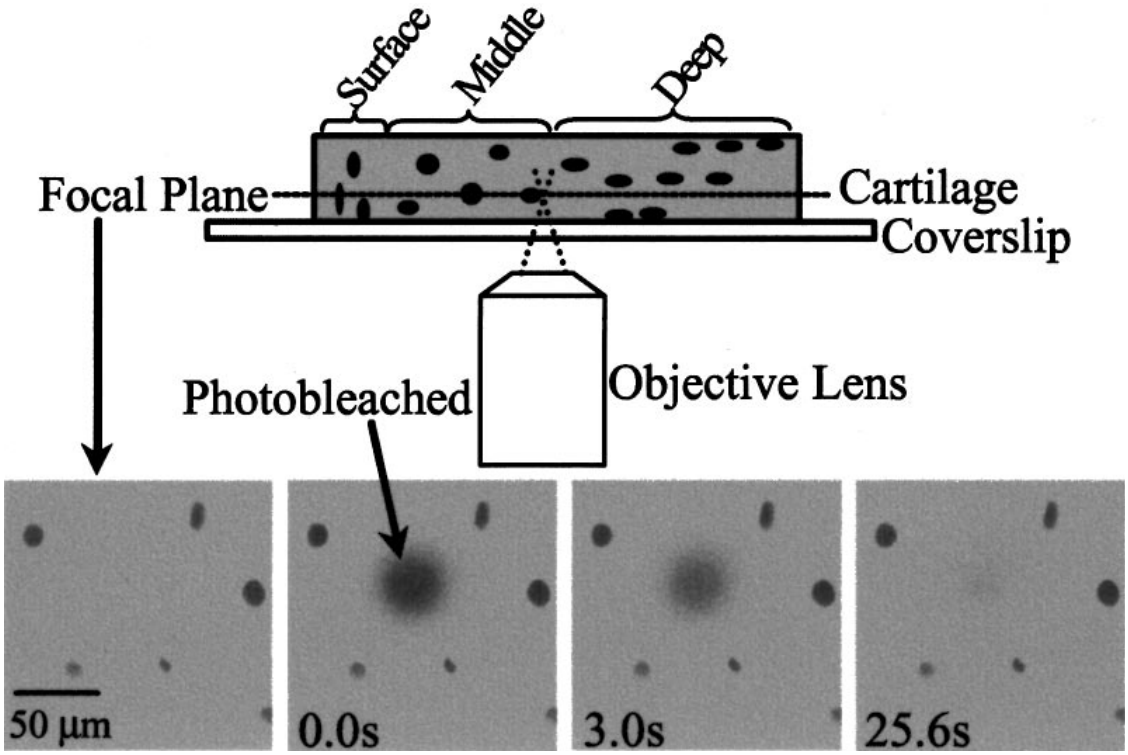

Figure 3.10 The setup for a FRAP experiment in cartilage tissues.
The cartilage specimen is placed on its side such that surface, middle, and deep zones are visible through the microscope. The confocal microscope allows the focal plane to be at a depth in the tissue away from the cut face. The lower panels show the photobleaching and recovery process on a cartilage sample. The smaller dark spots are viable chondrocytes that exclude the fluorescent dye. [5]

3.4 FRAP Techniques for 3D Diffusion Measurements

Most 2D FRAP methods and applications for use with convention fluorescence microscopes have already been reviewed in the previous sections. Since the FRAP applications have been extended from simple and thin cell membranes to the complex intracellular matrix and nuclei as well as the development of confocal and multiphoton laser scanning microscopy, the mathematical models and data analysis of 3D FRAP have become more important in recent years. Several research studies on 3D FRAP analyses will be reviewed in this section.

3.4.1 The Importance of 3D Analysis in FRAP Techniques

In traditional FRAP models, they describe the relation between the diffusion into a 2D bleached region and the fluorescence recovery as observed by the conventional fluorescence microscope. Currently, however, bleaching experiments can be easily implemented on confocal/multiphoton laser scanning microscopes (CLSMs or MP-LSMs) as they are often equipped with the feature to bleach arbitrary regions in the sample. When the bleaching geometry is defined in the software, the microscope scans the laser beam over the sample pixel-by-pixel and line-by-line, while modulating the beam intensity according to the designed pattern. New FRAP analyses are necessary to be studied for new applications and instrumentation setup. The importances of 3D analysis in FRAP techniques are summarized as below:

1) The protein mobility and activity studies have been developed from cell membranes to the intracellular matrix (*e.g.*, cytoplasm and cytoskeleton) and nuclei with complex structures. The common thickness of the cell membrane is about 3~5nm and the

size of bleached spot in FRAP experiments is usually several micrometers, thus the 2D infinite planar model could be satisfied in membrane diffusion studies, however, this is not the case when the solute diffusion takes place in the cytoplasm[123] or nuclei.[134] The 3D diffusion models should be more appropriate to describe the protein dynamics in this situation.

2) Beside the development to the tiny scale, the FRAP techniques also have been utilized to investigate the solute diffusion in the large size tissues, such as the mobility of molecules in interstitial spaces of tumor or brain tissues [130] and extracellular matrix of cartilage tissues.[85] 3D anisotropic diffusion predominates in these kinds of tissue and new mathematical models are needed to be established.

3) The bleaching profile of FRAP experiments performed on the conventional fluorescent microscope with single-photon absorption is shown in Figure 3.11(c,d). The fluorescent molecules are bleached through the whole z-axis, therefore the main fluorescence recovery only happens in x-y plane, which allows to assume a 2D diffusion. In the recent multiphoton-based bleaching experiments, due to the non-linear optical phenomenon, only the fluorophore within the focal spot is bleached and the bleaching profile yields a sharp and well-defined 3D geometry. [Figure 3.11 (a,b)] The diffusion in the z direction has to be considered in this configuration. The confocal microscope also can bring in the different bleaching profile when compared to the traditional fluorescent microscope and the scanning feature requires a new theory for the initial or boundary conditions.

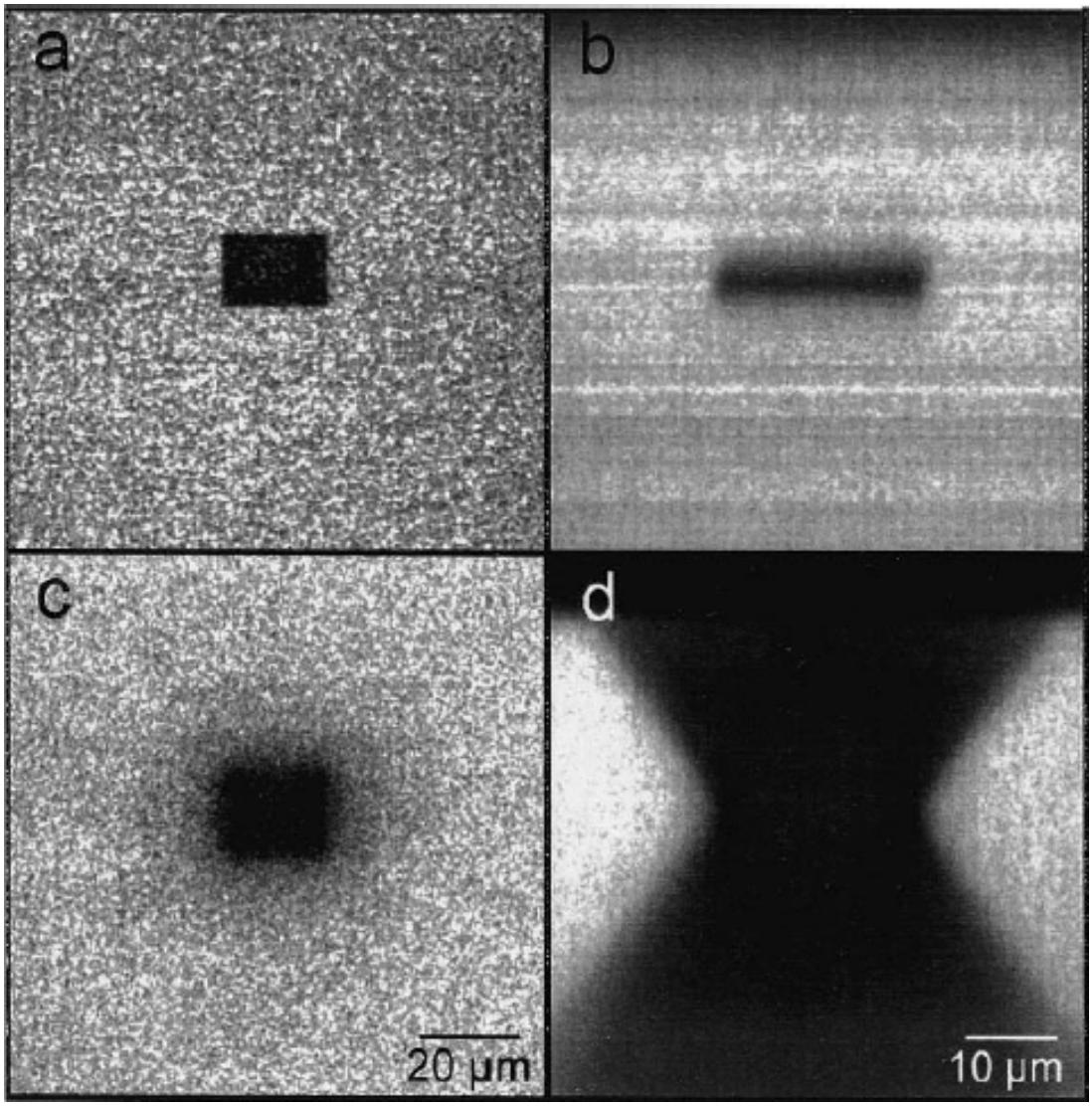

Figure 3.11 Spatial selectivity of two-photon-absorption-induced fluorescence photobleaching.
(a,b) A thick fluorescent gel layer was employed as the specimen. The microscope was focused several micrometers below the upper surface of the gel layer and a rectangular area irradiated at 30mW beam power. The total scanned area was then imaged at a largely reduced, nonbleaching beam power in both x-y plane (a) and the x-z plane (b). It can be recognized that photobleaching yielded an area sharply bounded in both the x-y and x-z planes. (c,d) For comparison the same experiment was performed with single-photon absorption using the 488-nm argon line. In this case a blurred cone is photobleached extending through the whole sample.[135]

3.4.2 3D FRAP using Confocal Laser Scanning Microscopy (CLSM)

The development of CLSMs provided biological researchers with an excellent standard tool to perform FRAP experiments. Currently, most commercially available CLSMs are equipped with acoustic-optic tunable filters (AOTF) that allow bleaching arbitrary regions in the sample. During bleaching, the microscope directs a moving excitation laser beam to the sample. The bleach region is thus scanned point by point and line by line, increasing the incident laser intensity inside the pattern defined. Due to bleaching and monitoring of fluorescence recovery, some assumptions of the models developed for nonscanning microscopes do not hold. To this end, new theories have to be developed for the FRAP technique with CLSMs, and the process must be completed in a totally different way.

A practical 3D model was first devised for use with objective lenses of low numerical aperture (NA) by Blonk *et al.* [11] They denoted the fluorescent concentration at any post-bleaching time *t*, at radial position *r*, and axial location *z*, by $c(r,z,t)$ then the 3D diffusion equation (3.17) in cylindrical coordinate system becomes:

$$\frac{\partial c}{\partial t} = D\left[\frac{1}{r}\frac{\partial}{\partial r}\left(r\frac{\partial}{\partial r}\right)+\frac{\partial^2}{\partial z^2}\right]c(r,z,t). \tag{3.17}$$

The initial condition is:

$$c(r,z,0) = c_0 \exp\left[-\alpha T I(r,z)\right] \tag{3.18}$$

$$I(r,z) = I_0 \exp\left[-2\left(\frac{r^2}{\omega^2}+\frac{z^2}{z_0^2}\right)\right] \tag{3.19}$$

where c_0 is the uniform per-bleaching fluorescent concentration and α denotes the first-order photobleaching rate constant. The laser beam profile $I(r,z)$ is Gaussian in the axial z-direction as well as the radial r-direction and ω and z_0 is the e^{-2} radii of the laser beam in the radial and axial directions respectively. They solved the equation (3.17) and solution is:

$$c(r,z,t) = c_0 z_0 \omega^2 \sum_{n=0}^{\infty} \frac{(-\kappa)^n}{n!} \times \frac{\exp\left[-2nz^2/(z_0^2+8nDt)\right]}{\sqrt{(z_0^2+8nDt)}} \times \frac{\exp\left[-2nr^2/(\omega^2+8nDt)\right]}{\sqrt{(\omega^2+8nDt)}} \quad (3.20)$$

The 3D fluorescence recovery time function based on the concentration function (3.20) was rather complicated, thus Blonk *et al.* had some reasonable assumptions to simplify it, such as z_0 is much greater than ω due to the low NA objective and 3D equation above reduced to their 2D counterparts. A series of line-scanning, x-t image, crossing the bleached spot was recorded for the fluorescence recovery. The diffusion of 45-nm latex spheres, FITC molecules and a 2.45nm protein-FITC complex in water-glycerol mixtures measured by this method was in close agreement with the theoretical values calculated by Stokes-Einstein equation.[11]

- ***Line-FRAP with CLSM***

Blonk *et al.* first mentioned the use of line-scanning model to get the fluorescence recovery images, but the bleached spot was still a circle in their studies. Wedekind *et al.* [83] further developed a FRAP technique, referred to as line-scanning microphotolysis (LINSCAMP) for the measurement of molecular transport at a high spatial and temporal resolution. Both bleaching and recording areas in their study were only a single line.

(Figure 3.12 and Figure 3.13) They derived the 2D mathematical model for line-FRAP data analysis by using equation (3.21) ~ (3.23).

$$\frac{\partial c(x,y,t)}{\partial t} = D\left[\frac{\partial^2}{\partial x^2} + \frac{\partial^2}{\partial y^2}\right]c(x,y,t) \tag{3.21}$$

$$c(x,y,0) = c_0(1 - e^{-\alpha TI(x,y)}) \text{ (Initial condition)} \tag{3.22}$$

$$I(x,y) = \int_{-a/2}^{+a/2} Ae^{-\left[(x-x')^2+y^2\right]/2\sigma_{Na}^2} dx' \text{ (Beam intensity profile)} \tag{3.23}$$

Kubitscheck *et al.* [136] extended the illumination geometry and models to 3D for Line-FRAP technique by using equation (3.24)~(3.26).

$$\frac{\partial c(\vec{\mathbf{X}},t)}{\partial t} = D\frac{\partial^2}{\partial \vec{\mathbf{X}}^2}c(\vec{\mathbf{X}},t) - k(\vec{\mathbf{X}},t)c(\vec{\mathbf{X}},t) \tag{3.24}$$

$$I(r,z) = I_0 \exp\left(-\frac{2r^2}{w_e^2(z)}\right)\exp\left(-\frac{2z^2}{w_{z,e}^2}\right) \tag{3.25}$$

$$w_e^2(z) = w_{0,e}^2\left[1 + \left(\frac{z}{z_{r,e}}\right)^2\right]; z_{r,e} = \frac{\pi w_{0,e}}{\lambda_e} \tag{3.26}$$

In Wedekind and Kubitscheck's studies, they all used numerical integration to simulate the fluorescent concentration distribution with several pre-defined parameters, the simulation results then were combined with microscope point spread function to generate a single time-dependent fluorescence recovery signal. The simulated recovery curve was compared with the experimental data obtained from line-scanning confocal images and the best estimation of parameters was acquired by many iterations and minimizing the function of the experimental and simulated data. (Figure 3.14)

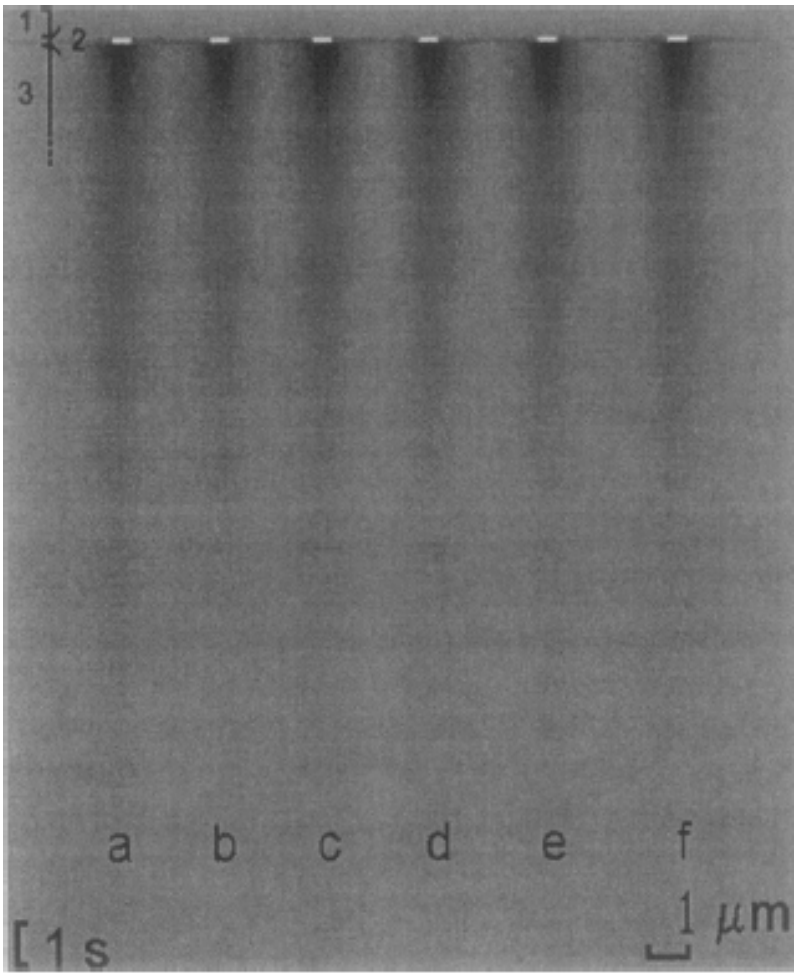

Figure 3.12 Measurements of lateral diffusion by line-scanning FRAP.
Six segments of 0.55µm length were chosen along a line for photobleaching. The experiment yielded an image with the x position and time as coordinates and with the origin at the left upper corner. [83]

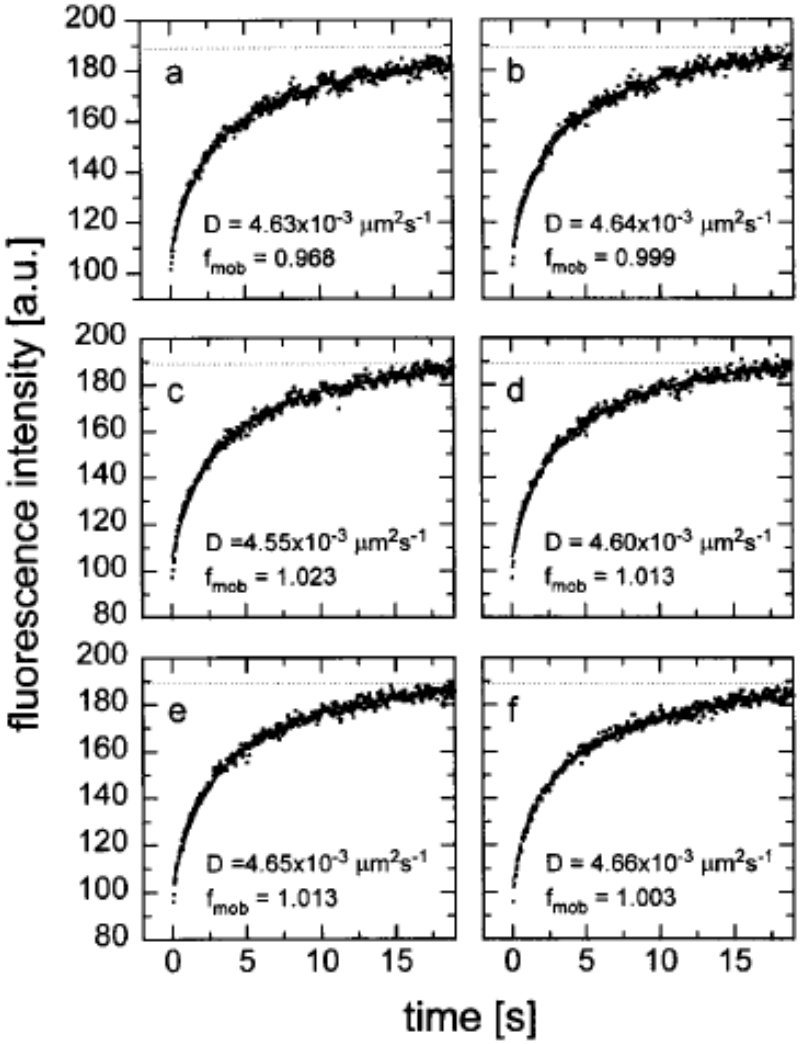

Figure 3.13 The fluorescence recovery curves.
The experiment shown in Figure 3.12 was evaluated by plotting the averaged intensities of the bleached segments vs. time after bleaching. This yielded the fluorescence recovery curves a-f. The diffusion coefficient D and the mobile fraction f_{mob} were indicated in the figure. [83]

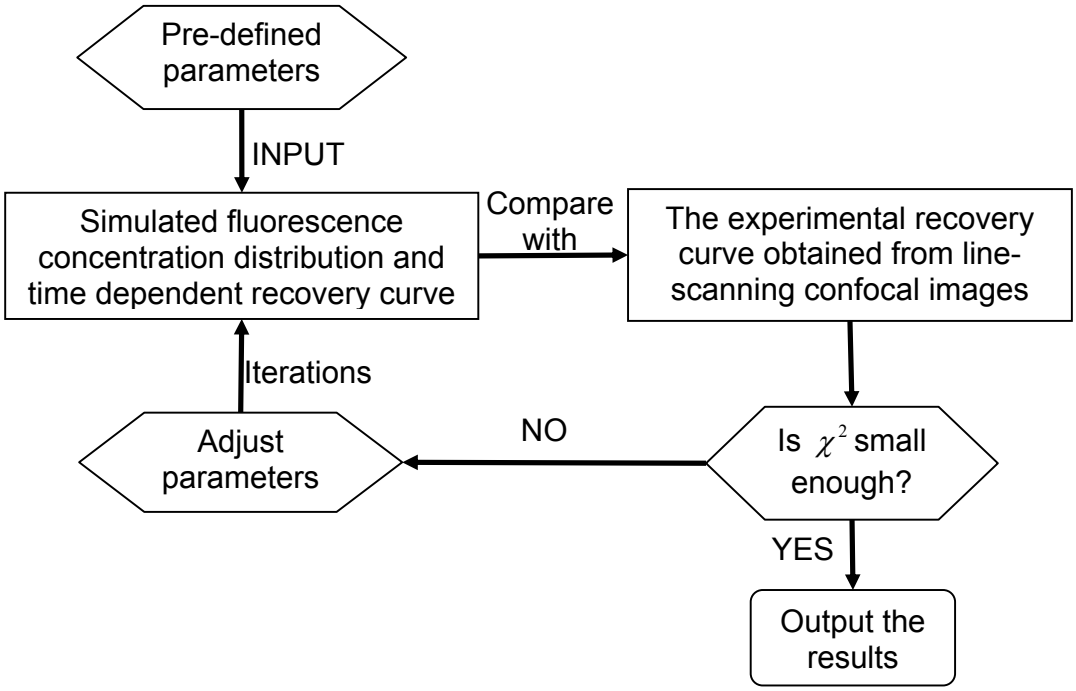

Figure 3.14 The flow chart of line-FRAP technique proposed by Wedekind. [83, 136]

Wedekind *et al.* [83] validated the line-FRAP model by measuring the diffusivities of b-phycoerythrin and FITC-dextrans of various average molecular weights in a glycerol/water mixtures. They also reported the first application of line-FRAP to the diffusion of a fluorescently labeled tracer inside the cell nucleus, which showed the potential of this method for the transport study of complex biological systems. The high spatial and temporal resolution is the most important advantage of line-FRAP technique with CLSM, however, the recovery signal is only from very tiny line area, this technique has the disadvantage of being less accurate due to a lower signal to noise ratio.[137]

Braeckmans *et al.* [137] presented a truly quantitative FRAP model for use with the CLSM based on the photobleaching of a long line segment. (Figure 3.15 and Figure 3.16) They derived the initial condition of concentration function from 3D spatial domain, but reduced it to 1D, as shown in equation (3.27), using low NA and long line bleaching assumptions. The solution of concentration function in line-FRAP experiment is shown in equation (3.28).

$$C_b(x,y,z) = C_0(x,y,z)e^{-K_0 e^{-2\frac{y^2}{r_{0e}^2}}} \tag{3.27}$$

$$C(y,t) = C_0 \sum_{n=0}^{+\infty} \frac{(-K_0)^n}{n!}(a_n - n)^{-1/2} e^{-\frac{2ny^2}{(a_n - n)r_{0e}^2}} \tag{3.28}$$

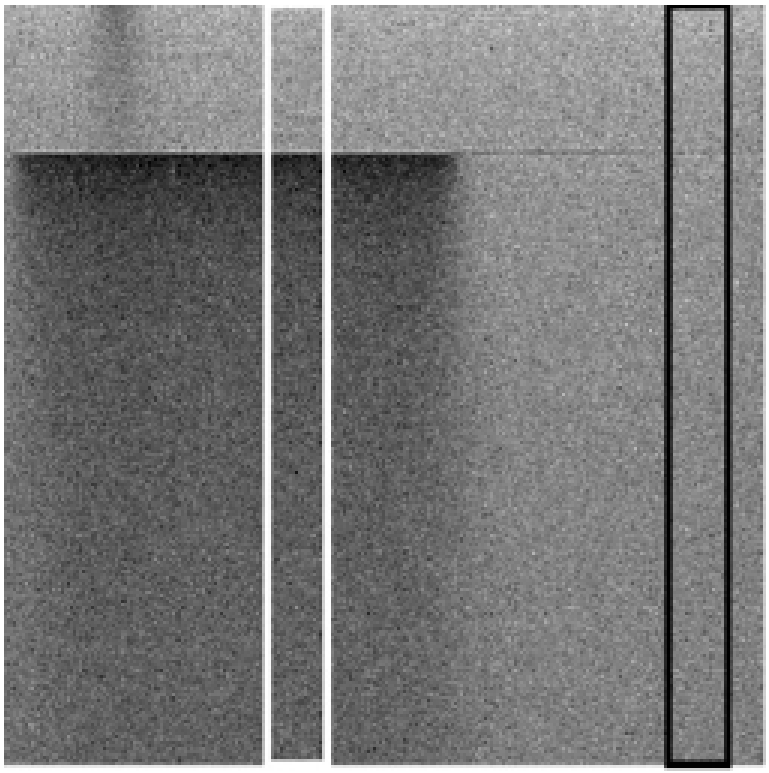

Figure 3.15 x-t image is shown of a line-FRAP experiment on a fluorescent solution. The FRAP curve is extracted from the x-t image by defining a main ROI (white rectangle) and a background ROI (black rectangle). [137]

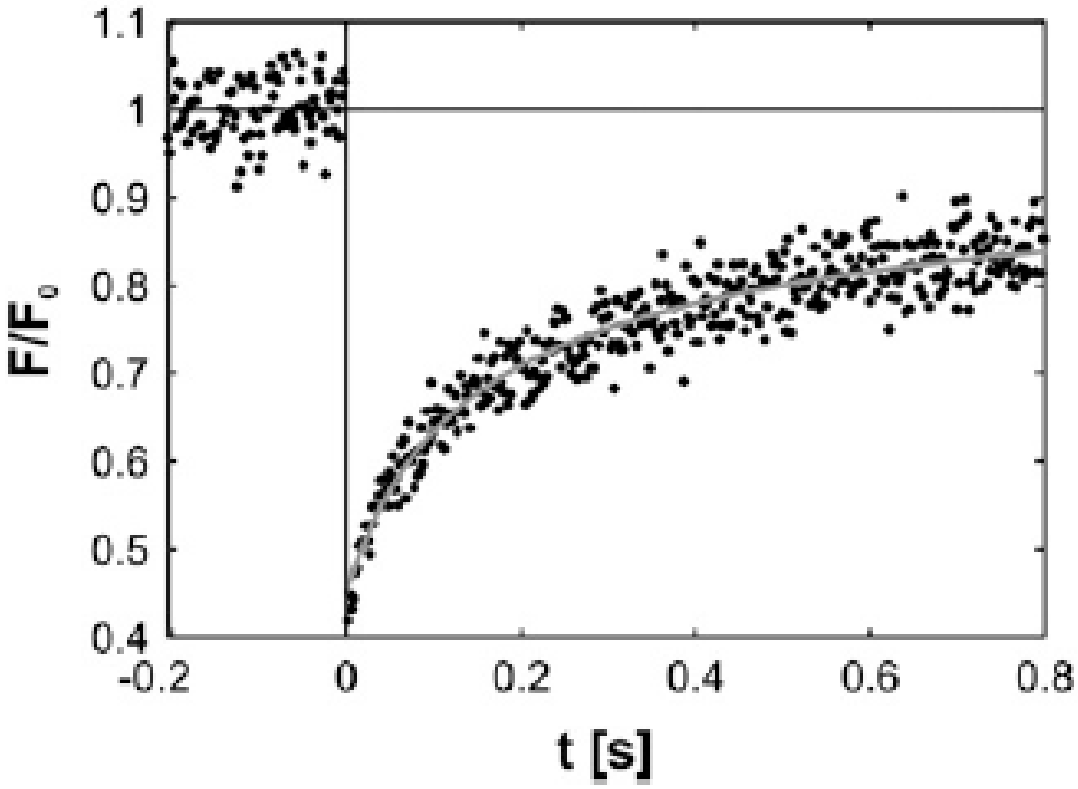

Figure 3.16 The final recovery curve (black data points) is shown and the solid gray line shows the best fit of the line-FRAP model to the experimental recovery curve. [137]

This method was validated by testing the diffusivities of R-phycoerythrin and FITC-dextrans of various molecular weights in solutions of different viscosities. They also applied this method to intracellular diffusion measurements of free GFP diffusion in living A549 cells and found a diffusivity of 26±3 $\mu m^2/s$ in the cytoplasm and 29±5 $\mu m^2/s$ in the nucleus, in good agreement with what other have reported. They concluded that the line-FRAP model offers a straightforward and fast way to measure diffusion coefficients and mobile fractions on a microscopic scale in 3-D samples with high spatial resolution. Because the bleaching of a line can be easily accomplished by commercial CLSMs, it can be applied by anyone familiar with the CLSM instrument.

Leddy *et al.* [138] modified the line-FRAP technique based on Kubitscheck's study [136] and applied it to quantify the diffusivities of FITC-dextrans within a pericellular matrix (PCM) of porcine articular cartilage. They found the diffusion coefficients of FITC-dextrans were significantly lower in the PCM than in the ECM of healthy articular cartilage probably due to difference in proteoglycan content, however, this difference was not detected in early-stage arthritic tissue.

- ***Disk-FRAP with CLSM***

Braeckmans *et al.* [23] used CLSM as a handy tool to perform FRAP measurements with a 3D disk-shaped bleaching geometry which was generated by the scanning laser beam of a CLSM.(Figure 3.17) The general mathematical basis was outlined describing the bleaching process for an arbitrary geometry bleached by a scanning beam, and the final analytical solution was derived with the assumptions of a disk-shaped geometry and low NA objective that described 3D fluorescence recovery

curve in the bleached area as observed by the CLSM. They concluded that 3D fluorescent recovery function for a disk bleached by a scanning beam reduced to the simpler 2D formula for a uniform disk bleached by a stationary beam.

The disk-FRAP model has the advantages of not requiring extensive mathematical or programming skills because the mathematical expressions are straightforward and can easily be programmed in a standard fitting routine and the detecting the solute diffusion in relative large areas with very high signal to noise ratio. However, the limitations are that the size of bleached regions cannot be too small, it should be more than 4× the resolution of the bleaching PSF to avoid boundary effects and the detection speed cannot be high because of the large scanning area.

Braga *et al.* [139] started to push the limit of disk-FRAP technique to the tiny bleaching regions for intracellular solute diffusion measurements in 3D and took into account diffusion of highly mobile molecules during the bleaching phase. The method was validated by determining the diffusion coefficients of fluorescence dextrans and green fluorescent protein in aqueous solution and in the nucleus of living HeLa cells. Diffusion coefficients were lower in the nucleoplasm, particularly for higher molecular weight dextrans. This was most likely caused by a sterical hindrance effect imposed by nuclear components. Decreasing the temperature from 37 to 22°C reduced the dextran diffusion rates by ~30% in aqueous solution but has little effect on mobility in the nucleoplasm. This suggested that spatial constraints to diffusion of dextrans inside the nucleus were insensitive to temperature.

Seifferts and Oppermann [140] simplified the line-FRAP and disk-FRAP models to 1D or 2D mathematical models (3.29) by introducing the parameter *d* for the diffusion dimension and used equation (3.30) to curve-fit the fluorescent intensity profile in the image at each time point to estimate two parameters, $w(t)^2$ and $A(t)$. Using equation (3.31) to curve-fit $w(t)^2$ data can yield diffusion coefficient and curve-fit $A(t)$ data can determine the dimensionality of the diffusion process.

$$C(r,t) = \frac{M}{(4\pi Dt)^{d/2}} e^{\frac{-r^2}{4Dt}} \tag{3.29}$$

$$I(r,t) = I_0 - \frac{M}{(4\pi Dt)^{d/2}} e^{\frac{-r^2}{4Dt}} = I_0 - A(t) e^{\frac{-r^2}{2w(t)^2}} \tag{3.30}$$

$$w(t)^2 = 2Dt \; ; \; A(t) = \frac{M}{(4\pi D)^{d/2}} \cdot t^{-d/2} \tag{3.31}$$

They found an interesting, smart and facile pathway to combine line-FRAP and disk-FRAP together in one model and applied it to FRPA experiments on solutions of Rhodamine B in glycerol and aqueous suspensions of polymethyl methacrylate (PMMA) microspheres. The method also has the potential to analyze and quantify diffusion processes in anisotropic media.

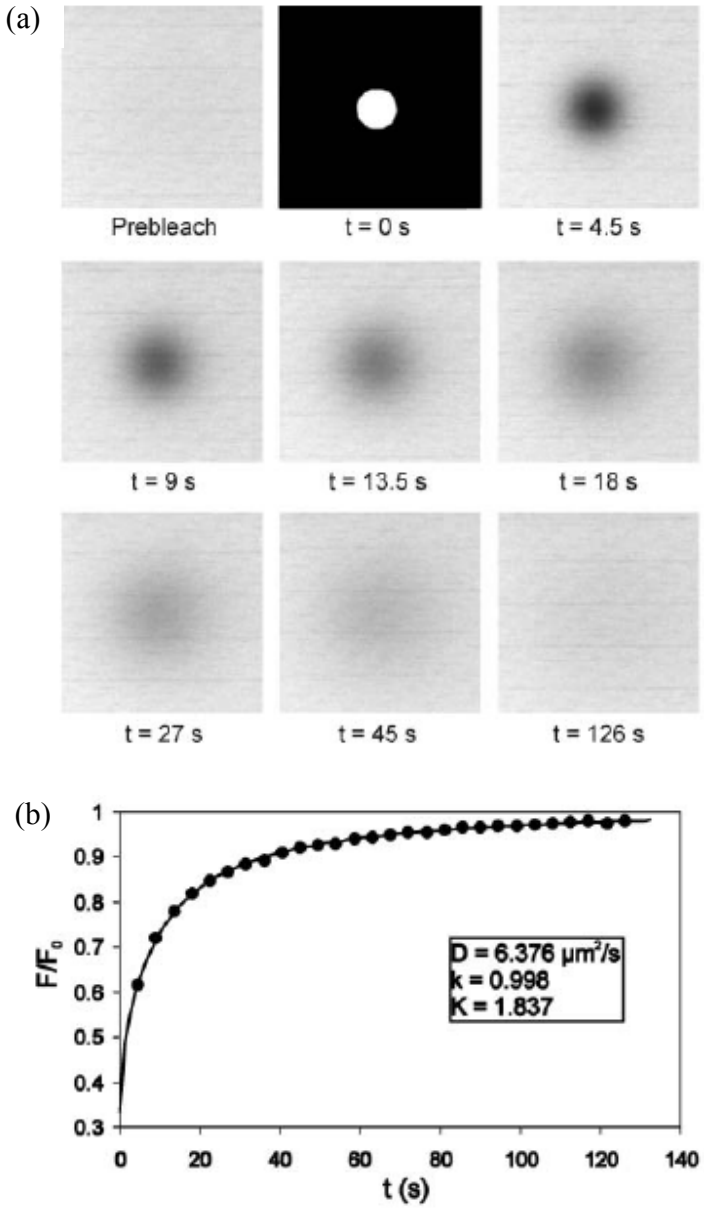

Figure 3.17 Experimental images and curves of disk-FRAP.
(a) A FRAP experiment is performed on the FD167 solution with 30% glucose (w/w). An image sequence is recorded of 30 images at regular time intervals of 4.5 s. The first image shows the sample before bleaching, the so-called pre-bleaching image. (b) A dedicated image processing program extracts the recovery curve from the image sequence, The experimental data are indicated by solid black circles. A best fit of the model (solid line) finally yields the translational diffusion coefficient D, the mobile fraction k, and the bleaching parameter K_0. [23]

3.4.3 3D FRPA based on Multiphoton Laser Scanning Microscopy (MPLSM)

Kubitscheck *et al.* [135] fully introduced the features of fluorescent photobleaching induced by multiphoton laser scanning microscope. (MP-FRAP) The photobleaching profile (Figure 3.19) showed a true spatial selectivity by restricting excitation to very small focal volumes due to the nonlinear optical processes.

- ***Studying protein dynamics in living cells***

Brown in Dr. Webb's lab [12] firstly demonstrated 3D multiphoton fluorescence photobleaching recovery (MP-FPR) technique in 1999 with spatial resolution of a few microns. An intense flash of mode-locked laser light pulses excites fluorescent molecules via multiphoton excitation in an ellipsoidal focal volume and photobleaches a fraction. The bleached region is restricted to a known, 3D defined volume. Fluorescence recovery in this focal volume is measured with multiphoton excitation, using the attenuated laser beam due to the surrounding unbleached fluorophores diffuse in. The fluorescence recovery curve after photobleaching can be analyzed to determine the diffusion coefficient of the fluorescent molecules. They applied MP-FRAP to measure the diffusion coefficient ($8.7\times10^{-7}\pm1.7\times10^{-7}cm^2s^{-1}$) of wild-type GFP in aqueous solution, which agreed with the value derived from the conventional FRAP experiment. This method also demonstrated the ability to quantify the mobility of calcein in the cytoplasm of RBL-2H3 cells. This study could be the first FRAP technique which can be utilized in thick tissue samples to determine the 3D diffusive transport of biological solutes within the cytoplasm or intracellular spaces.

In order to perform a detailed analysis of the dynamics of cytoskeleton proteins in a small domain, Waharte *et al.* [141] developed MP-FRAP and a theoretical framework for data analysis. Fast dynamics of proteins in the microvilli of the brush border of epithelial intestinal cells can be measured on the millisecond timescale in volumes smaller than 1 μm^3. The diffusion properties of myosin 1a and actin were quantified to be different and unrelated and the dynamics of myosin 1a in microvilli reflected its motor activity.

- ***The diffusion measurements by MP-FRAP in the extracellular matrix***

Stroh *et al.* [142] used MP-FRAP technique to quantify the dynamic behavior of nerve growth factor (NGF) in coronal, 400 μm thick, fresh rat brain tissue slices. They microinjected the fluorescent labeled NGF as a point source in the coronal slices and then monitored the dispersion of fluorescent dye using multiphoton microscope inside the tissue. The experimental data were analyzed by a two-step curve-fitting procedure to estimate the solute diffusivity. The results showed the diffusivity of NFG within rat coronal tissue is 2.14× lower than the diffusivity in the water, indicating the diffusion of NFG is hindered by the extracellular matrix.

Schnell *et al.* [143] validated Brown's 3D MP-FRAP model by measuring diffusion of macromolecules (150 KDa and 2 MDa FITC-dextran) in solution and gels, as well as in the extracellular matrix in multicellular spheroids and tumor tissue in dorsal chambers. They found the diffusion coefficients (Figure 3.18) decreased with increasing complexity of the sample matrix and increasing the amount of collagen in the gels. The diffusion coefficient was reduced for all the systems compared to values in solution.

Diffusion of 150-kDa dextrans was reduced 20 to 60% in spheroids and gels, and more than 70% in tumor tissue. The diffusion of 2-MDa dextrans was slower than the case of 150-kDa dextrans, and the diffusion coefficient was reduced 40 to 90% in spheroids and gels compared with solution.

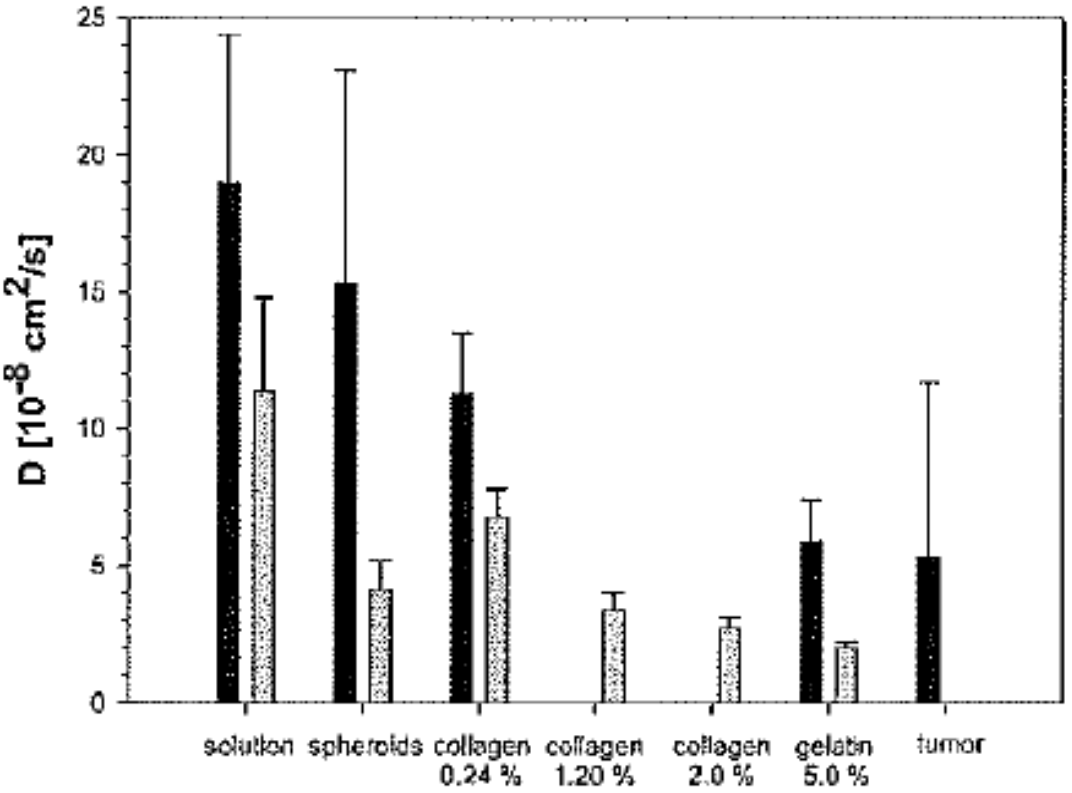

Figure 3.18 The diffusion coefficients of 150 KDa (black columns) and 2 MDa (gray columns) dextrans in solution, collagen gels, gelatin gels, multicellular spheroids, and tumor tissues.
The diffusion coefficient decreased as the complexity of the system and collagen concentration increased. The diffusion coefficient was reduced for all the systems compared to values in solution. Diffusion of 150-kDa dextrans was reduced 20 to 60% in spheroids and gels, and more than 70% in tumor tissue. The diffusion of 2-MDa dextrans was slower than the case of 150-kDa dextrans, and the diffusion coefficient was reduced 40 to 90% in spheroids and gels compared with solution. [143]

- ***The comparison of bleaching profile between one-photon and two-photon excitation***

Mazza *et al.* [144] mentioned when diffusion in 3D environment is considered in FRAP experiments, the description of the initial condition produced by the laser beam represented a crucial aspect. Therefore, they measured and compared the experimental 3D bleaching distributions (Figure 3.19) obtained in confocal and two-photon excitation schemes and analyzed the deviations from the ideal cases adopted in FRAP experiments. They also obtained the approximations for the one-photon and two-photon bleaching profile function (3.32) and (3.33).

$$f_0(r,z) = f_{ini} \exp\left(-K_{1ph} \exp\left(-\frac{2r^2}{w_r^2} - \frac{2z^2}{w_z^2} \right) \right) \tag{3.32}$$

$$f_0(r,z) = f_{ini} \exp\left(-K_{2ph} \exp\left(-\frac{4r^2}{w_r^2} - \frac{4z^2}{w_z^2} \right) \right) \tag{3.33}$$

where $K_{1ph} = k_b / (v\Delta y) I_{bl}(0,0)$ and $K_{2ph} = k_{2ph} / (v\Delta y) I_{bl}^2(0,0)$ is the bleaching parameter. They evidenced the inability of the approximation to describe the bleach distribution produced by conventional one-photon illumination and used finite-element computation to show that this can lead to considerable underestimation in the evaluation of diffusion coefficients. However, the same approximation provided more accurate results for bleaching profiles obtained in two-photon excitation, both at low and high illumination power.

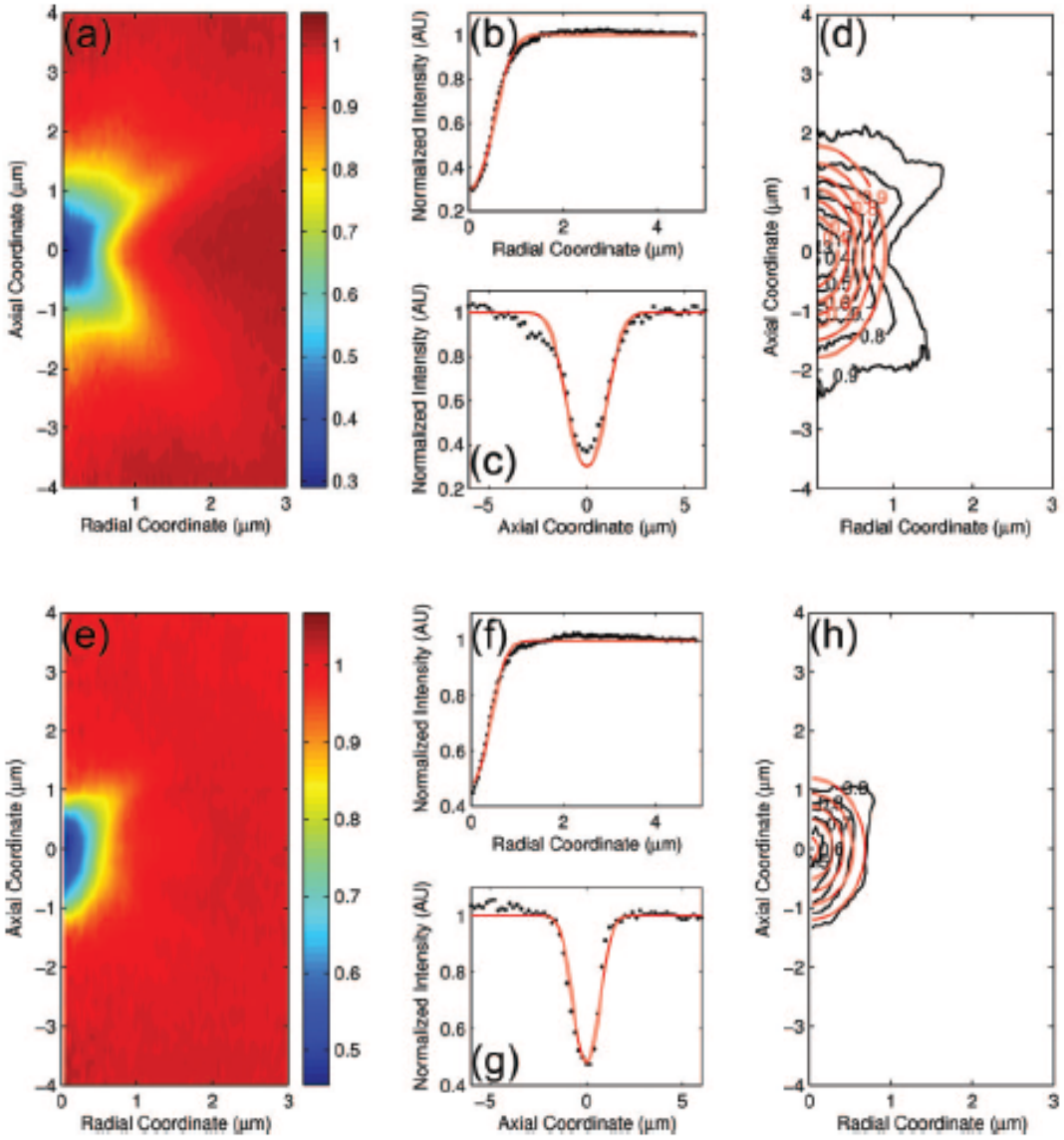

Figure 3.19 Exemplary 3D one-photon bleaching pattern obtained by confocal microscope [(a)-(d)] and two-photon bleaching pattern obtained by multiphoton microscope [(e)-(h)]. [144]

- ***A novel fluorescence recovery after photoactivation (FRAPa) technique***

Mazza *et al.* [145] presented a new convenient method for quantitative three-dimensionally resolved diffusion measurements based on the photobleaching (FRAP) or photoactivation (FRAPa) of a disk-shaped area by the scanning laser beam of a multiphoton microscope. The method was compatible with low as well as high numerical aperture objective lenses, allowing them to perform quantitative diffusion measurements in 3D extended samples as well as in very small volumes, such as cell nuclei. Furthermore, by photobleaching/photoactivating a large area, diffusion along the optical axis can be measured separately, which was potential to study anisotropic diffusion. They showed the mathematical model of FRAP and FRAPa technique based on multiphoton excitation and validated the methods using FITC-dextran in glycerol/water mixtures and photoactivatable green fluorescent protein (PA-GFP) in sucrose solutions. (Figure 3.18) They finally applied the method to PA-GFP diffusing freely in the nucleus of living NIH-3T3 mouse embryo fibroblasts. (Figure 3.21) The comparison between FRPA and FRAPa was reported in their paper and they mentioned FRAPa experiments are attractive since generally less laser energy is necessary for photoactivation compared to photobleaching, which could benefit them to shorten the photoperturbation and reduce the chance of photodamage effects in living cells.

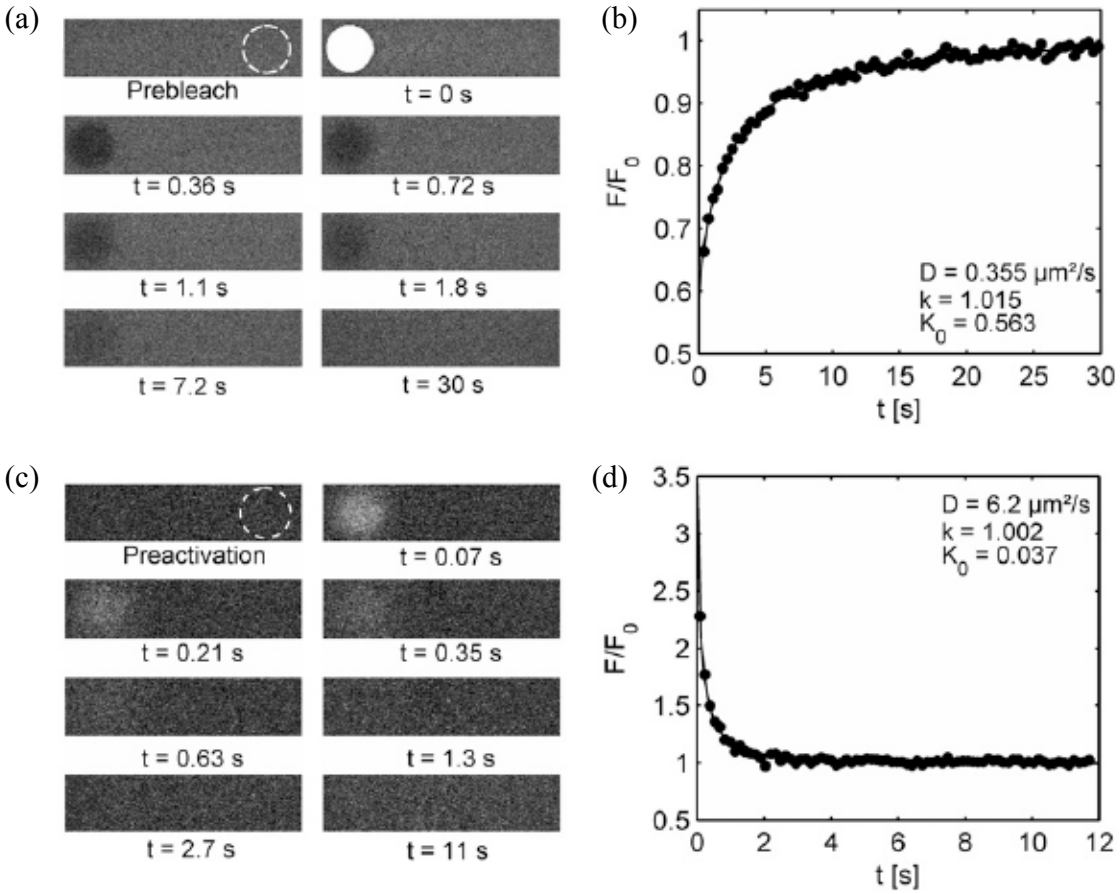

Figure 3.20 Two-photon FRAP and FRAPa images and curves.
(a) An example is shown of a two-photon disk-FRAP experiment on FD500 in an 85% (w/w) glycerol solution. (b) Custom image processing software is used to extract the normalized recovery curve from the images. The diffusion coefficient D, the mobile fraction k, and the bleaching parameter K_{0n} are calculated from a best fit of the model to the recovery data (solid line). (c and d) A corresponding two-photon FRAPa experiment is shown on PA-GFP in a 51% (w/w) sucrose solution. [145]

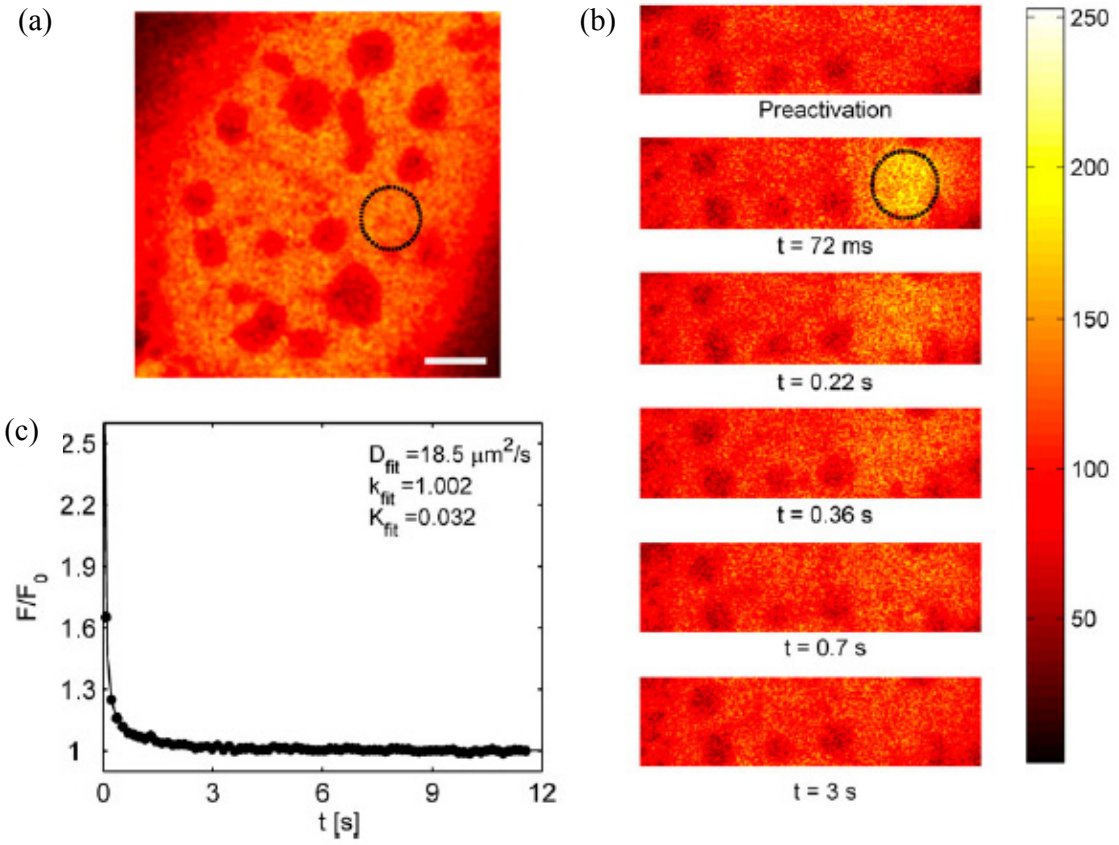

Figure 3.21 Two-photon FRAPa experiment on PA-GFP diffusing in the nucleus of a mouse embryo fibroblast.
(a,b) The first image shows the sample before photoactivation in the selected region (2.5 mm in radius). The subsequent images show the fluorescence redistribution after photoactivation of the selected region. The scale bar in (a) is 5 µm. (c) The redistribution curve is the average of seven experiments in different cells to obtain a smoother curve. The diffusion coefficient was obtained of (19±4) $\mu m^2/s$. [145]

CHAPTER 4 ANISOTROPIC SOLUTE DIFFUSION TENSOR IN PORCINE TMJ DISC MEASURED BY 2D FRAP

4.1 Introduction

The temporomandibular joint (TMJ) is a synovial, bilateral joint with unique morphology and function.[146] The TMJ disc, a fibrocartilaginous tissue, is a major component of jaw function by providing stress distribution and lubrication in the joint.[147, 148] Disc derangement (e.g., dislocation of the disc) is a common clinical finding in patients with TMJ disorders (affecting more than 35 million Americans with an annual health care cost of $4 billion).[149, 150] It has been suggested that degenerative processes predispose the disc to displacement and result in significant changes in disc morphology, biochemistry, function, and material properties.[151, 152]

The TMJ disc has a distinctive extracellular matrix (ECM) composition when compared to hyaline cartilage and other fibrocartilaginous tissues [*e.g.*, the intervertebral disc (IVD)]. The TMJ disc is comprised primarily of water with a significant amount of collagen (mainly type I) and a very small amount of proteoglycan.[153-157] The TMJ disc is a large avascular structure with human discs being wider mediolaterally than anteroposteriorly (approximately 19×13 mm).[158] The nutrients required by disc cells for maintaining healthy matrix are supplied by synovial fluid at the margins of the disc, as well as from nearby blood vessels at the posterior bilaminar zone connection.[159] Diffusive transport of nutrient solutes through the ECM plays a key role in maintaining the normal function of TMJ discs while the dysfunctional transport of those solutes is believed to contribute to the degeneration of the disc over time. Solute diffusivities in articular cartilage and IVD have been measured using a variety of techniques, including

magnetic resonance imaging (MRI), [33, 34] tracking the net movement of radiolabeled solutes, [35, 160] and fluorescence [36] or radiotracer desorption.[37, 38] However, to our knowledge the solute diffusivities in the TMJ disc have not been determined. Moreover, differences in biochemical composition and structure distinguish the disc into three regions: the anterior band, intermediate zone, and posterior band.[158] Collagen fibers in the anterior and posterior bands run primarily in the mediolateral direction, while in the intermediate zone these fibers run predominately in an anteroposterior direction.[161] Studies have shown that the mechanical properties of the TMJ disc are region-dependent and anisotropic.[159, 162] Therefore, it is reasonable to hypothesize that the solute diffusion in the TMJ disc is inhomogeneous and anisotropic. The objective of this study was to determine the region-dependent anisotropic diffusion tensor in TMJ discs using a new fluorescence recovery after photobleaching (FRAP) technique coupled with spatial Fourier analysis (SFA).

FRAP is a versatile and widely used tool for the determination of local diffusion properties within solutions, tissues, cells, and membranes.[10] Due to the high spatial resolution, FRAP offers the possibility to microscopically examine a specific region of a sample. For instance, the site-specific (*i.e.*, inhomogeneous) solute diffusion in articular cartilage has been previously studied using FRAP.[5, 132] The basic principle of FRAP is based on photobleaching the fluorescence of molecular probes and analyzing the recovery of the bleached area.[13, 87, 163] To date, most FRAP analyses are based on the method proposed by Axelrod *et al.* for isotropic diffusion.[13] Another approach for FRAP analysis is based on the spatial Fourier analysis of the recovery images and has the

advantage of potential detection of anisotropic diffusion.[14-16, 63, 101, 164, 165] Tsay and Jacobson, using SFA of FRAP images, developed a method for the determination of a two-dimensional (2D) diffusion tensor along the fixed coordinate system.[15] Most recently, Travascio *et al.* reported a method for calculating an anisotropic diffusion tensor based on two independent analyses of FRAP images: the Fourier transform (FT) and the Karhunen-Loeve transform (KLT).[17] The KLT analysis of FRAP images could determine the principal direction of the diffusion tensor. By combining the FT and KLT analyses, all components of the anisotropic diffusion tensor can be solved for in a single FRAP experiment. This method has been used to characterize anisotropic diffusion in knee meniscus and intervertebral disc tissues.[6, 17] In this chapter, we proposed a new method solely based on the SFA to completely determine the anisotropic diffusion tensor, avoiding all of the limitations imposed by KLT analysis.

We first discussed the theoretical basis of this new analysis. Next, we applied this analysis to computer simulated anisotropic FRAP experiments to validate the method, as well as made a comparison to the method proposed by Travascio *et al.* in terms of accuracy and robustness. And finally, we applied this analysis to characterize anisotropic solute diffusion in different regions of the TMJ disc by using the new FRAP technique.

4.2 Theory

Diffusional transport is governed by Fick's second law and in two dimensions, the partial differential equation has been shown in equation (3.8), where (x, y) are the spatial coordinates of the imaging system and t is the time. The function $C(x, y, t)$ represents the spatial concentration distribution of solutes in the x-y plane and **D** is the diffusion

tensor which is assumed symmetric. Within the small observation field of FRAP experiments, it is assumed that the diffusion tensor (**D**) is independent of position and time. Therefore, equation (3.8) could be rewritten as:[101]

$$\frac{\partial}{\partial t}C(x,y,t) = D_{xx}\frac{\partial^2 C(x,y,t)}{\partial x^2} + 2D_{xy}\frac{\partial^2 C(x,y,t)}{\partial x \partial y} + D_{yy}\frac{\partial^2 C(x,y,t)}{\partial y^2} \tag{4.1}$$

where D_{xx}, D_{xy}, and D_{yy} are components of diffusion coefficient tensor (**D**) in the (x,y) coordinate system.

Given that $\widetilde{C}(u,v,t) = \int_{-\infty}^{\infty}\int_{-\infty}^{\infty} C(x,y,t)e^{-i2\pi(ux+vy)}dxdy$ is the Fourier transform of $C(x,y,t)$, with an arbitrary initial condition and a boundary condition that $C(x,y,t)$ is a constant as (x, y) → ±∞, equation (4.1) can be solved by using 2D SFA in the frequency domain:[14-17, 101]

$$\widetilde{C}(u,v,t) = \widetilde{C}(u,v,0)e^{-4\pi^2(u^2+v^2)D(u,v)t} \tag{4.2}$$

where $\widetilde{C}(u,v,0)$ is the initial solute concentration and $D(u,v)$ represents the diffusion coefficient in Fourier space (with frequencies u and v) and is defined as:

$$D(u,v) = \frac{u^2 D_{xx} + 2uvD_{xy} + v^2 D_{yy}}{u^2 + v^2} \tag{4.3}$$

The function $D(u,v)$ can be determined by curve fitting the light intensity of a time series of fluorescence recovery images (in the Fourier space) to equation (4.2).

The average of $D(u,v)$ over the arc of a circumference (Integral curve L: $u^2 + v^2 = a^2$, a is an arbitrary constant, see Figure 4.1) over an angle range from α to β can be given as:

$$D_{\alpha,\beta} = \frac{\int_{L:u^2+v^2=a^2} D(u,v)ds}{\int_{L:u^2+v^2=a^2} ds} = \frac{1}{\beta-\alpha}\int_{\alpha}^{\beta}(D_{xx}\cos^2\xi + 2D_{xy}\sin\xi\cos\xi + D_{yy}\sin^2\xi)d\xi \quad (4.4)$$

The auxiliary variable ξ is a function of the frequencies *u* and *v*:[14, 15, 17]

$$\xi = \tan^{-1}(v/u),\ (\alpha \le \xi \le \beta) \quad (4.5)$$

Based on equation (4.4), the average of $D(u,v)$ over the arc from 0 to π can be related to the components of the diffusion tensor **D** as:[14, 17]

$$D_{0,\pi} = \frac{D_{xx}+D_{yy}}{2} = \frac{tr(\mathbf{D})}{2} \quad (4.6)$$

Similarly, the average of $D(u,v)$ over the arc from 0 to $\pi/2$ can be calculated as:[17]

$$D_{0,\frac{\pi}{2}} = \frac{D_{xx}+D_{yy}}{2} + \frac{2D_{xy}}{\pi} = \frac{tr(\mathbf{D})}{2} + \frac{2D_{xy}}{\pi} \quad (4.7)$$

The average of $D(u,v)$ over the arc from 0 to $\frac{\pi}{4}$ can be calculated as:

$$D_{0,\frac{\pi}{4}} = \frac{D_{xx}+D_{yy}}{2} + (\frac{D_{xx}-D_{yy}}{\pi}) + \frac{2D_{xy}}{\pi} = \frac{tr(\mathbf{D})}{2} + (\frac{D_{xx}-D_{yy}}{\pi}) + \frac{2D_{xy}}{\pi} \quad (4.8)$$

According to equations (4.6), (4.7) and (4.8), all components of the diffusion tensor (i.e., D_{xx}, D_{yy} and D_{xy}) can be obtained and expressed as the functions of $D_{0,\frac{\pi}{4}}$, $D_{0,\frac{\pi}{2}}$ and $D_{0,\pi}$:

$$\begin{cases} D_{xx} = D_{0,\pi} + \dfrac{\pi(D_{0,\frac{\pi}{4}} - D_{0,\frac{\pi}{2}})}{2} \\ D_{yy} = D_{0,\pi} - \dfrac{\pi(D_{0,\frac{\pi}{4}} - D_{0,\frac{\pi}{2}})}{2} \\ D_{xy} = \dfrac{\pi}{2}(D_{0,\frac{\pi}{2}} - D_{0,\pi}) \end{cases} \tag{4.9}$$

Using all components of the diffusion tensor two principal diffusivities (eigenvalues) of the 2D diffusion tensor can be calculated by:

$$\begin{cases} D_{\text{Eig\_Min}} = \dfrac{D_{xx} + D_{yy} - \sqrt{(D_{xx} - D_{yy})^2 + 4D_{xy}^2}}{2} \\ D_{\text{Eig\_Max}} = \dfrac{D_{xx} + D_{yy} + \sqrt{(D_{xx} - D_{yy})^2 + 4D_{xy}^2}}{2} \end{cases} \tag{4.10}$$

where $D_{\text{Eig\_Min}}$ is the relatively smaller of the two eigenvalues and $D_{\text{Eig\_Max}}$ is the relatively larger one. The ratio of $D_{\text{Eig\_Min}}$ to $D_{\text{Eig\_Max}}$ can be used to represent the anisotropy of the diffusion.

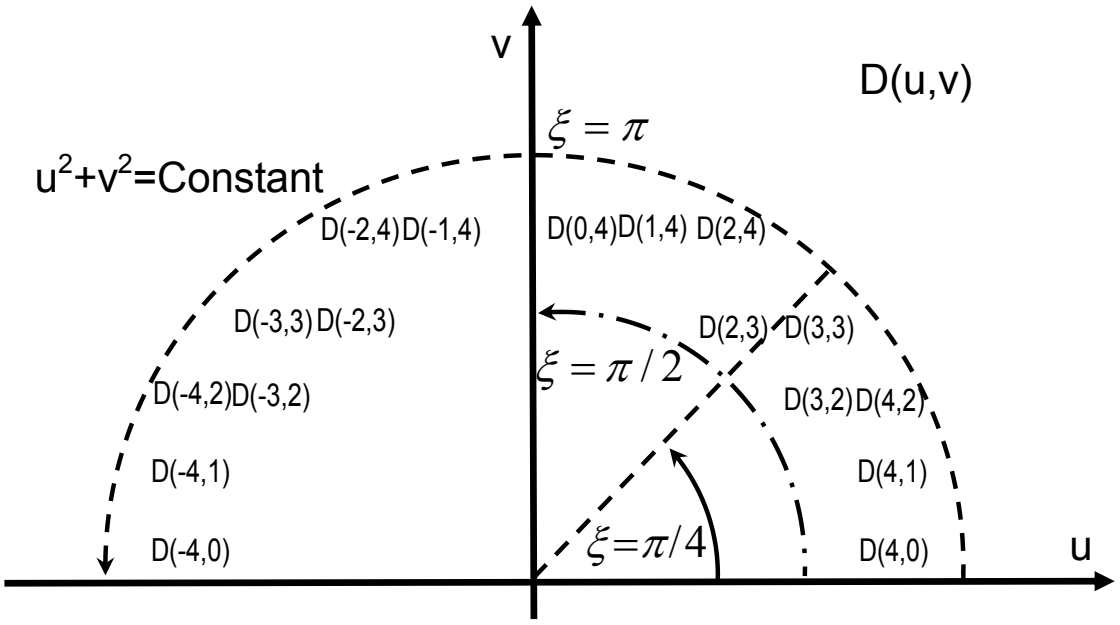

Figure 4.1 Diffusion coefficient $D(u,v)$ in frequency domain (*u,v*).

The averages of $D(u,v)$ over the arcs from 0 to π, 0 to $\pi/2$ and 0 to $\pi/4$ can be used to determine the components (D_{xx}, D_{yy} and D_{xy}) of the diffusion tensor. On the 'Ring4':

$$D_{0,\frac{\pi}{4}} = \left[D(4,0) + D(4,1) + D(4,2) + D(3,2) + D(3,3)\right]/5$$

$$D_{0,\frac{\pi}{2}} = \left[D(4,0) + D(4,1) + D(4,2) + D(3,2) + D(3,3) + D(2,3) + D(2,4) + D(1,4) + D(0,4)\right]/9$$

$$D_{0,\pi} = \left[D(4,0) + D(4,1) + D(4,2) + D(3,2) + D(3,3) + D(2,3) + D(2,4) + D(1,4) + D(0,4) + D(-1,4) + D(-2,4) + D(-2,3) + D(-3,3) + D(-3,2) + D(-4,2) + D(-4,1) + D(-4,0)\right]/17$$

4.3 Materials and Methods

4.3.1 Computer Simulation of Anisotropic FRAP Experiment

The 2D anisotropic diffusion process of the fluorescent molecule recovery after photobleaching was simulated using finite element analysis software (COMSOL Multiphysics 3.4, COMSOL Inc., Burlington, MA). At the boundaries of the sample (i.e., simulation domain, $4\times4mm^2$), the concentration of the fluorescent molecules satisfied the constancy assumption ($C=C^*$). Initially, the concentration distribution of fluorescent molecules was assumed to be uniform ($C=C^*$) outside the photobleached spot and zero within the photobleached area. The diameter of the bleached area was set to 26.71μm according to the optimum value of 8 for the ratio of the imaging frame size (213.68μm) to the initial diameter of the bleached spot as suggested by Travascio and Gu.[17] The mesh used in the simulation experiments included 8,784 quadratic Lagrange triangular elements. The convergence criterion for the solution was the relative error tolerance of less than 0.001. The simulation was stopped when the concentration in the bleached spot reached 95% of C^*. For data analysis purposes, an image sequence containing 101 frames (0.6s/frame) representing the FRAP experiment was extracted from the central region of the simulation domain and digitalized to 128pixels×128pixels [Figure 4.2(a)]. The frame size was set to $213.68\times213.68\mu m^2$, which was used in the following TMJ disc FRAP experiment.

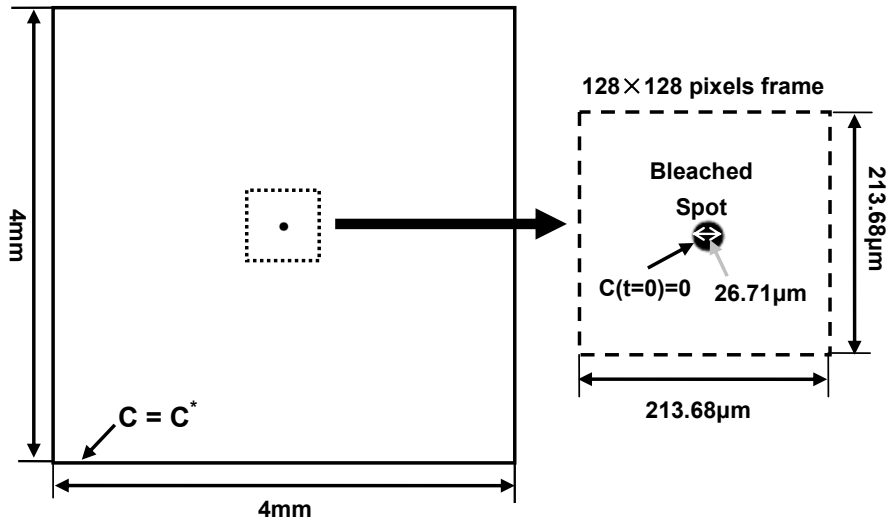

(a)

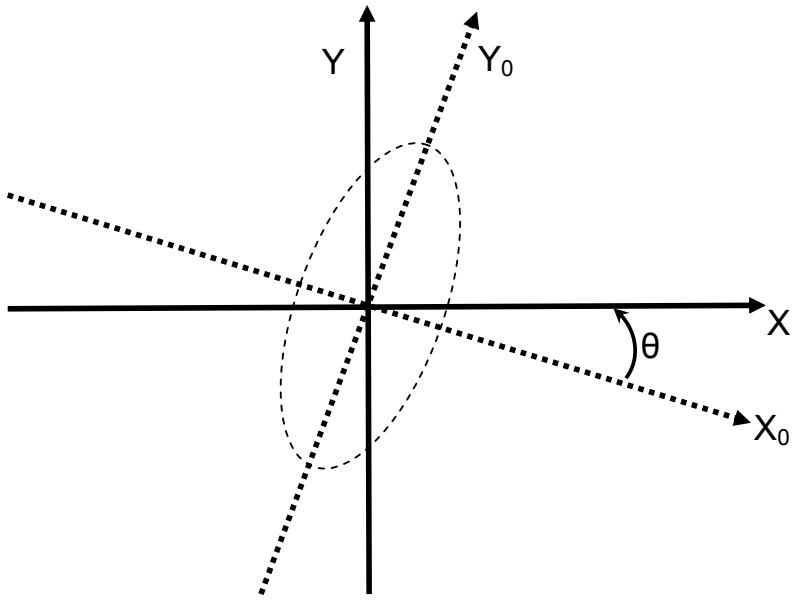

(b)

Figure 4.2 The schematic of simulation FRAP experiments and rotation angle.
(a) The computational domain with the initial and boundary conditions for FRAP simulation experiments. (b) The orientation of pre-defined anisotropic diffusion tensor generated using various rotation angles. θ is the rotation angle from the principal diffusion tensor coordinate (X_0, Y_0) to the observed diffusion tensor coordinate (X, Y).

Three groups of anisotropic diffusion were investigated in the simulation experiments and there were seven pre-defined diffusion tensors in each group. In the first group, a base diffusion tensor of $\mathbf{D_0} = \begin{bmatrix} 10 & 0 \\ 0 & 15 \end{bmatrix} \mu m^2 / s$ was selected and rotated at seven different angles $\theta_i, i = 0 \sim 6$ ($\theta_{0\sim6}$=0, π/6, π/4, π/3, 3π/8, and π/2) using a rotation matrix $\mathbf{R}_i$ defined as:

$$\mathbf{R}_i = \begin{bmatrix} \cos\theta_i & -\sin\theta_i \\ \sin\theta_i & \cos\theta_i \end{bmatrix} \tag{4.11}$$

The seven pre-defined diffusion tensors, see Figure 4.2(b), were calculated by:

$$\mathbf{D}_i = \mathbf{R}_i^T \mathbf{D}_0 \mathbf{R}_i \qquad (i = 0 \sim 6) \tag{4.12}$$

In the second and third group, the base diffusion tensors were $\mathbf{D_0} = \begin{bmatrix} 10 & 0 \\ 0 & 20 \end{bmatrix} \mu m^2 / s$ and $\mathbf{D_0} = \begin{bmatrix} 10 & 0 \\ 0 & 30 \end{bmatrix} \mu m^2 / s$, respectively. The computer simulations of these three groups allowed investigation into the effects of anisotropy and orientation of the diffusion tensors on the accuracy of the new SFA based FRAP data analysis.

To study the effect of experimental noise on this anisotropic FRAP data analysis photon noise was added to the ideal simulated FRAP images. Although photon noise has a Poisson distribution, for large photon fluxes (*e.g.*, during FRAP experiments) Gaussian noise represents a close approximation of Poisson noise.[166] Similarly to previous studies,[15, 17, 165] different magnitudes of Gaussian noise were added to the purely simulated recovery images to estimate how image noise affected the analysis. The

magnitude of the Gaussian noise was characterized by its standard deviation, σ. Two magnitudes of spatial Gaussian noise (i.e., σ = 5 and 10) were generated by ImageJ software (Version 1.39f, by Wayne Rasband, National Institutes of Health, USA) and were then superimposed onto the simulated recovery images. For each level of σ investigated, ten FRAP experiments were simulated.

4.3.2 FRAP Experiment on Porcine TMJ Disc

Nine fresh porcine TMJ discs from five young adult pigs (~8-10 months) were used for testing. Razor blades were used to prepare tissue slices from the intermediate, posterior, anterior, lateral, and medial regions of the discs (Figure 4.3). One tissue slice (about $4\times4mm^2$) was obtained from each region. The final specimens with ~650μm thickness were obtained from each tissue slice using a microtome (SM24000, Leica Microsystems GmbH, Wetzlar, Germany) with a freezing stage (Model BFS-30, Physitemp, Clifton, NJ). The tissue slice was microtomed on both inferior and superior surfaces to remove the natural concave shape of the tissue to maintain a flat cartilage surface for the FRAP experiment. Diffusion tensors for FITC-dextran molecules with a molecular weight of 4kDa (FD4, λ_{ex} 490 nm; λ_{em} 520 nm, Sigma-Aldrich®, St. Louis, MO, USA) were measured with FRAP in the horizontal X-Y plane in Figure 4.3 (parallel to the surface of the TMJ disc). Correspondingly, the three components (*i.e.*, D_{xx}, D_{yy} and D_{xy}) and two principal diffusivities (D_{Eig_Min} and D_{Eig_Max}) of the anisotropic diffusion tensor were obtained from the FRAP experiment.

Specimens were immersed in FITC-Dextran solution (0.1mM) for 48 hours (tissue swelling was not significant), to allow the concentration distribution of fluorescent

solutes to reach equilibrium throughout the tissue. The FRAP experiment was performed on a Leica TCS-SP2 Confocal Microscope System (Leica Microsystems, Inc., Exton, PA) at room temperature (22ºC). The specimen was photobleached using an Ar-488nm laser to create a circular bleached spot with a diameter about 27μm. A Multi-Layer Bleaching (MLB) protocol was used to ensure a 2D fluorescent recovery in the X-Y plane by minimizing the diffusion in the Z-direction along the thickness of the specimen.[14] The depth of the bleaching spot was about 70μm from the surface into the specimen and fluorescence recovery was observed on the focal plan at 7μm beneath the surface of the specimen. A HC PlanAPO 20×/0.7NA dry objective (Leica Microsystems, Inc., Exton, PA) was used to collect fluorescent recovery images of 128 ×128 pixels (213.68 ×213.68μm^2). For each experiment, 100 frames of recovery images, plus 5 images prior to bleaching, were acquired at a rate of 0.6s per frame. To minimize the contribution of the fluorescence emission of the background, pre-bleaching images were averaged and then subtracted from the post-bleaching image series.

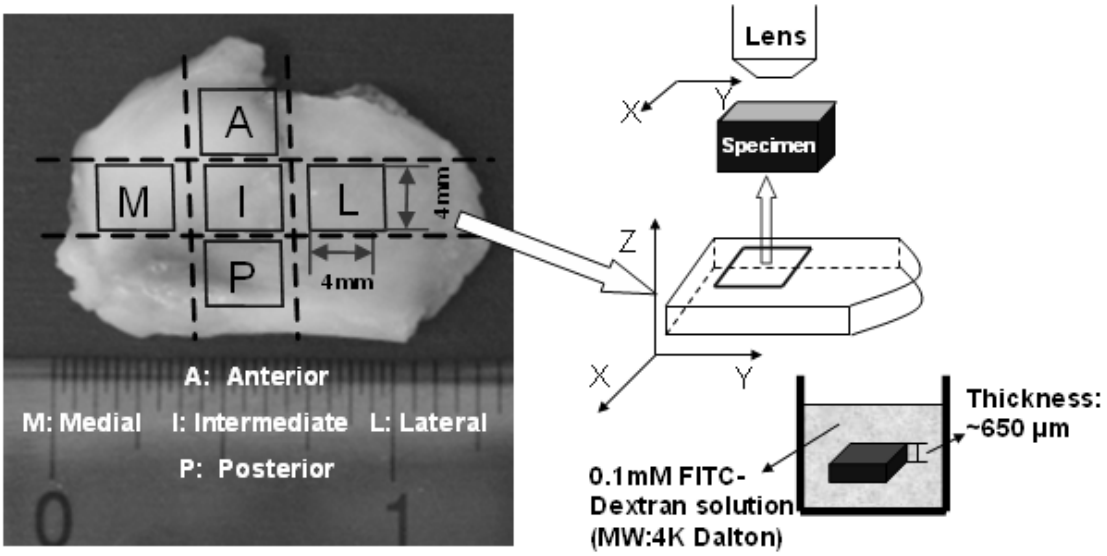

Figure 4.3 The schematic of FRAP experiments on porcine TMJ discs.
Tissue specimens were prepared from the anterior, posterior, intermediate, lateral, and medial regions of the discs. The diffusion tensor of 4kDa FITC-Dextran was measured with FRAP in the horizontal X-Y plane (parallel to the surface of the TMJ disc).

4.3.3 Images and Data Processing

For both computer simulated and experimental FRAP tests, the image processing was completed using custom written codes in MATLAB (MATLAB 7.0, The MathWorks Inc., Natick, MA). Based on equation (4.2), the code performed a two-dimensional Fourier Transform and nonlinear curve-fit to yield solutions for $D(u,v)$, which was the diffusion coefficient in the frequency domain. Based on Equation (5), averaging $D(u,v)$ on 'Ring 4' over different angle ranges generated $D_{0,\pi}$, $D_{0,\frac{\pi}{2}}$ and $D_{0,\frac{\pi}{4}}$. The selection of Ring 4 was suggested by previous studies,[17] and the frequency couples (*u,v*) for Ring 4 are shown in Figure 4.1. Using equation (4.11), the code calculated all components of the diffusion tensor: D_{xx}, D_{yy} and D_{xy}. Finally, the calculation of the principal diffusivities, $D_{\text{Eig\_Min}}$ and $D_{\text{Eig\_Max}}$, were completed according to equation (4.12). The average values, as well as the ratio of the two principal diffusivities for each specimen were determined.

4.3.4 Statistical Analysis

An independent t-test was performed on the principal diffusivities, $D_{\text{Eig\_Min}}$ and $D_{\text{Eig\_Max}}$, to examine the anisotropy of solute diffusion in each disc region. One-way ANOVA and Tukey's post hoc tests were performed on the average diffusivities to examine the regional effect on the diffusion rate in porcine TMJ discs. This effect was also examined through the ratio of the principal diffusivities. SPSS 16.0 software (SPSS

Inc., Chicago, IL) was used for all statistical analysis and significant differences were reported at p-values < 0.05.

4.4 Results

4.4.1 Validation Using Computer Simulated FRAP Experiments

2D anisotropic FRAP experiments were simulated by using pre-defined components of the anisotropic diffusion tensor. Numerically simulated FRAP digital images were transformed into the frequency domain using SFA. The principal diffusivities of the anisotropic diffusion process were calculated based on our proposed method. The accuracy of the new method was assessed by the relative error (ε) which is defined as:[17]

$$\varepsilon = \frac{\left|\text{Pre-defined Value - Calculated Value}\right|}{\text{Pre-defined Value}} \times 100(\%) \qquad (4.13)$$

The effects of anisotropic ratio (D_{0xx}/D_{0yy}) and diffusion tensor orientation (θ) on the accuracy of the new method were evaluated. The relative errors (ε) of the two principal diffusivities for three different anisotropic ratios (D_{0xx}:D_{0yy}=1:1.5, 1:2.0 and 1:3.0) with seven diffusion tensor orientations (θ = 0~π/2) are shown in Figure 4.4. Overall, the relative errors of $D_{\text{Eig\_Min}}$ were less than 1.5% for all simulated cases [Figure 4.4(a)], while the relative errors of $D_{\text{Eig\_Max}}$ were less than 1% [Figure 4.4(b)]. This result indicated that the accuracy of the new method was not significantly sensitive to D_{0xx}:D_{0yy} and θ. The highest accuracy was achieved when the diffusion tensors were oriented in alignment with the axes of the coordinate system (i.e., θ = 0 or π/2). The accuracy

slightly decreased when the orientation of the diffusion tensor deviated from the axes of the coordinate system. The accuracy of this method increased when the anisotropic ratio (D_{0xx}:D_{0yy}) decreased.

The effects of imaging noise (σ) on the accuracy of the new method were also investigated for the cases of D_{0xx}:D_{0yy}=1:1.5, 1:2.0 and 1:3.0, with $\theta = \pi/4$. The typical FRAP images with and without spatial Gaussian noise (σ = 0, 5, 10) as well as the corresponding curve-fits to determine $D(u, v)$ are shown in Figure 4.5. The relative errors of the two principal diffusivities increased with increasing σ. The average relative errors were less than 8% at σ = 5, while the average values were less than 12.5% at σ = 10 (Figure 4.6). In this study, the accuracy of the new method was not sensitive to the anisotropic ratio.

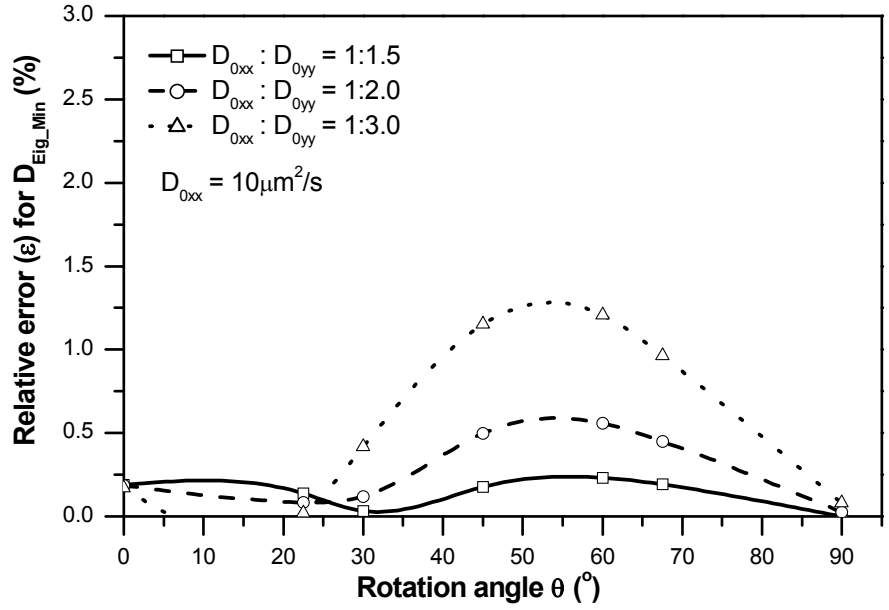

(a)

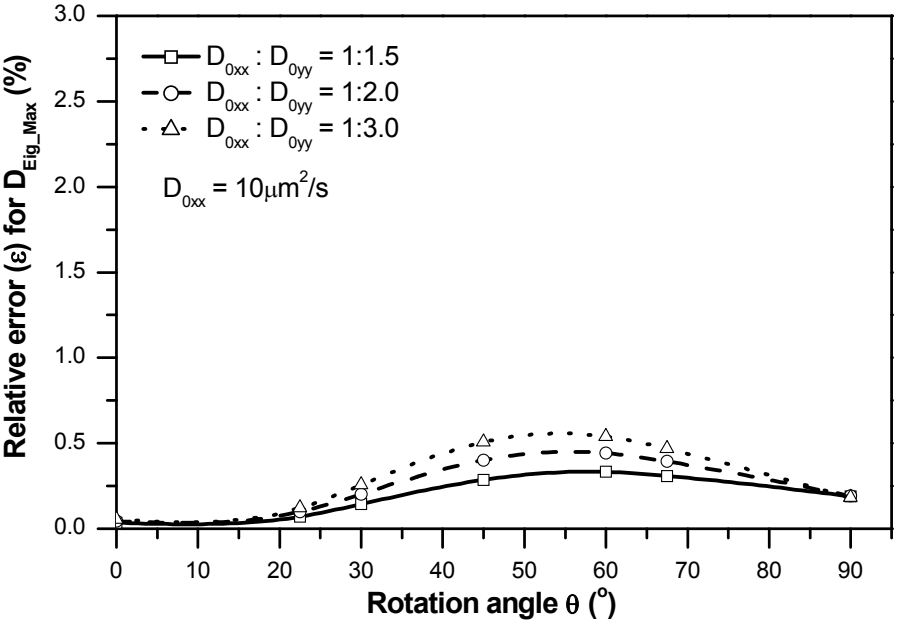

(b)

Figure 4.4 Effects of the orientation (θ) and anisotropic ratio (D_{0xx}/D_{0yy}) of the diffusion tensor on the relative error (ε) for the determination of (a) $D_{\text{Eig\_Min}}$ and (b) $D_{\text{Eig\_Max}}$.

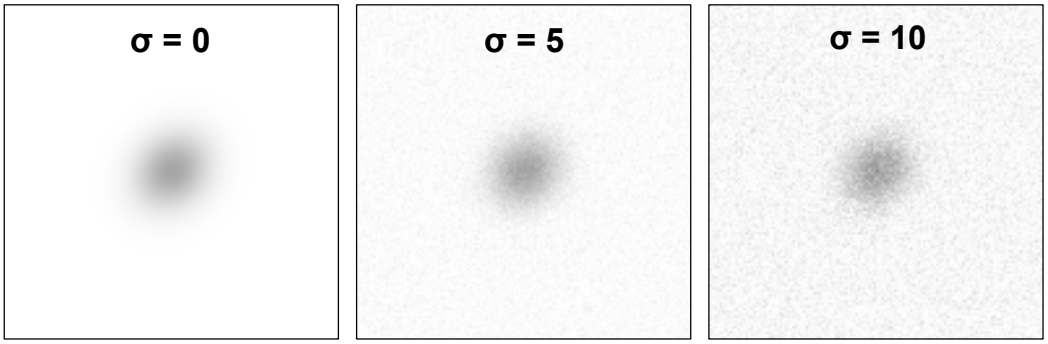

(a)

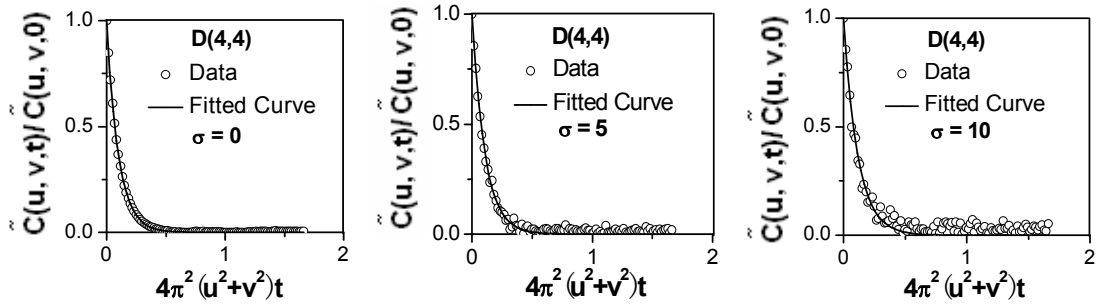

(b)

Figure 4.5 Effect of the imaging noise on the determination of the D(u, v).
(a) Typical computer simulated FRAP images without and with spatial Gaussian noise (σ = 0, 5, 10). (b) Typical curve-fits to determine D(4,4) for the simulated FRAP image sequences without and with spatial Gaussian noise (σ = 0, 5, 10).

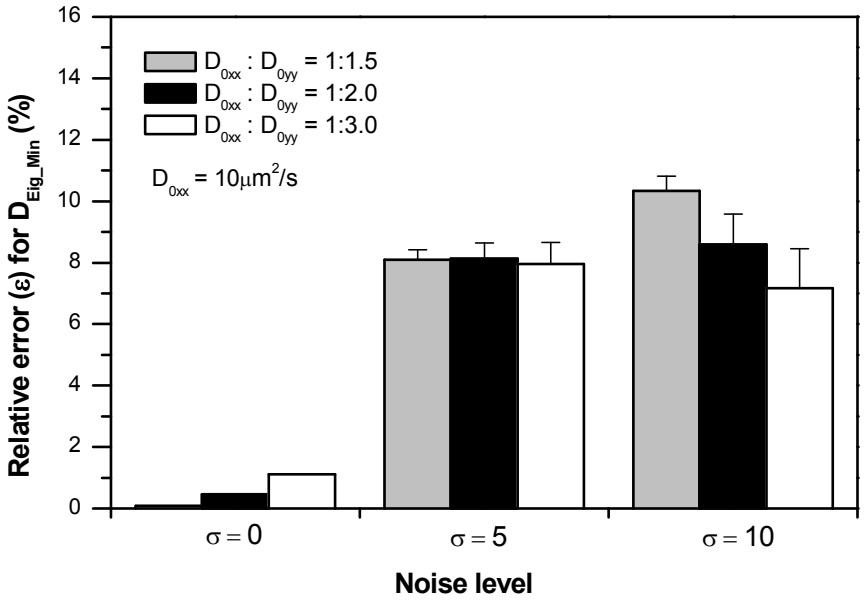

(a)

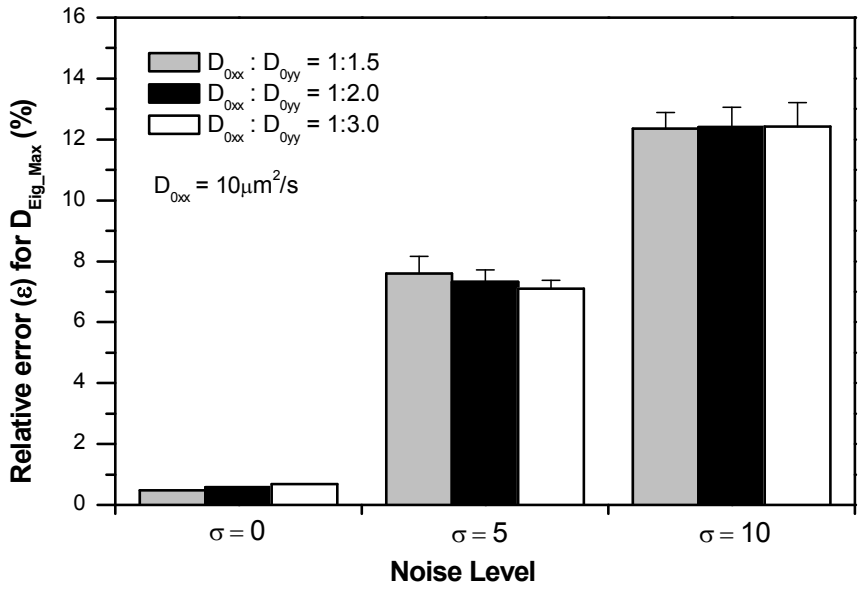

(b)

Figure 4.6 Effect of the imaging noise on the precision of determined diffusion tensors with different anisotropy: (a) The relative error (ε) for $D_{\text{Eig\_Min}}$ and (b) the relative error (ε) for $D_{\text{Eig\_Max}}$.

4.4.2 FRAP Experiments on Porcine TMJ Discs

The two principal diffusivities of the 2D anisotropic diffusion tensor of 4kDa FTIC-Dextran in the five regions of porcine TMJ disc were determined using our new method and listed in Table 4.1. The characteristic diffusivity defined as $\left(D_{\text{Eig\_Min}} + D_{\text{Eig\_Max}}\right)/2$ was calculated to represent the average solute diffusion rate in each disc region. The ratio of $D_{\text{Eig\_Min}}$ to $D_{\text{Eig\_Max}}$ was also calculated to evaluate the anisotropy of solute diffusion in the disc.

The average characteristic diffusivity across the disc was 26.05±4.32 $\mu m^2/s$. Regional differences in characteristic diffusivity were observed in the anteroposterior and mediolateral directions [Figure 4.7(a)]. In the anteroposterior direction, the anterior region (30.99±5.93 $\mu m^2/s$) had significantly higher characteristic diffusivity than the intermediate region (20.49±5.38$\mu m^2/s$, p = 0.0003) and posterior region (20.97±2.46 $\mu m^2/s$, $p < 0.0001$). In the mediolateral direction, the medial region (26.51±6.30$\mu m^2/s$) and lateral region (26.71±5.50$\mu m^2/s$) had higher characteristic diffusivities than the intermediate region, although this trend was not statistically significant.

Figure 4.7(b) showed that there was a significant difference between $D_{\text{Eig\_Min}}$ and $D_{\text{Eig\_Max}}$ in each disc region ($p < 0.001$). The ratio of $D_{\text{Eig\_Min}}$ to $D_{\text{Eig\_Max}}$ was approximately 0.45~0.51 (with 1.0 indicating isotropic) across the disc without significant regional differences [Figure 4.7(c)]. These results indicated that the diffusion of 4kDa FTIC-Dextran was highly anisotropic in the porcine TMJ disc.

Table 4.1 The results (mean±SD) of the diffusion tensor of 4kDa FTIC-Dextran in the five regions of porcine TMJ discs. $D_{\text{Eig\_Min}}$ to $D_{\text{Eig\_Max}}$ are the two principal diffusivities of the diffusion tensor. $\left(D_{\text{Eig\_Min}} + D_{\text{Eig\_Max}}\right)/2$ is the characteristic diffusivity that represents the averaged solute diffusion rate in each disc region. $D_{\text{Eig\_Min}} / D_{\text{Eig\_Max}}$ was calculated to evaluate the anisotropy of solute diffusion in each disc region. (* $D_{\text{Eig\_Max}}$ was significantly larger than $D_{\text{Eig\_Min}}$ in each region, $p < 0.05$).

	Anterior	Medial	Intermediate	Lateral	Posterior	Average
$D_{\text{Eig\_Min}}$ ($\mu m^2/s$)	**18.32±4.18**	**17.10±4.72**	**13.57±3.97**	**15.61±4.28**	**13.37±4.15**	**15.75±1.56**
$D_{\text{Eig\_Max}}$ ($\mu m^2/s$)	**43.67±11.39**	**35.92±8.95**	**27.40±8.31**	**37.80±11.95**	**28.58±5.90**	**36.35±8.66**
$\left(D_{\text{Eig\_Min}} + D_{\text{Eig\_Max}}\right)/2$ ($\mu m^2/s$)	**30.99±5.93**	**26.51±6.30**	**20.49±5.38**	**26.71±5.50**	**20.97±2.46**	**26.05±4.32**
$D_{\text{Eig\_Min}} / D_{\text{Eig\_Max}}$	**0.45±0.17***	**0.48±0.10***	**0.51±0.14***	**0.47±0.24***	**0.49±0.18***	**0.47±0.12**

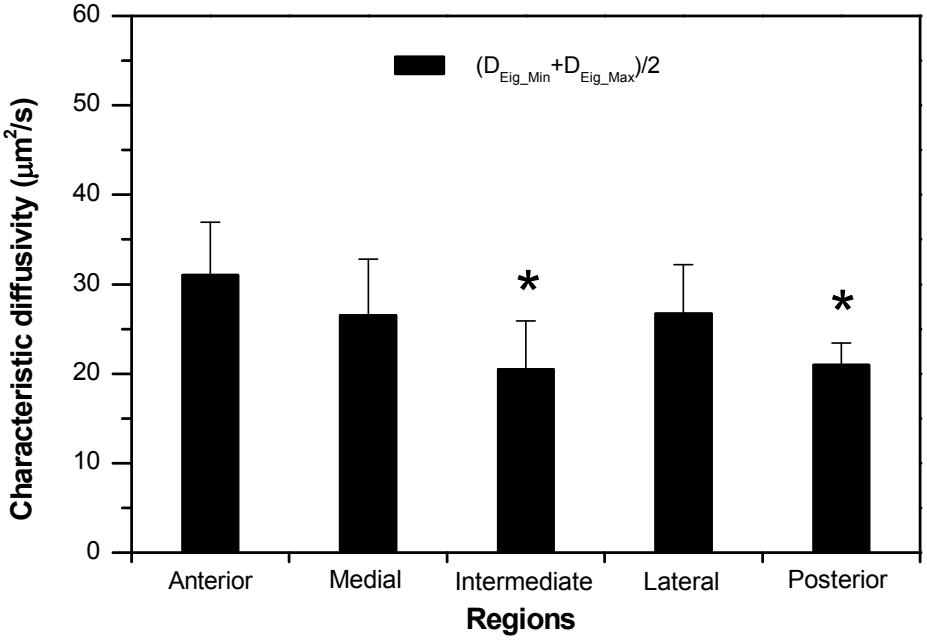
60
50
40
30
20
10
0
Characteristic diffusivity (μm²/s)
(D_Eig_Min+D_Eig_Max)/2
*
*
Anterior
Medial
Intermediate
Lateral
Posterior
Regions

(a)

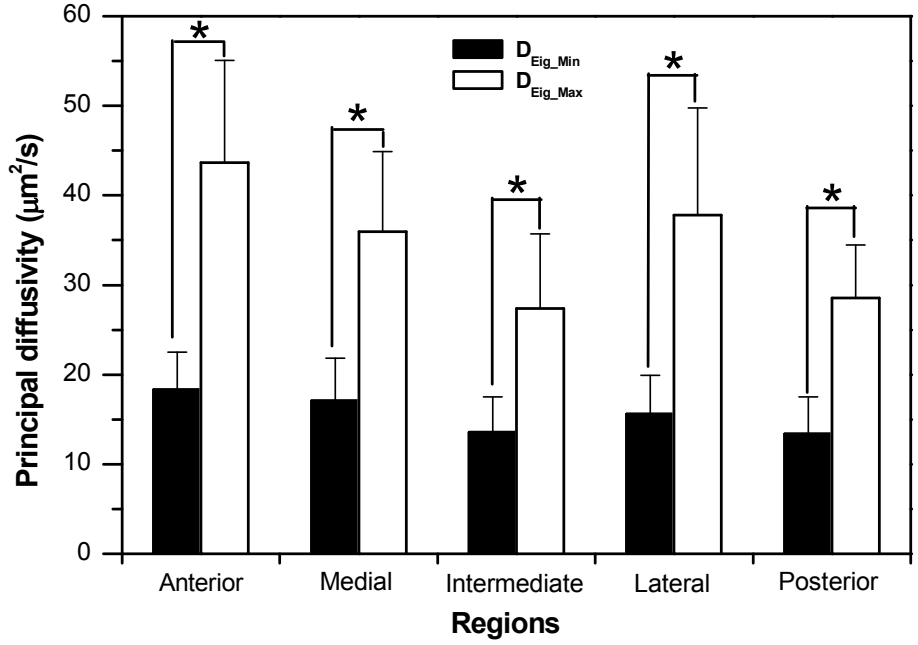
60
50
40
30
20
10
0
Principal diffusivity (μm²/s)
D_Eig_Min
D_Eig_Max
*
*
*
*
*
Anterior
Medial
Intermediate
Lateral
Posterior
Regions

(b)

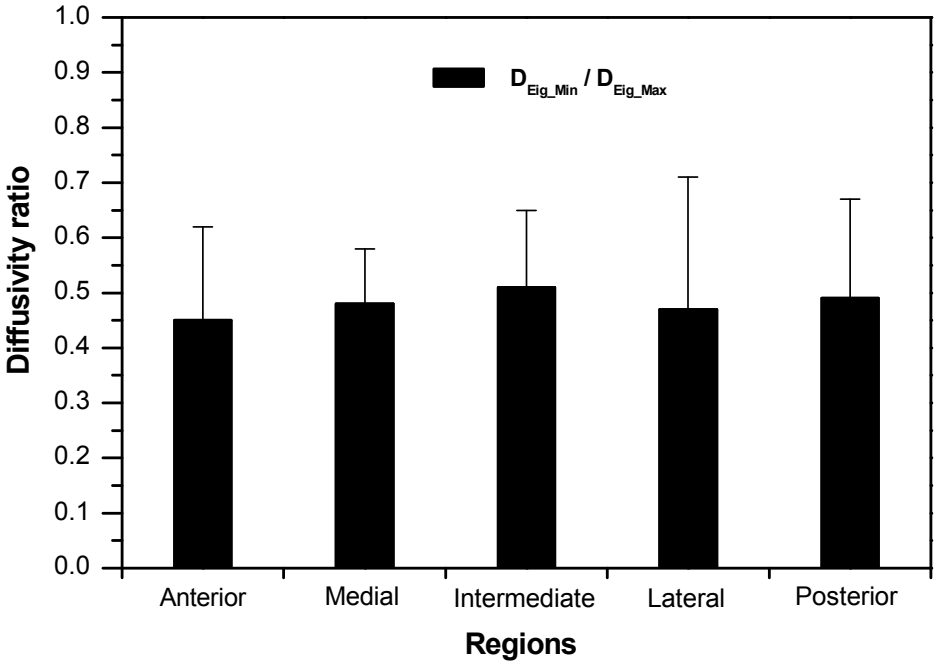

(c)

Figure 4.7 The results of statistical analysis of determined diffusion tensors in porcine TMJ disc.
(a) Characteristic diffusivities [$(D_{\text{Eig\_Min}} + D_{\text{Eig\_Max}})/2$] were significantly region-dependent (* $p < 0.05$ compared to Anterior). (b) Significant differences between $D_{\text{Eig\_Min}}$ and $D_{\text{Eig\_Max}}$ were detected in all disc regions (* $p < 0.05$). (c) The ratio of $D_{\text{Eig\_Min}}$ to $D_{\text{Eig\_Max}}$ was not region-dependent.

4.5 Discussion

In this study, a new method solely based on the SFA of FRAP images was developed to completely determine the anisotropic diffusion tensor in hydrated soft tissues. This method was used to determine the region-dependent anisotropic diffusion tensor in porcine TMJ discs.

The accuracy and robustness of our new method was validated by the computer simulated FRAP experiments. Our method demonstrated several key advantages over the previous studies on the SFA based FRAP methods for anisotropic diffusion. Most of all, it makes possible to deal with any orientation of the diffusion tensor ($\theta = 0\text{-}\pi/2$). The complete diffusion tenor, including both diagonal and off-diagonal components, can be determined using this new method.

Compared to the method recently reported by Travascio *et al.*,[17] our method is more accurate and robust. In their method, an anisotropic diffusion tensor was determined based on two independent analyses of FRAP images: the Fourier transform and the Karhunen-Loeve transform. The KLT analysis of FRAP images can determine the orientation of the diffusion tensor and by combining the FT and KLT analyses, Travascio's method can determine all components of the anisotropic diffusion tensor in a single FRAP experiment. In this study, we proposed a method solely based on the SFA to completely determine the anisotropic diffusion tensor which avoids all of the limitations imposed by KLT analysis. For example, due to the limitations of the KLT the Travascio's method is not applicable when the orientation of the diffusion tensor

coincides with the fixed coordinate system (i.e., $\theta = 0$ or $\pi/2$).[17] More importantly, the major limitation of their method, as recognized by the authors, is the robustness to deal with the imaging noise which is unavoidable in real experiments. In their simulation results the average relative errors reached 40% at $\sigma = 10$ noise level, while the average values reached 20% at $\sigma = 5$ level.[17] Under the same noise conditions the average relative errors of our method were less than 12.5% at $\sigma = 10$ level and less than 8% at $\sigma = 5$ level. It is apparent that our new method is more robust against the noise and our method only needs one image analysis (i.e., the SFA) resulting in fewer numerical errors for the determination of the diffusion tensor. In our simulation without imaging noise, the relative errors of $D_{\text{Eig\_Min}}$ were less than 1.5% [Figure 4.4(a)] while under the similar conditions, the relative errors reached 14% in simulations performed by Travascio *et al*.[17] In the above accuracy comparison, it needs to be noted that the sizes of the bleaching spot and imaging frame in this study were only about half the values of those parameters used in the study by Travascio *et al*.[17] This implies that the imaging sampling might also affect the precision of the results.

This study represents the first measurement of solute diffusion in TMJ disc tissues. The average diffusivity of 4kDa FITC-Dextran in porcine TMJ discs (26 $\mu m^2/s$) was approximately 16% of the diffusivity in water (162 $\mu m^2/s$, based on the Stokes-Einstein equation with the hydraulic radius of 1.4nm) and was comparable to the diffusivity of the similar sized solute (3kDa FITC-Dextran) in porcine articular cartilage ($75\mu m^2/s$) measured by FRAP.[5] Most recently, Benavides *et al.* reported that there is a region-dependency of water diffusion in porcine TMJ disc using diffusion tensor MRI.[167] In

the anteroposterior direction, the mean water diffusivity was higher in the anterior and posterior bands compared with the intermediate zone. In the mediolateral direction, the mean water diffusivity was higher in the medial and lateral aspects than in the center. Our study of 4kDa FITC-Dextran diffusion showed exactly the same trends.

The results of this study indicated that the diffusion rates of uncharged dextran molecules vary by region in the TMJ disc. The anterior region had higher characteristic diffusivity than the intermediate region and posterior region in the anteroposterior direction, while the medial and lateral regions had higher characteristic diffusivities than the intermediate region in the mediolateral direction. Previous studies showed that solute diffusivity in cartilaginous tissues depended on tissue water content in a manner that a decrease in the solute diffusivity occurs as tissue water content decreased,[14, 17, 132] and these findings were also observed in our study. For the porcine TMJ disc, it has been reported that along the anteroposterior axis, the anterior band (74.5±2.9%) had higher water content than the intermediate zone (73.7±3.1%) and posterior band (70.1±4.0%), while along the mediolateral axis, the medial region (75.3±2.1%) had a higher water content than the central (71.3±3.7%) and lateral (71.3±4.1%) regions.[168] The correlation between the diffusivity and tissue water content suggests that the diffusive transport in porcine TMJ discs is dependent on tissue composition. The inhomogeneous distribution of tissue components results in region-dependent diffusivity in TMJ disc tissues.

The results of this study also demonstrated that solute diffusive transport in porcine TMJ discs is highly anisotropic with the ratio of $D_{\text{Eig\_Min}}$ to $D_{\text{Eig\_Max}}$ around

0.45~0.51 across the disc. Studies on meniscus and annulus fibrosus showed that the anisotropic solute diffusion in fibrocartilage is due to the orientation of collagen fibers.[6, 17] The orientation of the largest principal component (D_{Eig_Max}) of the diffusion tensor is parallel to the direction of the bundles of collagen fibers, while the smallest principal component (D_{Eig_Min}) is perpendicular to the fibers. Inside the porcine TMJ disc, Detamore *et al.* reported that collagen fibers were well organized and had a ring-like structure around the periphery and were oriented anteroposteriorly through the intermediate zone.[168] Our results suggested that the diffusive transport in TMJ disc is not only dependent upon tissue composition but also tissue structure, especially collagen structure.

In this study, we measured diffusivities of 4kDa FTIC-Dextran (hydraulic radius equivalent to insulin)[5] to examine the region-dependent anisotropic diffusion in porcine TMJ discs. However, it is important to note that the dextran molecules have a linear structure that may not duplicate the molecular structure of other physiologically relevant molecules in the TMJ disc, which may be more globular in structure. Pluen *et al.* have shown that flexible macromolecules have greater mobility than similarly sized globular molecules in a random fiber matrix.[164] It is also important to note that the diffusion tensor was determined in the horizontal plane in this study. The diffusion in the vertical direction (*i.e.*, superior-inferior direction) could be the main pathway for nutrient transport through the TMJ disc. Therefore, in order to fully understand solute transport in the TMJ disc, it is necessary to determine the 3D diffusion tensor in each disc region and correlate it to tissue composition and structure.

In summary, a new method solely based on the SFA has been developed to determine the 2D anisotropic solute diffusion tensor in the fibrous tissues using FRAP. The accuracy and robustness of this method was validated using computer simulated FRAP experiments. The new method was applied to determine the 2D diffusion tensor of 4kDa FITC-Dextran in the porcine TMJ discs. It was determined that the diffusion of this solute in TMJ discs was inhomogeneous and anisotropic. These findings suggested that diffusive transport in TMJ disc is dependent upon tissue composition (*e.g.*, water content) and structure *(e.g.*, collagen orientation). This study provides a new method to quantitatively investigate the relationship between transport properties and tissue composition and structure. The obtained transport properties are crucial for future development of numerical models studying nutritional supply within the TMJ disc.

CHAPTER 5 RELATIONSHIP BETWEEN ANISOTROPIC DIFFUSION PROPERTIES AND TISSUE STRUCTURE IN PORCINE TME DISC

5.1 Introduction

The temporomandibular joint (TMJ) is a synovial, bilateral joint with unique morphology and function.[146] The TMJ disc has a distinctive extracellular matrix (ECM) composition and structure when compared to hyaline cartilage and other fibrocartilaginous tissues [*e.g.*, the intervertebral disc (IVD)]. The TMJ disc tissue is composed primarily of water with a significant amount of collagen (mainly type I) and a very small amount of proteoglycan.[153-157] The human TMJ disc is a large avascular structure being wider mediolaterally than anteroposteriorly (approximately 19×13 mm).[158] The nutrients required by disc cells for maintaining healthy matrix are supplied by synovial fluid at the margins of the disc as well as through nearby blood vessels at the connection to the posterior bilaminar zone.[169, 170] The balance between the rate of nutrient transport through the matrix and the rate of consumption by disc cells establishes a concentration gradient across the disc. The concentration levels of essential nutrients, such as oxygen and glucose, can profoundly affect TMJ disc cell viability, matrix synthesis, and response to inflammatory factors.[171, 172] This suggests that deviation from physiological nutrient levels in the TMJ disc due to the lack of nutrient supply may initiate tissue remodeling and matrix degradation. Although convection due to interstitial fluid flow induced by mechanical loading may affect large solute transport,[173-175] the transport of small solutes (*e.g.*, ions, oxygen, and glucose) within avascular cartilaginous tissues mainly depends on diffusion.[175, 176] The rate of solute diffusion in tissue is governed by solute diffusivities which are affected by the

composition and structure of the matrix, as well as mechanical strains on the tissue. Many studies have been conducted to determine diffusivities of various solutes in articular cartilage and IVD.[177] However, very few data of solute diffusivities are available for the TMJ disc. Recently, we examined the effect of mechanical loading on small ion diffusivity in TMJ discs using the electrical conductivity method. The results indicated that compressive strain significantly impeded solute transport in the TMJ disc.[73] Furthermore, the solute diffusivities in porcine TMJ disc were also measured by using a fluorescence recovery after photobleaching (FRAP) technique.[7] The results showed that the tissue matrix significantly hindered solute diffusion and the solute diffusivities were anisotropic (*i.e.*, orientation dependent) and inhomogeneous (*i.e.*, region dependent).[7] A recent diffusion tensor imaging (DTI) study also showed the anisotropic and region-dependent behavior of water diffusion in porcine TMJ discs.[167]

The unique transport behavior in the TMJ disc tissue may be attributed to the complex tissue composition and structure (*i.e.*, tissue morphology) of the disc. Differences in biochemical composition and structure distinguish the disc into three regions: the anterior band, intermediate zone, and posterior band.[158] Collagen fibers in the posterior band run primarily in the mediolateral direction and in the intermediate zone align predominately in an anteroposterior direction, while mixed fiber orientations have been found mainly in the anterior band. Knowledge of transport properties for small nutrient molecules (*e.g.*, oxygen and glucose) and their relationship with tissue morphology is important for elucidating the mechanism and pathways of nutrient transport in the TMJ disc and better understanding the etiology of TMJ disc degeneration.

While several studies have been published about the effect of tissue morphology on anisotropic diffusion in articular cartilage,[5] ligament,[85] knee meniscus,[17] and IVD,[17] little is known regarding the relationship between solute diffusion properties and tissue structure of the TMJ disc.

Therefore, the objective of this study was to investigate the relationship between solute diffusion properties and tissue morphology in porcine TMJ disc. We hypothesized that solute diffusion in the TMJ disc is anisotropic and inhomogeneous, and transport properties are associated with tissue morphology. The diffusivities of fluorescein in five TMJ disc regions (anterior, medial, intermediate, lateral, and posterior) were determined by a FRAP technique previously developed in our lab. The anisotropic diffusion behavior of fluorescein in the TMJ disc was investigated by measuring the diffusion coefficient in three orthogonal directions (medial-lateral, anterior-posterior, and superior-inferior) in each disc region. To investigate the relationship between tissue morphology and solute diffusivity, the three-dimensional (3D) collagen fiber structures in each disc region were examined by utilizing scanning electron microscopy (SEM). The anisotropy of fiber structures in five disc regions were quantified through the analyses of the SEM images.

5.2 Materials and Methods

5.2.1 Specimen Preparation

A total of eleven pig heads (Yorkshire, male, aged 6~8 months) were collected from a local abattoir within 2 hours of slaughter. The entire TMJ with capsule intact was removed *en bloc*. Joints were opened under a sterile dissection hood; TMJ discs were

then removed from peripheral attachments. All discs were assessed visually, and were not used if signs of degeneration were apparent. The transport properties and tissue morphology were investigated in three orthogonal orientations (*i.e.*, mediolateral, anteroposterior, and superoinferior) for each of the five different regions (*i.e.*, anterior, medial, intermediate, lateral, and posterior) (Figure 5.1). Eleven TMJ discs of the right joints were used to determine the anisotropic diffusivities via FRAP protocols. Eleven TMJ discs of the corresponding left joints were used to examine the tissue morphology via SEM. When the specimens were observed under the microscopes, the material coordinates of the samples were fixed to the microscopy coordinates [*i.e.*, mediolateral (ML) axis→X axis, anteroposterior (AP) axis→Y axis, and superoinferior (SI) axis→Z axis] in order to correlate the diffusion properties to the tissue morphology of the TMJ discs.

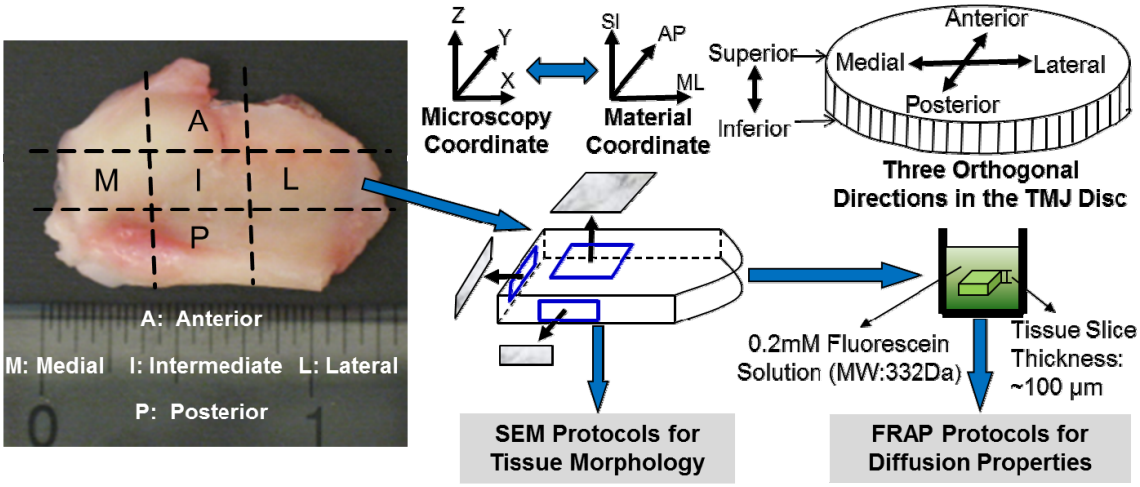

Figure 5.1 The schematic of specimen preparation and testing protocols.
Each disc was examined in five regions: anterior, intermediate, posterior, lateral and medial. In each region, solute diffusion properties and tissue morphology of these specimens were investigated in three orthogonal planes (*i.e.*, XY, ZX and ZY). The right side discs were tested by FRAP protocols for the diffusion properties and the corresponding left side discs were examined by SEM protocols for tissue morphology.

5.2.2 Diffusivity Measurement using FRAP Techniques

Three tissue blocks were harvested from each region for the diffusivity measurements (Figure 5.1). Three tissue blocks were harvested from each region for the diffusivity measurements (Figure 5.1). One tissue block was for the diffusivity measurement on the XY horizontal plane (*i.e.*, ML-AP plane), one was for the ZX vertical plane (*i.e.*, SI-ML plane), and the other one was for the ZY vertical plane (*i.e.*, SI-AP plane). The disc tissue blocks were sectioned to 100μm slices using a microtome (SM24000, Leica Microsystems GmbH, Wetzlar, Germany) with a freezing stage (Model BFS-30, Physitemp, Clifton, NJ). The specimens were marked to identify the material coordinates. The tissue slices were then immersed in a phosphate buffered saline (PBS) solution (Sigma®, St. Louis, MO) with 0.2mM fluorescein (332 Da, λ_{ex} 490 nm; λ_{em} 514 nm, Fluka-Sigma-Aldrich®, St. Louis, MO) for 48 hours. The anisotropic diffusion tensors of fluorescein in the specimens on the sectioned plane were determined using a Spatial Fourier Analysis (SFA) based FRAP technique developed in our previous study.[7] The FRAP experiments were performed on a Leica TCS-SP5 confocal laser scanning microscope (Leica Microsystems, Inc., Exton, PA) at room temperature (22ºC). Briefly, the specimens were photobleached using an Ar-488nm laser to create a circular bleached spot with a diameter of 48μm. For each FRAP measurement, 300 frames of recovery images of 128×128 pixels (387.5μm×387.5μm), plus 5 images prior to photobleaching, were acquired at a scanning rate of 0.355 seconds per frame. To minimize the contribution of the fluorescence emission of the background, pre-bleaching

images were averaged and then subtracted from the post-bleaching image series. The confocal series images were analyzed by implementing custom written codes in MATLAB (MATLAB 7.0, The MathWorks Inc., Natick, MA) to calculate the 2D solute diffusion tensor in the specimen on the section plane. For the specimen sectioned on the XY horizontal plane (*i.e.*, ML-AP plane), the diffusivities along the mediolateral (D_{ML}) and anteroposterior (D_{AP}) orientations were determined. Similarly, for the specimen sectioned on the ZX vertical plane (*i.e.*, SI-ML plane), the diffusivities along the superoinferior (D_{SI}) and mediolateral (D_{ML}) were determined. For the specimen sectioned in the ZY vertical plane (*i.e.*, SI-AP plane), the diffusivities along the superoinferior (D_{SI}) and anteroposterior (D_{AP}) orientations were determined. Finally, for each disc region, the diffusivities along the anteroposterior (D_{AP}), mediolateral (D_{ML}), and superoinferior (D_{SI}) orientations were calculated by averaging the corresponding diffusivities of the three specimens prepared from the same disc region in three orthogonal planes. The mean diffusivities [$(D_{ML}+D_{AP}+D_{SI})/3$] in each region were calculated as well.

5.2.3 Fractional Anisotropy

To quantify the solute diffusion anisotropy, the fractional anisotropy (FA) [178] was calculated for each disc region by following the equation:

$$FA = \sqrt{\frac{3}{2}} \frac{\sqrt{(D_{ML} - D_{Mean})^2 + (D_{AP} - D_{Mean})^2 + (D_{SI} - D_{Mean})^2}}{\sqrt{D_{ML}{}^2 + D_{AP}{}^2 + D_{SI}{}^2}} \qquad (5.1)$$

Here, the diffusivities of D_{AP}, D_{ML}, and D_{SI} were used to represent the three eigenvalues of the 3D diffusion tensor. Our data showed that values of the off-diagonal

components of the diffusivity tensor in the material coordinates were much smaller (at least one order of magnitude smaller) compared to the diagonal components (*i.e.,* D_{AP}, D_{ML}, and D_{SI}). The FA is a scalar and rotationally invariant quantity that describes the degree of anisotropy of diffusion in a tissue sample. A FA value of zero means that diffusion is isotropic (*i.e.* it is equally restricted in all directions). In contrast, a FA value of one represents that diffusion occurs only along one axis and is fully restricted along all other directions.

5.2.4 Tissue Structure Examination using SEM

To determine the fiber structure on the horizontal plane (*e.g.*, XY plane), a whole disc sample was microtomed to remove the concave shape of the disc and expose the collagen fiber structure on the horizontal plane which is parallel to the superior surface. To determine the fiber structure on the two vertical planes (*e.g.*, ZX and ZY planes), the discs were cut mediolaterally or anteroposteriorly to uncover the tissue structure on the vertical planes. The specimens were marked to distinguish the different regions and identify the material coordinates. The specimens were then fixed with a solution of 2.5% glutaraldehyde in PBS at 4°C for 72 hours. The fixed tissues were dehydrated using a graded series of ethanol. Afterwards, the specimens were dried by immersion in hexamethyldisilazane (HMDS) solution. In order to enhance the contrast of SEM images, the specimens were coated with a layer (20μm thickness) of gold. Finally, the coated specimens were examined via SEM (Hitachi TM-1000) at 3000x magnification.

5.2.5 Collagen Fiber Alignment Measurement

The SEM images in each disc region were used to assess the degree of collagen fiber alignment. The fiber alignment measurement was characterized by using an ImageJ (Version 1.45s, by Wayne Rasband, National Institutes of Health, USA) plug-in (OrientationJ) that calculates the directional coherency coefficient of the collagen fibers.[179, 180] The coherency coefficient indicates if the local fibers are aligned or not. A coherency coefficient close to one demonstrates a significantly coherent orientation of the local fibers in one direction. A coherency coefficient close to zero represents no dominant orientation of the fibers.[179]

5.2.6 Statistical Analysis

One-way ANOVA and Tukey's *post hoc* tests were performed on D_{ML}, D_{AP} and D_{SI} to examine in the anisotropy of solute diffusion in each disc region. The mean solute diffusivities, diffusion fractional coefficients, and fiber coherency in the five disc regions were also analyzed using the same statistical methods to examine the regional effect on the solute diffusion rate, diffusional anisotropy, and fiber alignment in porcine TMJ discs. SPSS 16.0 software (SPSS Inc., Chicago, IL) was used for all statistical analyses and significant differences were reported at p-values < 0.05.

5.3 Results

5.3.1 Solute Diffusivities in the TMJ discs (FRAP)

The diffusivities of fluorescein in each TMJ disc region were significantly anisotropic, except the anterior region (Figure 5.2). In the medial region, anteroposterior

diffusivity [mean, 95% confidence interval (CI), 65.2 (49.4-81.1) $\mu m^2/s$] was significantly larger than the diffusivities in the mediolateral [51.6 (36.4-66.7) $\mu m^2/s$, p = 0.031] and superoinferior [50.8 (35.9-65.7) $\mu m^2/s$, p = 0.023] directions. In the lateral region, anteroposterior diffusivity [60.2 (45.4-75.0) $\mu m^2/s$] was also significantly larger than the diffusivities in the mediolateral [48.1 (36.7-59.5) $\mu m^2/s$, p = 0.023] and superoinferior [39.7 (26.9-52.5) $\mu m^2/s$, $p < 0.0001$] directions. Similarly, in the intermediate region, anteroposterior diffusivity [64.3 (48.3-80.4) $\mu m^2/s$] was significantly larger than the diffusivities in the mediolateral [50.7 (38.8-62.5) $\mu m^2/s$, p = 0.013] and superoinferior [43.7 (31.1-56.4) $\mu m^2/s$, p = 0.0001] directions. In contrast, in the posterior region, mediolateral diffusivity [72.0 (56.8-87.2) $\mu m^2/s$] was significantly larger than anteroposterior [49.1 (34.7-63.6) $\mu m^2/s$, p = 0.0003] and superoinferior diffusivity [57.7 (42.9-72.5) $\mu m^2/s$, p = 0.04]. However, in the anterior region, there were no significant differences in diffusivity between anteroposterior [67.8 (50.1-85.6) $\mu m^2/s$], mediolateral [62.6 (43.7-81.4) $\mu m^2/s$], and superoinferior [66.3 (46.3-81.8) $\mu m^2/s$] directions (ANOVA, p = 0.66). The degree of the diffusional anisotropy was quantified by the fractional anisotropy in the five disc regions (Figure 5.4). The value of fractional anisotropy in the anterior region [0.13 (0.10-0.16)] was significantly lower than those of the medial [0.24 (0.15-0.34)], lateral [0.26 (0.19-0.35)], intermediate [0.28 (0.19-0.38)], and posterior [0.30 (0.20-0.41)] regions (ANOVA, p = 0.0002).

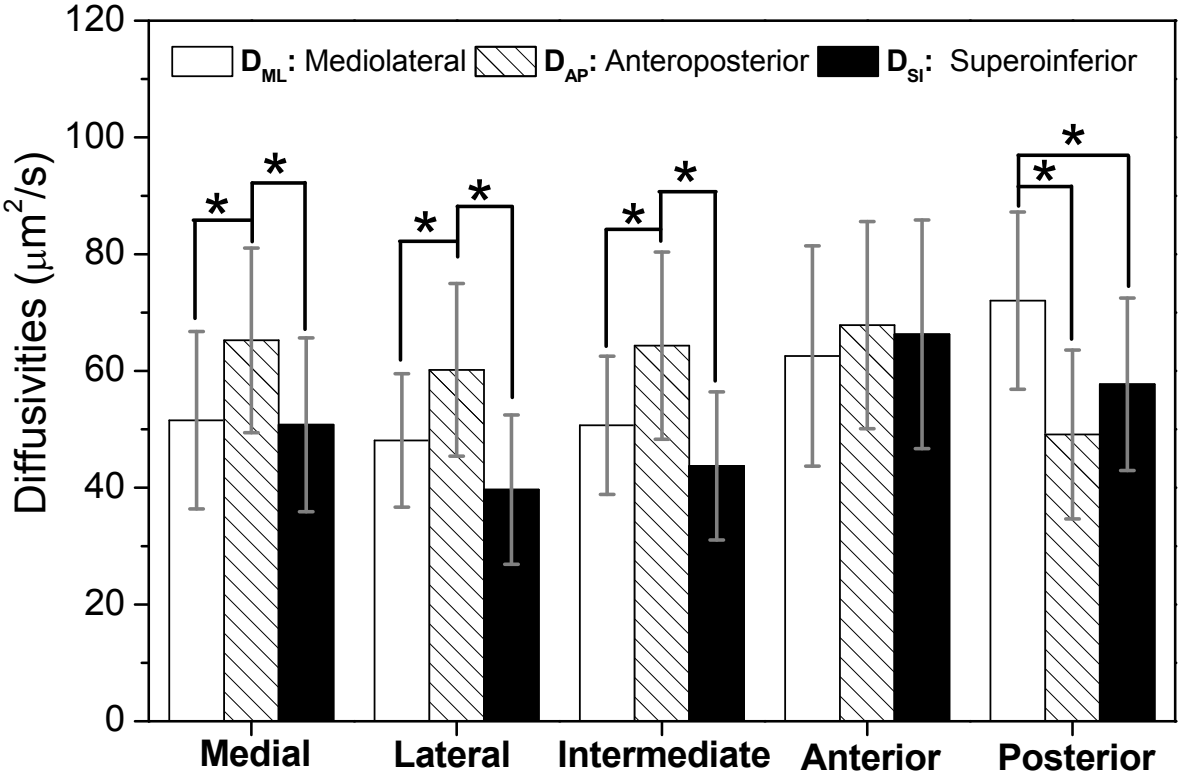

Figure 5.2 The results of anisotropic solute diffusivities in porcine TMJ discs (The data shown are means ± 95% CIs).
In the medial, lateral and intermediate regions, anteroposterior diffusivity was significantly larger than the diffusivities in the other two directions (* $p < 0.04$ compared to D_{AP}). The mediolateral diffusion predominated in the posterior region (* $p < 0.05$ compared to D_{ML}). In the anterior region, there were no significant differences for diffusivity between the orientations likely due to the multi-directional fiber arrangement.

The mean diffusivities of fluorescein in porcine TMJ discs were region-dependent (ANOVA, p = 0.013). The anterior region [65.6 (49.3-81.8) $\mu m^2/s$] had significantly higher mean diffusivity than the intermediate region [53.5 (41.0-66.0) μm2/s, p = 0.048] and lateral region [51.2 (39.0-63.3) $\mu m^2/s$, p = 0.01]. Moreover, the anterior region also had higher value of mean diffusivity than the medial region [56.2 (42.7-69.7) $\mu m^2/s$, p = 0.221] and posterior region [58.7 (44.9-72.5) $\mu m^2/s$, p = 0.544], although the differences were not statistically significant (Figure 5.3). The overall average diffusivity of fluorescein cross the TMJ disc was 57.0 (43.0-71.0) $\mu m^2/s$.

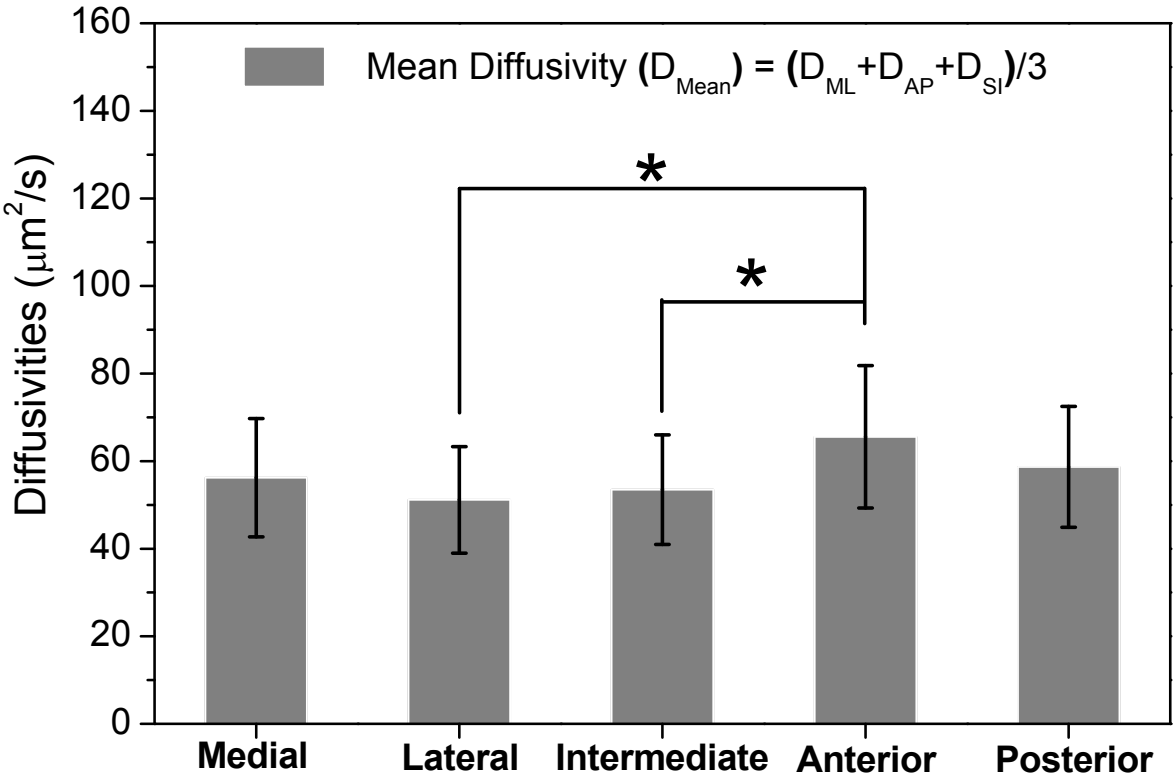

Figure 5.3 The results of inhomogenous solute diffusivities in porcine TMJ discs (The data shown are means ± 95% CIs).
Region-dependent diffusion properties were found in the TMJ disc. The anterior region had higher mean diffusivity than the lateral and intermediate regions (* ANOVA, $p <$ 0.02 compared to anterior) probably due to the higher water content and random fiber arrangement in this region.

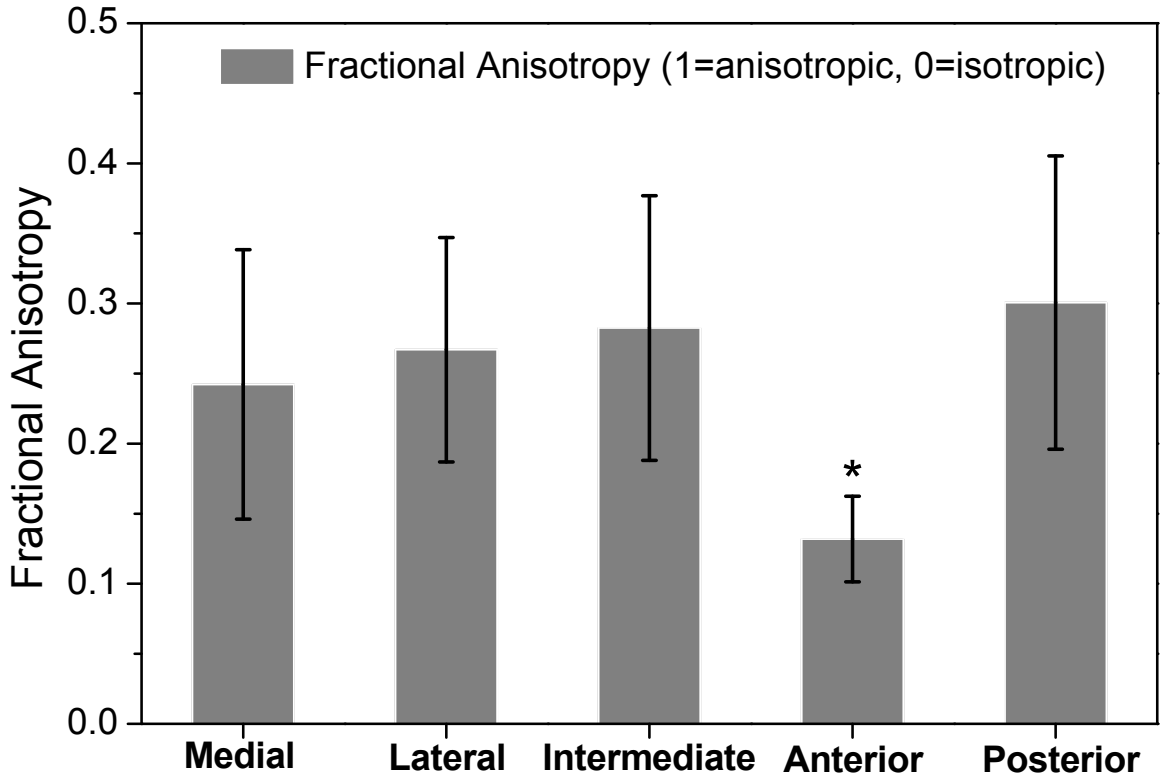

Figure 5.4 The results of solute diffusional anisotropy in five regions of the TMJ disc (The data shown are means ± 95% CIs).
The results of fractional anisotropy showed the region-dependent solute diffusion properties in the TMJ disc. The anterior region had lower FA than other four regions (*ANOVA, $p = 0.0002$).

5.3.2 Collagen Fiber Orientations (SEM)

Typical SEM images of porcine TMJ discs in the horizontal XY, vertical ZX, and vertical ZY sections (Figure 5.6) showed differences in the organization of collagen fibers among five disc regions. In the horizontal XY plane (*i.e.*, ML-AP plane), the collagen fibers aligned anteroposteriorly in the medial, intermediate, and lateral regions while fibers were aligned mediolaterally in the posterior region. Interestingly, fibers aligned in both anteroposterior and mediolateral directions were found in the anterior region [Figure 5.6(a)]. In the vertical ZX plane (*i.e.*, SI-ML plane), there was no clear fiber orientation in the medial, intermediate and lateral regions, likely due to their orientation perpendicular to the sectioned plane. There was also no clear fiber orientation in the anterior region. Conversely, the fibers clearly aligned in the mediolateral direction in the posterior region [Figure 5.6(b)]. In the vertical ZY plane (*i.e.*, SI-AP plane), anteroposterior fibers were found again in the medial, intermediate, and lateral regions while fibers with two orientations existed in the anterior region. There was no clear fiber orientation in the posterior region, likely due to fibers being oriented perpendicular to the section plane [Figure 5.6(c)].

The degree of collagen fiber alignment was quantified by the coherency coefficient in the five disc regions (Figure 5.5). The results indicated that the values of the coherency coefficient were region-dependent in the TMJ disc. The collagen fibers highly aligned in the medial [0.43 (0.33-0.53)], lateral [0.42 (0.37-0.48)], intermediate [0.41 (0.33-0.50)], and posterior [0.39 (0.36-0.42)] regions. In contrast, the anterior [0.12 (0.06-0.17)] region had a significant lower coherency coefficient than the other four

regions (ANOVA, $p < 0.0001$), likely due to the multi-directional fiber arrangement in this region.

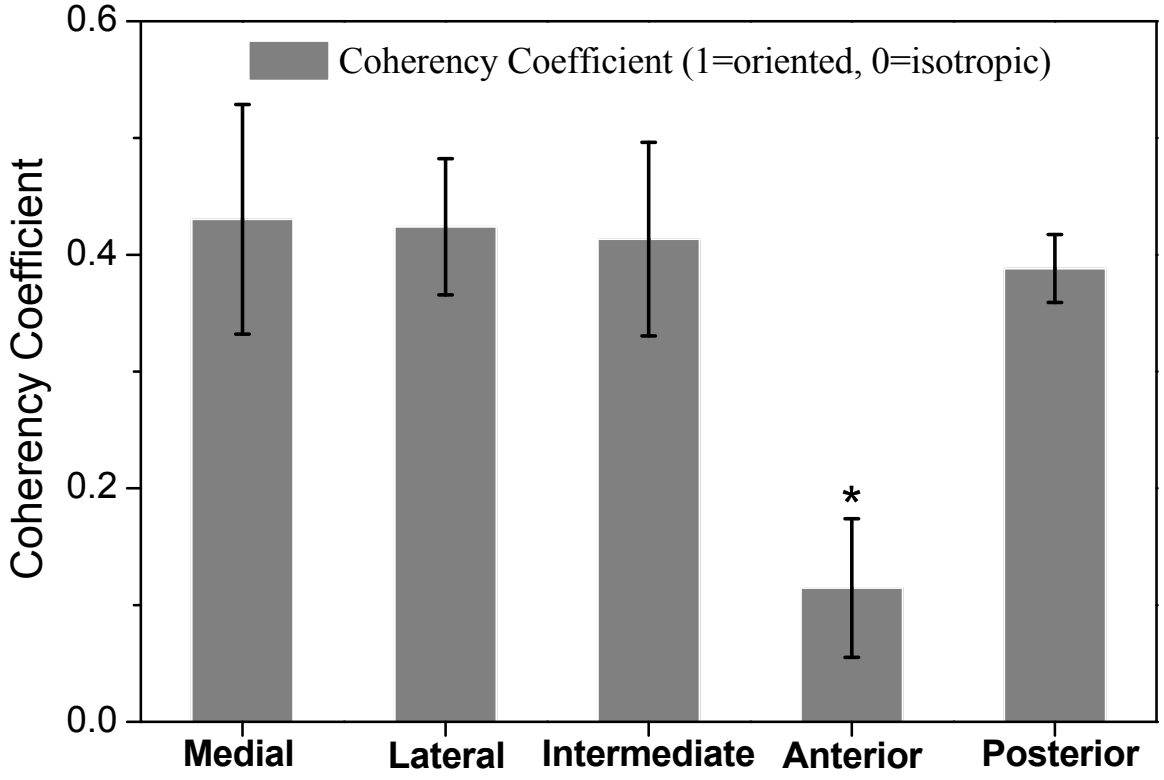

Figure 5.5 The results of collagen fiber alignment anisotropy in five regions of the TMJ disc (The data shown are means ± 95% CIs).
The measurements of coherency coefficient demonstrated the region-dependent collagen fiber alignment properties in the TMJ disc. The anterior region had lower coherency coefficient than other four regions (* ANOVA, $p < 0.0001$) probably caused by the random fiber arrangement in the anterior region.

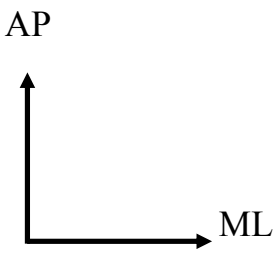

Horizontal XY plane

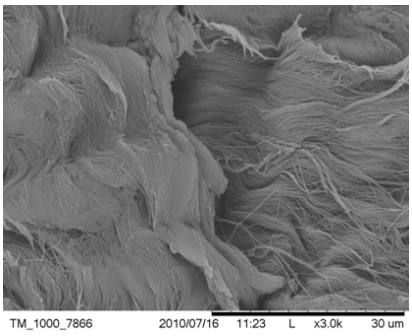

Anterior

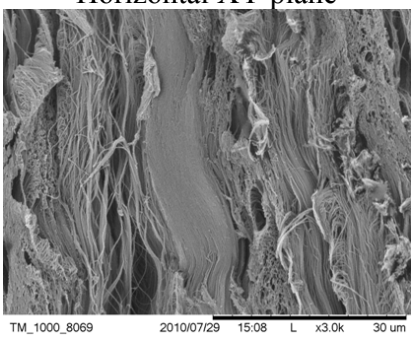

Medial

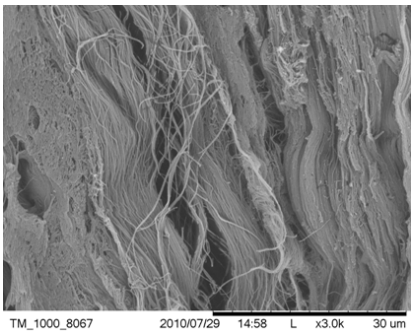

Intermediate

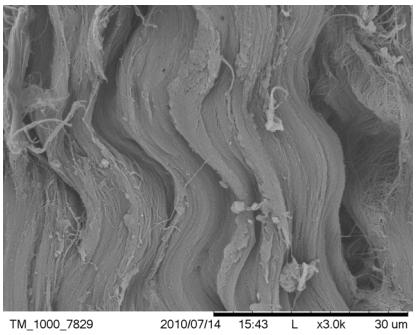

Lateral

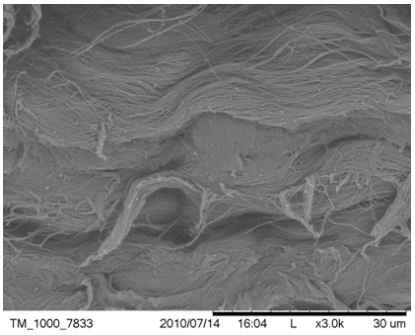

Posterior

(a)

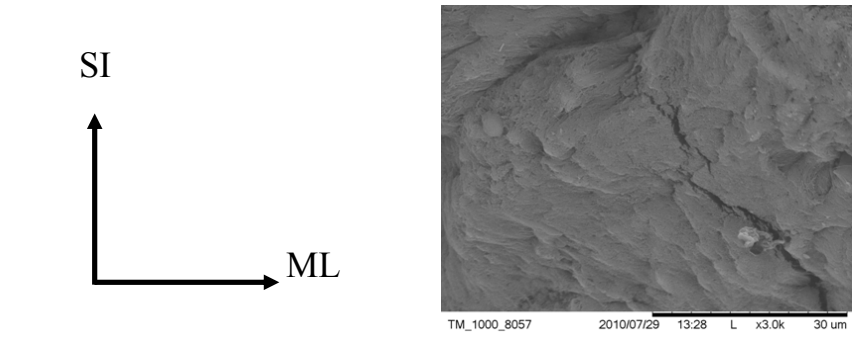

Vertical ZX plane Anterior

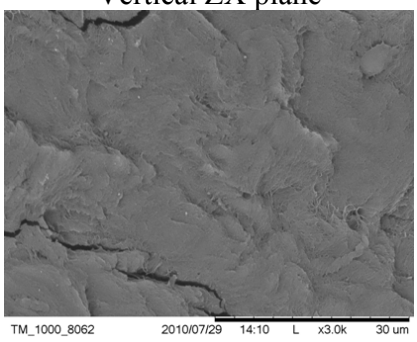

Medial

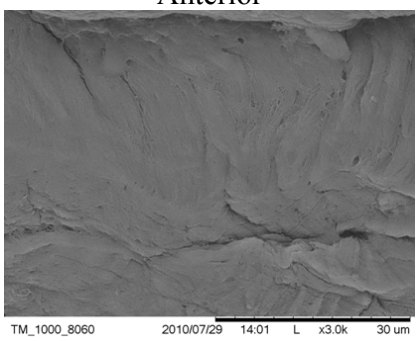

Intermediate

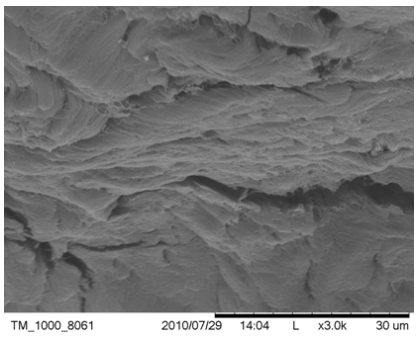

Lateral

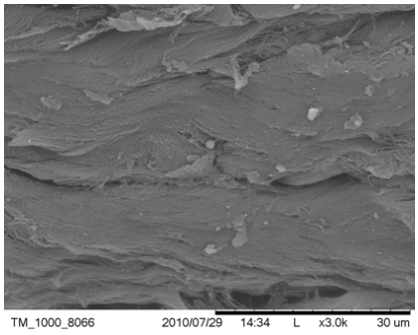

Posterior

(b)

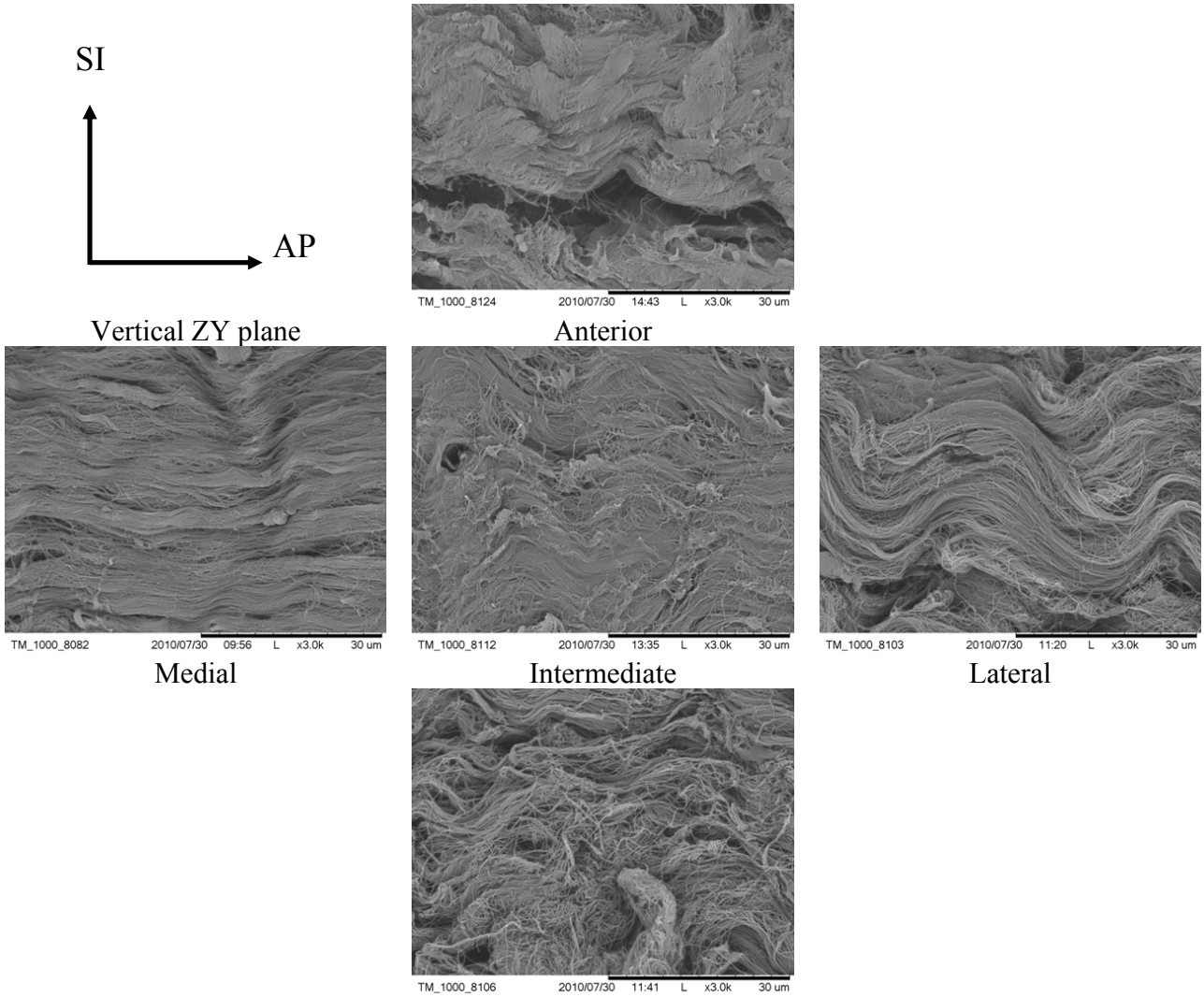

Figure 5.6 SEM images of collagen fiber orientations in the TMJ disc.
In the XY plane, the collagen fibers aligned anteroposteriorly in the medial, intermediate and lateral regions. The collagen fibers run mediolaterally in the posterior region and fibers in both directions were found in the anterior region. (b) In the ZX plane, there was no clear fiber orientation in the anterior, medial, intermediate and lateral regions, but the fibers in the posterior region aligned mediolaterally. (c) In the ZY plane, anteroposterior fibers were found again in the medial, intermediate and lateral regions, and fibers with both orientations existed in the anterior region and were randomly distributed in the posterior region.

5.4 Discussion

The 3D solute diffusion properties and tissue morphology in porcine TMJ discs were determined in this study by using FRAP and SEM techniques, respectively. The results of the FRAP measurements demonstrated that the solute diffusion in porcine TMJ discs was anisotropic. Moreover, the degrees of the diffusional anisotropy and main orientations of diffusion were region-dependent. The SEM results showed that the collagen fiber structure in the TMJ discs was highly organized and the degree and orientation of collagen fiber alignment were region-dependent as well. The 3D anisotropic diffusion properties were strongly correlated with tissue morphology (*i.e.*, collagen fiber structure) in each disc region.

The collagen fiber orientations observed by SEM in this study were in agreement with the experimental results reported in the literature. Detamore *et al.* found collagen fibers inside the porcine TMJ discs have a ring-like structure around the periphery and are oriented anteroposteriorly through the intermediate zone.[168] The anterior band has the merging of anteroposterior fibers with mediolateral fibers and the collagen fibers primarily align in a mediolateral direction within the posterior region. The collagen fibers in human and other animal TMJ discs [161, 181-183] have similar structures as the results shown in this study.

The mean diffusivity of fluorescein across the TMJ disc measured in this study was comparable to the values in other fibro-cartilaginous tissues (*e.g.*, intervertebral disc) (Table 5.1). The diffusivity of fluorescein was lower than that of ions (Na^+ and Cl^-),[73]

but higher than that of 4kDa FITC-dextran [7] in porcine TMJ discs determined in our previous studies (Table 5.1). This was expected since the fluorescein molecular weight lies in between the other solute weights. The results of this study demonstrated that the solute diffusion in the TMJ disc was highly anisotropic, which was also found in our previous study examining 2D anisotropic diffusion in the horizontal X-Y plane.[7] This study of 3D anisotropic solute diffusion further indicated that the main diffusion directions were greatly associated with the main collagen fiber orientations. In the medial, intermediate, and lateral regions, the fluorescein diffusion along the fiber orientation (*i.e.*, anteroposterior direction) was significantly faster than the diffusion transverse to the fiber orientation (*i.e.*, mediolateral and superoinferior directions). In the posterior regions (*i.e.*, posterior band), the fluorescein diffusion along the fiber orientation (*i.e.*, mediolateral direction) was significantly faster than the diffusion transverse to the fiber orientation (*i.e.*, anteroposterior and superoinferior directions) as well. In contrast, the diffusion in the anterior region was mostly isotropic, likely due to the multi-directional fiber arrangements.

Furthermore, the degree of collagen fiber alignment was correlated to the degree of diffusional anisotropy. The collagen fibers were highly aligned in the medial, lateral, intermediate, and posterior regions. However, the anterior region had a significantly lower coherency coefficient than the other four regions (Figure 5.5). Correspondingly, the value of fractional anisotropy in the anterior region was significantly lower than those of the other disc regions (Figure 5.4). Similar results were also found by DTI measurements of 3D water diffusion in porcine TMJ discs.[167] However, the fractional

anisotropy of water diffusion (0.36-0.55) in the DTI study was higher than the fluorescein diffusion (0.13-0.30) in this study. The possible reason for this difference might be the age difference of the animals used between the DTI study (12-16 months) and this study (6-8 months). The existence of more aligned collagen fibers in the skeleton matured pigs may cause a relatively higher fractional anisotropy. The studies on bovine [17] and human [6] annulus fibrosus (AF) also showed highly anisotropic fluorescein diffusion properties exist because of the well-organized tissue structures.

The mean diffusivity of fluorescein in the TMJ disc is about 10% of its diffusivity in water, indicating the solute diffusion is significantly hindered by the ECM of the tissue. The comparison of mean diffusivities between different regions showed the inhomogeneous solute diffusion properties in the TMJ disc. The anterior region had a higher mean diffusivity of fluorescein than the other disc regions probably due to the high water content. Our previous study showed that the ion diffusivities were highly associated with the tissue water content in porcine TMJ discs.[73] The anterior region has the highest ion diffusivities as well as tissue water content. Studies [6, 14, 132] on other cartilaginous tissues also showed that the solute diffusivity is positively correlated to the tissue water content. The diffusivity was lower in the TMJ disc when compared to AF (Table 5.1) likely due to the low water content in the TMJ disc. Therefore, in addition to the tissue structure, the tissue composition also could influence the solute diffusion properties in hydrated soft tissues.

In this study, fluorescein was utilized as a molecular probe to investigate the relationship between solute diffusion properties and tissue morphology. The molecular

weight of fluorescein (332 Da) is about two times higher than the molecular weight of glucose (180 Da). Generally, the tissue ECM has a greater impact on the diffusivity of larger solutes.[177] Therefore, it is necessary to determine the impact of tissue ECM on the diffusivities of other essential solutes, such as oxygen and glucose. In this study, the measurement of 3D anisotropic diffusivities was achieved by measuring 2D diffusion tensors in three orthogonal tissue sections. However, this tissue sectioning process might alter the collagen fiber alignment. Therefore, it is necessary to develop a FRAP technique to measure local 3D solute diffusion tensor without tissue sectioning. Although pigs have been considered as a good animal model to study human TMJ disc mechanics, the determination of the solute diffusivity on human samples is also needed.

Table 5.1 The diffusivities (mean ± standard deviation) of different solutes in various fibrocartilaginous tissues (unit: $\mu m^2/s$).

Type of tissues and species	Type of Solute	Diffusivities	References
Porcine TMJ disc	Chloride ion	439.5 ± 88.6	73
	Sodium ion	316.7 ± 63.8	
Porcine TMJ disc	FITC-Dextran (4K Da)	26.1 ± 4.3	7
Porcine TMJ disc	Fluorescein	57.0 ± 20.9	Current study
Bovine AF	Fluorescein	111.2 ± 33.3	17
Human AF	Fluorescein	153.0 ± 54.5	6

5.5 Conclusion

In summary, this study investigated the relationship between small solute diffusion properties and tissue morphology in porcine TMJ discs. Both FRAP and SEM techniques were utilized to determine the 3D solute diffusion properties and collagen fiber orientations, respectively. It was found that the diffusion of fluorescein in the TMJ disc was anisotropic and inhomogeneous. This suggests that tissue structure (*i.e.*, collagen fiber alignment) and composition (*e.g.*, water content) could be key factors affecting the solute diffusion properties within TMJ discs. The fluorescein diffusion along the fiber orientation was significantly faster than the diffusion transverse to the fiber orientation. Interestingly, the quantitative measurements showed the degree of diffusional anisotropy was positively correlated the degree of collagen fiber alignment, which strongly indicated the anisotropic diffusion properties were highly associated with tissue morphology. Furthermore, this study also demonstrated that the regional difference in tissue composition resulted in the region-dependent solute diffusion properties. This study has provided a baseline investigation on the relationship between solute transport properties and tissue morphology. These findings are important for understanding transport properties as well as further developing numerical models on nutritional supply within the TMJ disc.

CHAPTER 6 THREE-DIMENSIONAL ANISOTROPIC DIFFUSION MEASUREMENTS BY MP-FRAP TECHNIQUE

6.1 Introduction

Fluorescence recovery after photobleaching (FRAP) is a versatile and widely used tool for the determination of local diffusion properties within solutions, cells, tissues, and biomaterials. Due to the high spatial resolution, FRAP offers the possibility to microscopically examine a specific region of a sample. For instance, the hindered solute diffusion properties in the mitochondrial matrix have been studied using FRAP [184]. The diffusion properties of macromolecules in the hydrogels were measured by FRAP to investigate the effect of molecular configurations on the transport properties [164]. Moreover, this technique was also utilized in the tumor tissue study which showed that the structure and orientation of collagen fibers in the tumor extracellular matrix (ECM) leads to diffusion anisotropy [131].

The basic principle of FRAP is based on photobleaching the fluorescence of molecular probes and analyzing the recovery of the photobleached area. To date, most FRAP analyses are based on the method proposed by Axelrod *et al.* by analyzing the FRAP data in the spatial domain over time to mainly determine the two-dimensional (2D) and isotropic diffusion [13]. Another approach for 2D FRAP analysis is based on the spatial Fourier analysis (SFA) of the recovery images in the frequency domain and has the advantage of potential detection of anisotropic diffusion [6, 7, 14-17, 101]. Tsay and Jacobson, using SFA on FRAP images, developed a method for the determination of 2D diffusion tensor [15]. Most recently, Travascio *et al.* [17] reported a study on calculating an anisotropic diffusion tensor based on frequency analyses of FRAP images. This

method has been applied to characterize 2D anisotropic diffusion in knee meniscus and intervertebral disc (IVD) tissues [6, 17]. Shi *et al.* proposed another FRAP technique solely based on the SFA to completely determine the 2D anisotropic diffusion tensor. The anisotropic solute diffusion in the temporomandibular joint (TMJ) disc was found by utilizing this technique [7].

The dramatic development of confocal and multiphoton laser scanning microscopy (CLSM and MPLSM) in the last two decades has made the FRAP technique become the standard tool to measure the solute diffusion properties in the biological samples. Many three-dimensional (3D) FRAP studies have started to compensate the effect of axial diffusion by adding the diffusion in the z direction to their mathematical models, but they have still assumed the diffusion is isotropic (*i.e.*, the diffusivities are identical in all directions), so only a scalar diffusion coefficient was adopted to characterize the diffusion properties in their models.

A CLSM-based 3D FRAP model was first devised for use with objective lenses of low numerical aperture (NA) by Blonk *et al.* [11]. Wedekind et al. [83] developed a FRAP technique, referred to as line-scanning microphotolysis, (LINSCAMP) for the measurement of molecular transport at a high spatial and temporal resolution. Kubitscheck *et al.* [136] extended LINSCAMP from 2D thin cell membranes to 3D thick samples by considering the complicated geometries of 3D diffusion measurements. Later on, Braeckmans *et al.* presented a quantitative FRAP model for use with the CLSM by photobleaching a long line segment, named line FRAP [137]. This technique possesses the advantage of a small bleaching region, thus it's perfectly suitable to measure the

faster and more site-specific diffusion in the intracellular space. However, for the diffusion studies in the relatively larger bulk samples such as biological solutions, gels and tissue ECM, disk-FRAP technique proposed by Braeckmans *et al.* [23] exhibits the advantages of higher signal-to-noise ratio (SNR) and more possibilities to be applied on the common commercial CLSMs.

In the recent multiphoton-based photobleaching experiments, due to the non-linear optical phenomenon, only the fluorophore within the focal spot was photobleached and the photobleaching profile yielded a sharp and well-defined 3D geometry [135, 144]. The multiphoton fluorescence recovery after photobleaching (MP-FRAP) can be implemented within thick samples and the deeper penetration of multiphoton imaging [185] allows MP-FRAP to be realized deeply within scattering samples [130, 186].

The theoretical framework of MP-FRAP was firstly presented by Brown et al. in 1999 [12], MP-FRAP experiments were performed with a stationary laser beam and spot-bleaching protocol to measure the mobility of fluorescent molecule with spatial resolution of a few microns. However, this method only works for the isotropic diffusion measurements. Sullivan *et al.* [186] improved the initial MP-FRAP model by additionally considering the effects of convective flows within the system. This diffusion-convection model extended MP-FRAP technique to simultaneously measure the diffusion coefficient and flow speed within tumor vessels. Due to the non-neglectable molecule diffusion during the photobleaching pulse and photobleaching during the recovery in some situations, Waharte *et al.* [141] used a new numerical simulation model to interpret the MP-FRAP data with taking into account the spatial depletion and

observational photobleaching in the analysis. This study further improved the accuracy of MP-FRAP technique which can determine the millisecond dynamics of proteins in volumes smaller than $1\mu m^3$ [141].

Meanwhile, FRAP techniques based on scanning laser beam of multiphoton microscope have also been developed in several studies. Schnell *et al.* [143] determined the bleaching profile of scanning multiphoton excitation by using the convolution of the point spread function (PSF) and a circular scanning area. Mazza *et al*. [145] fully accomplished the mathematical model of a FRAP method based on multiphoton photobleaching of a large uniform disk which was generated by a scanning protocol. In this study, by photobleaching a large area, diffusion along the optical axis can be detected separately, offering a potential opportunity for investigating anisotropic diffusion.

So far, most MP-FRAP models and techniques focus on the measurements of 3D solute diffusion in volumes of a few cubic micrometers due to the dominant applications of this technique are to study protein mobilities within the intracellular structures. A general assumption made for the interpretation of these experimental data is that the diffusion is isotropic and a scalar diffusion coefficient D could fully characterize the diffusion properties of molecules of interest. However, this assumption is difficult to be satisfied when the diffusion is examined in a larger scale, such as a tissue level [142]. The common observational volume in tissue diffusion studies is more than $100\times100\times100\mu m^3$ and also includes very complex biological structures (*e.g.*, the collagen fiber alignment), therefore, the anisotropic diffusion model is more appropriate to quantify the diffusion process by applying anisotropic diffusion tensor in a large 3D tissue space.

Fourier analysis has showed a decent capability to calculate the 2D anisotropic diffusion tensor in the cartilaginous tissues [6, 7, 17], it's reasonable to extend it to 3D diffusion measurements. However, to our knowledge, there are no 3D models for anisotropic diffusion measurements by using SFA and multiphoton excitation photobleaching experiments. Thus, the goal of this study was to develop the mathematical theory and technique of 3D MP-FRAP with SFA to determine the anisotropic solute diffusion tensors in the solutions and cartilaginous tissues (e.g., ligament).

In this article, we firstly derived the mathematical theory of MP-FRAP model with 3D anisotropic diffusion tensor and SFA. Next, we applied this analysis to computer simulated 3D anisotropic FRAP data in order to validate the method. After that, we showed a throughout experimental validation of model by measuring the diffusion of FITC-Dextran in the glycerol solutions with different concentrations. And finally, an application example was reported in which this new method is adopted to characterize 3D anisotropic solute diffusion tensors in the porcine ligament tissues.

6.2 Theory

6.2.1 Solving 3D Diffusion Equation by SFA

Diffusional transport is governed by Fick's second law in 3D and the partial differential equation becomes:[19]

$$\frac{\partial}{\partial t} C(x, y, z, t) = \nabla \bullet \{\mathbf{D}[\nabla C(x, y, z, t)]\} \tag{6.1}$$

where (x,y,z) are the spatial coordinates of the imaging system and t is the time. The function $C(x, y, z, t)$ represents the spatial concentration distribution of solute in the X-

Y-Z coordinates and **D** is the diffusion tensor which is assumed symmetric. Within the observation field of MP-FRAP experiments, it is assumed that the diffusion tensor (**D)** is independent of position and time. Therefore, equation (6.1) could be rewritten as:

$$\frac{\partial}{\partial t}C(x,y,z,t) = D_{xx}\frac{\partial^2 C(x,y,z,t)}{\partial x^2} + D_{yy}\frac{\partial^2 C(x,y,z,t)}{\partial y^2} + D_{zz}\frac{\partial^2 C(x,y,z,t)}{\partial z^2} + 2D_{xy}\frac{\partial^2 C(x,y,z,t)}{\partial x \partial y} + 2D_{xz}\frac{\partial^2 C(x,y,z,t)}{\partial x \partial z} + 2D_{yz}\frac{\partial^2 C(x,y,z,t)}{\partial y \partial z} \tag{6.2}$$

where D_{xx}, D_{yy}, D_{zz}, D_{xy}, D_{xz}, and D_{yz} are six independent components of **D** in the (x,y,z) coordinate system.

Given $\widetilde{C}(u,v,w,t) = \int_{-\infty}^{\infty}\int_{-\infty}^{\infty}\int_{-\infty}^{\infty} C(x,y,z,t)e^{-i2\pi(ux+vy+wz)}dxdydz$ is the Fourier transform of $C(x,y,z,t)$, with an arbitrary initial condition and a boundary condition that $C(x,y,z,t)$ is a constant as $(x,y,z) \rightarrow \pm\infty$,equation (6.2) can be solved by using 3D SFA in the frequency domain [14-17, 101] , which are the similar strategies in the 2D condition:

$$\frac{\widetilde{C}(u,v,w,t)}{\widetilde{C}(u,v,w,0)} = \exp\left[-4\pi^2(u^2+v^2+w^2)D(u,v,w)t\right] \tag{6.3}$$

where $\widetilde{C}(u,v,w,0)$ is the initial solute concentration and $D(u,v,w)$ represents the diffusion coefficient in the Fourier space (with frequencies *u*, *v, and w*) and is defined as:

$$D(u,v,w) = \frac{u^2D_{xx} + v^2D_{yy} + w^2D_{zz} + 2uvD_{xy} + 2uwD_{xz} + 2vwD_{yz}}{u^2+v^2+w^2} \tag{6.4}$$

The function $D(u,v,w)$ can be determined by curve-fitting the light intensity of a time series of 3D fluorescence recovery image stacks in the Fourier space to equation (6.3).

6.2.2 Averaging the Diffusivity in the Frequency Domain over a Shell

The diffusivity $D(u,v,w)$ can be averaged over a shell of a spherical surface in the frequency domain. The geometry of a shell is defined in the Figure 6.1 by three parameters (i.e., radius $a=\sqrt{u^2+v^2+w^2}$, polar angle $\theta=\arccos^{-1}(w/a)$, and azimuthal angle $\varphi=\arctan(v/u)$).

When φ and θ ranges from α_1 to β_1 and α_2 to β_2 respectively, $D_{\alpha_1,\beta_1,\alpha_2,\beta_2}$, representing the average of $D(u,v,w)$ over a shell, can be given as:

$$D_{\alpha_1,\beta_1,\alpha_2,\beta_2}=\int_{\alpha_2}^{\beta_2}\int_{\alpha_1}^{\beta_1} D(\varphi,\theta)\sin\theta d\varphi d\theta \Big/ \left[(\beta_1-\alpha_1)(\cos\alpha_2-\cos\beta_2)\right] \tag{6.5}$$

where

$$\begin{aligned} D(\varphi,\theta) = {} & D_{xx}\sin^2\theta\cos^2\varphi + D_{yy}\sin^2\theta\sin^2\varphi + D_{zz}\cos^2\theta \\ & + D_{xy}\sin^2\theta\sin 2\varphi + D_{xz}\sin 2\theta\cos\varphi + D_{yz}\sin 2\theta\sin\varphi \end{aligned} \tag{6.6}$$

Based on equations (6.5) and (6.6), the average of $D(u,v,w)$ over the shell with $\alpha_1=0,\beta_1=\pi,\alpha_2=0,\beta_2=\pi$ can be related to the components of the diffusion tensor **D** as:

$$D_{0,\pi,0,\pi}=\frac{D_{xx}+D_{yy}+D_{zz}}{3}=tr(\mathbf{D}) \tag{6.7}$$

Similarly, the other averages of $D(u,v,w)$ over the different shells can be calculated as follow:

$$D_{0,\pi/2,0,\pi}=tr(\mathbf{D})+\frac{4}{3\pi}D_{xy} \quad (\alpha_1=0,\beta_1=\frac{\pi}{2},\alpha_2=0,\beta_2=\pi) \tag{6.8}$$

$$D_{0,\pi,0,\pi/2} = tr(\mathbf{D}) + \frac{4}{3\pi} D_{yz} \quad (\alpha_1 = 0, \beta_1 = \pi, \alpha_2 = 0, \beta_2 = \frac{\pi}{2}) \tag{6.9}$$

$$D_{0,\pi/2,0,\pi/2} = tr(\mathbf{D}) + \frac{4}{3\pi}(D_{xy} + D_{xz} + D_{yz}) \quad (\alpha_1 = 0, \beta_1 = \frac{\pi}{2}, \alpha_2 = 0, \beta_2 = \frac{\pi}{2}) \tag{6.10}$$

$$D_{0,\pi/4,0,\pi} = tr(\mathbf{D}) + \frac{4}{3\pi} D_{xy} + \frac{2}{3\pi}(D_{xx} - D_{yy}) \quad (\alpha_1 = 0, \beta_1 = \frac{\pi}{4}, \alpha_2 = 0, \beta_2 = \pi) \tag{6.11}$$

$$D_{0,\pi,0,3\pi/4} = \frac{3+\sqrt{2}}{12}(D_{xx} + D_{yy}) + \frac{3-\sqrt{2}}{6} D_{zz} + \frac{2\sqrt{2}-2}{3\pi} D_{yz}$$

$$(\alpha_1 = 0, \beta_1 = \pi, \alpha_2 = 0, \beta_2 = \frac{3\pi}{4}) \tag{6.12}$$

6.2.3 Obtaining all Components of Diffusion Tensor

According to equations (6.7)-(6.12), all components of the diffusion tensor (i.e., D_{xx}, D_{yy}, D_{zz}, D_{xy}, D_{xz}, and D_{yz}) can be obtained and expressed as the functions of $D_{0,\pi,0,\pi}$, $D_{0,\pi/2,0,\pi}$, $D_{0,\pi,0,\pi/2}$, $D_{0,\pi/2,0,\pi/2}$, $D_{0,\pi/4,0,\pi}$, and $D_{0,\pi,0,3\pi/4}$:

$$\begin{cases} D_{xy} = \frac{3\pi}{4}(D_{0,\pi/2,0,\pi} - D_{0,\pi,0,\pi}) \\ D_{yz} = \frac{3\pi}{4}(D_{0,\pi,0,\pi/2} - D_{0,\pi,0,\pi}) \\ D_{xz} = \frac{3\pi}{4}(D_{0,\pi/2,0,\pi/2} + D_{0,\pi,0,\pi} - D_{0,\pi/2,0,\pi} - D_{0,\pi,0,\pi/2}) \\ D_{xx} = (2\sqrt{2}+2)D_{0,\pi,0,3\pi/4} - 2\sqrt{2}D_{0,\pi,0,\pi} - D_{0,\pi,0,\pi/2} + \frac{3\pi}{4}(D_{0,\pi/4,0,\pi} - D_{0,\pi/2,0,\pi}) \\ D_{yy} = (2\sqrt{2}+2)D_{0,\pi,0,3\pi/4} - 2\sqrt{2}D_{0,\pi,0,\pi} - D_{0,\pi,0,\pi/2} - \frac{3\pi}{4}(D_{0,\pi/4,0,\pi} - D_{0,\pi/2,0,\pi}) \\ D_{zz} = (4\sqrt{2}+3)D_{0,\pi,0,\pi} + 2D_{0,\pi,0,\pi/2} - (4\sqrt{2}+4)D_{0,\pi,0,3\pi/4} \end{cases} \tag{6.13}$$

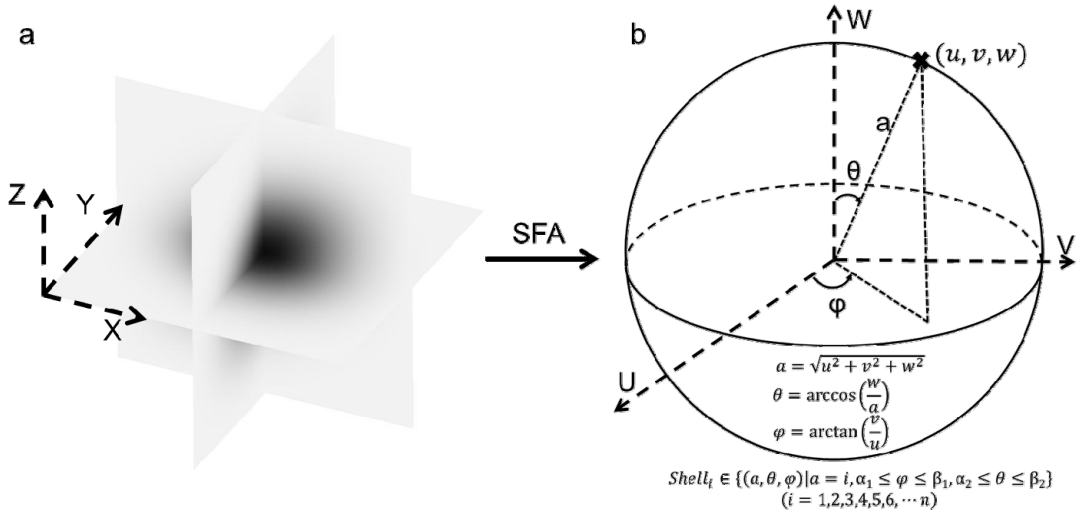

Figure 6.1 The Schematic of SFA and averaging the diffusivity in the frequency domain over a shell.

In the SFA, the solute concentration distribution is transformed from spatial domain in (a) to the frequency domain in (b) by using Fourier transform. In the frequency domain, the diffusivity $D(u,v,w)$ is averaged over a shell of a spherical surface to obtain all components of 3D diffusion tensor. The level of shell is defined by the radius a (i.e., commonly positive integers) and the range of shell is determined by polar angle θ, and azimuthal angle φ (i.e., six different ranges at each shell level).

6.3 Materials and Methods

6.3.1 Computer-Simulated MP-FRAP Experiments

The 3D anisotropic diffusion processes of the fluorescent molecule recovery after photobleaching were simulated using a finite element analysis software (COMSOL Multiphysics 3.5, COMSOL Inc., Burlington, MA). Figure 6.2 shows the simulation setup. At all boundaries of the simulation domain ($102\times102\times102\mu m^3$), the concentration of the fluorescent solutes satisfied the constancy assumption ($C=C^*$). Initially, the concentration distribution of fluorescent molecules was assumed to be uniform ($C=C^*$) outside the photobleached geometry and zero within the photobleached volume. The photobleached geometry was set to a cubic block with a side length (d) of 12.75μm according to the optimum value of 8 for the ratio of the imaging frame size to the initial length of the bleached volume as suggested by Travascio and Gu [17]. The mesh used in the simulation experiments included 7,554 quadratic Lagrange triangular elements. The convergence criterion for the solution was the relative error tolerance of less than 0.00001. The simulation was stopped when the concentration in the beached block reached 95% of C^*. For data analysis purposes, a number of Z-stack images representing the 3D FRAP experiment were extracted from the simulation and digitalized to 64pixels×64pixels×64pixels in the x-y-z coordinates.

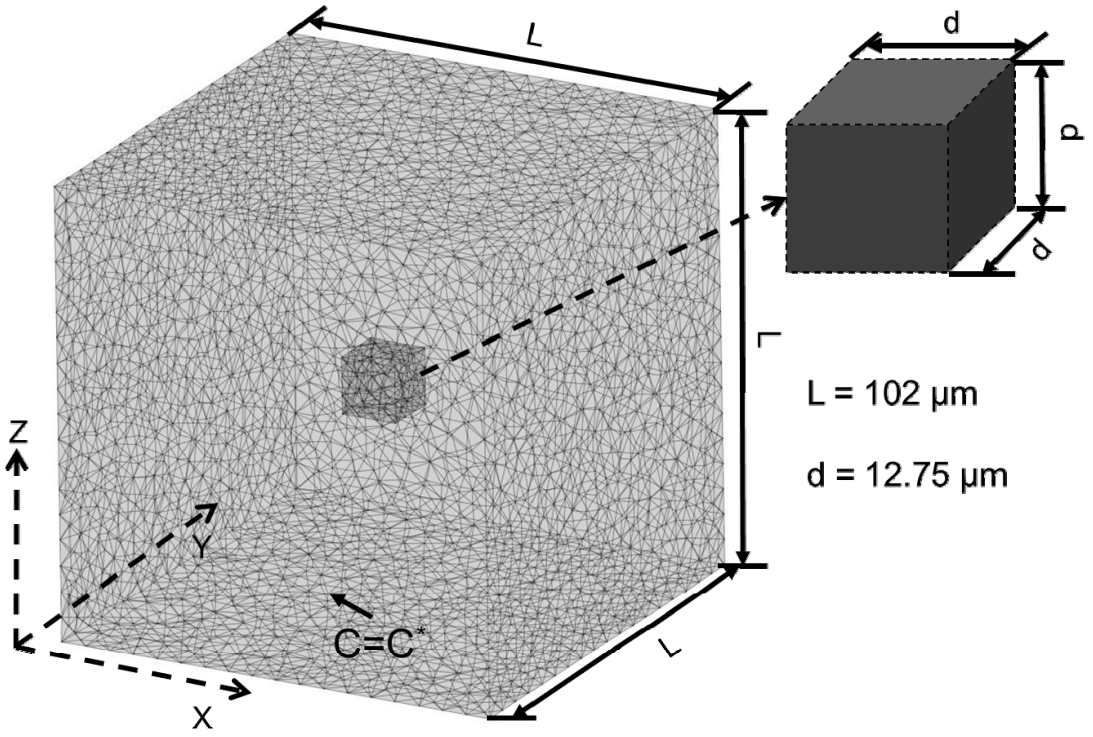

Figure 6.2 Schematic representation of the computational domain with the initial and boundary conditions for 3D MP-FRAP simulation experiments.
At all boundaries of the simulation domain ($102\times102\times102\mu m^3$), the concentration of the fluorescent solutes satisfies the constancy assumption ($C=C^*$). Initially, the concentration distribution of fluorescent molecules is assumed to be uniform ($C=C^*$) outside the photobleached geometry and zero within the photobleached volume. The photobleached geometry (insert) is set to a cubic block with a side length (d) of 12.75µm. The mesh used in the simulation experiments includes 7,554 quadratic Lagrange triangular elements.

In order to validate the capability of our MP-FRAP method, five groups of 3D anisotropic diffusion were investigated via setting different pre-defined diffusion tensors. In the first group, a base diffusion tensor of $\mathbf{D_0} = \begin{bmatrix} 0.1 & 0 & 0 \\ 0 & 0.2 & 0 \\ 0 & 0 & 0.3 \end{bmatrix} \mu m^2 / s$ was selected and rotated in other four groups at different angles using 3D rotation matrices $\mathbf{R}_{3Dj}$ $(i = 0 \sim 4)$ defined as:

$$\mathbf{R}_{3Dj} = \mathbf{R}_{xj}\mathbf{R}_{yj}\mathbf{R}_{zj} \tag{6.14}$$

where

$\mathbf{R}_{xj} = \begin{bmatrix} 1 & 0 & 0 \\ 0 & \cos\eta_1 & -\sin\eta_1 \\ 0 & \sin\eta_1 & \cos\eta_1 \end{bmatrix}$, $\mathbf{R}_{yj} = \begin{bmatrix} \cos\eta_2 & 0 & \sin\eta_2 \\ 0 & 1 & 0 \\ -\sin\eta_2 & 0 & \cos\eta_2 \end{bmatrix}$, and

$\mathbf{R}_{zj} = \begin{bmatrix} \cos\eta_3 & -\sin\eta_3 & 0 \\ \sin\eta_3 & \cos\eta_3 & 0 \\ 0 & 0 & 1 \end{bmatrix}$. These matrices represented counterclockwise rotations of a tensor relative to X, Y, and Z axes by rotation angles of η_1, η_2, and η_3, respectively (Figure 6.3). The detailed values of rotation angles in each group were listed in the Table 6.1. Their products were $\mathbf{R}_{3Dj}$ meaning the sequential rotations of a tensor about the x, y, and z axes at the certain angles. The five pre-defined diffusion tensors were calculated by:

$$\mathbf{D}_j = \mathbf{R}_{3Dj}{}^T \mathbf{D}_0 \mathbf{R}_{3Dj} \tag{6.15}$$

The simulated MP-FRAP data were analyzed by the new method and the principal components of diffusion tensor were determined based on the calculated diffusion tensors

and were compared to the pre-defined one in each group to assess the accuracy of this method. The time interval (ΔT) between each Z-stack was set to 18s.

The preference of the method for the shell radii [see Figure 6.1(b)] was studied. The pre-defined diffusion tensor was set to $\begin{bmatrix} 0.1 & 0 & 0 \\ 0 & 0.2 & 0 \\ 0 & 0 & 0.3 \end{bmatrix} \mu m^2 / s$, the accuracy of the method was compared between the shells ranging from "$Shell_1$ " to "$Shell_6$". The ΔT between each Z-stack was fixed to 18s.

The sufficiency of MP-FRAP recovery data sampling may significantly affect the accuracy of the MP-FRAP method. To study this effect, an isotropic diffusion tensor, $\begin{bmatrix} 0.1 & 0 & 0 \\ 0 & 0.1 & 0 \\ 0 & 0 & 0.1 \end{bmatrix} \mu m^2 / s$, was pre-defined to reduce the numerical error which may be caused by the different magnitudes of diffusion tensor components. The ΔT varied from 6s to 144s with the fixation of the characteristic diffusion time (T_D) which was defined by the equation below.

$$T_D = \frac{(d/2)^2}{tr(\mathbf{D})}, \ \mathbf{Ratio} = \Delta T / T_D \tag{6.16}$$

The side length, d, of bleaching block was a constant in the simulation, so the ratio of ΔT to T_D was only dependent on the values of ΔT. This ratio represented the effective sampling rate during the recovery data acquisition process. Therefore, different FRAP experiments with varying ratios were analyzed to examine the sampling effect to the accuracy of our method. Furthermore, this effect was also investigated under different

image noise conditions. Similarly to previous studies [7, 17], two magnitudes of spatial Gaussian noise (i.e., $\sigma = 5$ and 10) were generated by ImageJ software (Version 1.39f, National Institutes of Health, USA) and were then superimposed onto the simulated recovery Z-stack image sequences. These experiments were used to estimate how image noise affected the analyses as well.

Table 6.1 The detailed values of rotation angles (η_1, η_2, and η_3) in five groups of computer-simulated 3D MP-FRAP experiments for capability validation.

Rotation Angles	**j=0**	**j=1**	**j=2**	**j=3**	**j=4**
η_1	**0**	$\frac{\pi}{4}$	**0**	**0**	$\frac{\pi}{4}$
η_2	**0**	**0**	$\frac{\pi}{4}$	**0**	$\frac{\pi}{4}$
η_3	**0**	**0**	**0**	$\frac{\pi}{4}$	$\frac{\pi}{4}$

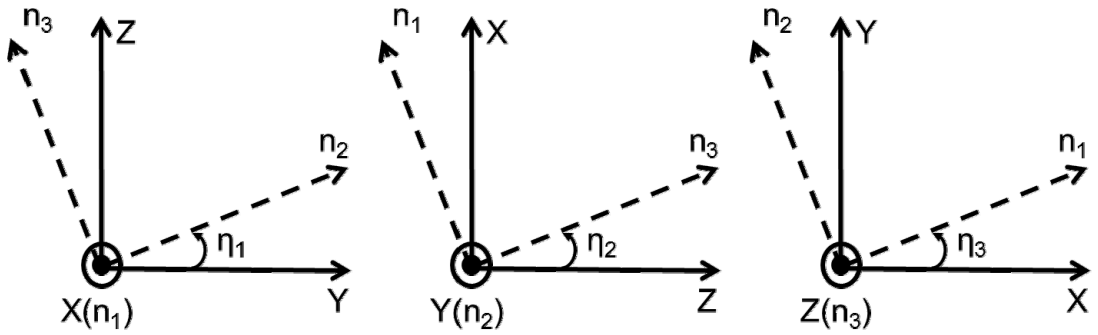

Figure 6.3 The orientation of pre-defined 3D anisotropic diffusion tensor generated using various rotation angles in the computer-simulated MP-FRAP experiments for capability validation.

η_1, η_2, and η_3 are the rotation angles which characterize the counterclockwise rotations of a diffusion tensor relative to X, Y, and Z axes in the spatial coordinates system, respectively.

6.3.2 Experimental MP-FRAP Apparatus and Protocol

All MP-FRAP experiments were performed on a Zeiss LSM 510 META NLO confocal laser scanning microscope (Carl Zeiss Microscopy, LLC, Thornwood, NY) equipped with a Coherent Mira 900 femtosecond pulsed Ti:Sapphire laser for multiphoton excitation (Coherent, Santa Clara, CA) at room temperature (22ºC). Multiphoton excitation of fluorescein isothiocyanate-dextran (FITC-Dextran, FD) (Sigma-Aldrich®, St. Louis, MO) in the specimens was accomplished by a 790-nm light from the Ti:Sapphire laser. To minimize the contribution of the fluorescence emission of the background, one pre-bleaching image stack was firstly obtained in the observation volume (e.g., 150×150×150μm^3 for 40× lens or 102×102×102μm^3 for 63× lens) and subsequently subtracted from the post-bleaching image stack series. Imaging mode with low multiphoton laser energy (6%~30% laser energy) was applied during this course and auto gain compensation function was also applied when the imaging plane moved deep into the specimen in order to enhance the fluorescence signal inside the scattering sample. Images were collected as 64×64×64 pixel X-Y-Z-scans at 8-bit intensity resolution using a 40×/1.2NA water immersion objective (working distance: 0.22mm) for the glycerol samples with concentrations of 75%, 80%, and 85% (see Glycerol/PBS solutions section) or a 63×/1.3NA water immersion objective (working distance: 0.17mm) for the rest of samples. The central region of the observation volume was then photobleached by a high energy multiphoton laser (85%~100% laser power) at the different Z-levels to create a cubic bleached block with a dimension about 18.75×18.75×18.75μm^3 (40× lens) or

$12.75 \times 12.75 \times 12.75 \mu m^3$ (63× lens). The system was switched back to the imaging mode afterward to acquire the post-bleaching image stack series in the exactly same observation volume. For each experiment, 40 stacks (30 stacks for the glycerol samples with concentrations of 75%, 80%, and 85%) of recovery images, plus 1 stack prior to photobleaching, were acquired at an approximate rate of 18s/stack.

6.3.3 Glycerol/PBS Solutions

FD molecules (500KDa, 4mg/mL) in the glycerol/phosphate buffered saline (PBS) solutions with five different concentrations (v/v: 75%, 80%, 85%, 90%, and 95%) were used to test the MP-FRAP technique. 14 mL of the solutions was pipetted to a small chamber obtained by attaching two layers of 120-μm-thick double-side adhesive spacer (Secure-Seal spacers, Life Technologies, Grand Island, NY) on a microscope slide. The chamber was then sealed with a microscope coverslip. The sample was located on the microscope stage and then MP-FRAP experiment was started after 30 minutes of waiting to eliminate any detectable flow in the sample. The diffusion properties of FD500 molecules in the glycerol/PBS solutions were quantified by MP-FRAP technique.

6.3.4 Porcine Ligament Tissues

The porcine ligament tissues from adult pigs were used for testing as an application example of our MP-FRAP technique. Tissue slices were prepared by cutting the ligament tissues into 6mm segments. These tissue segments were then sliced along the fiber direction into 150μm slices by using a microtome (SM24000, Leica Microsystems GmbH, Wetzlar, Germany) with a freezing stage (Model BFS-30, Physitemp, Clifton, NJ). Ligament tissue specimens were then immersed in two types of

FD molecules (FD70 and FD150, 6mg/mL) for 72 hours, so the concentration distribution of fluorescent solutes reached equilibrium inside the tissue slices. Next, each tissue slice was transferred into a small chamber made up of two layers of 120-μm-thick double-side adhesive spacer and a microscope slide. After then, a certain amount of glycerol/PBS solutions (v/v: 60%) containing FD70 or FD150 molecules (6mg/mL) was added in the chamber to enhance the penetration depth in multiphoton microscopy.[187, 188] Finally, the chamber was sealed with a coverslip and then moved to the microscope stage to start the MP-FRAP experiment. The anisotropic diffusion tensors of FD molecules with molecular weights of 70KDa and 150KDa in the ligament tissue slices were measured by the MP-FRAP technique. Each specimen was firstly tested when the fiber orientation aligned with X-axis of microscopy coordinate [X-Alignment in Figure 6.4(a)], and then, the field of view (FOV) was rotated 90 degree to allow the fiber direction align with Y-axis and the specimen was tested again. [Y-Alignment in Figure 6.4(b)] Correspondingly, the six components (i.e., D_{xx}, D_{yy}, D_{zz}, D_{xy}, D_{xz}, and D_{yz}) and the traces of the diffusion tensors were obtained from those MP-FRAP experiments.

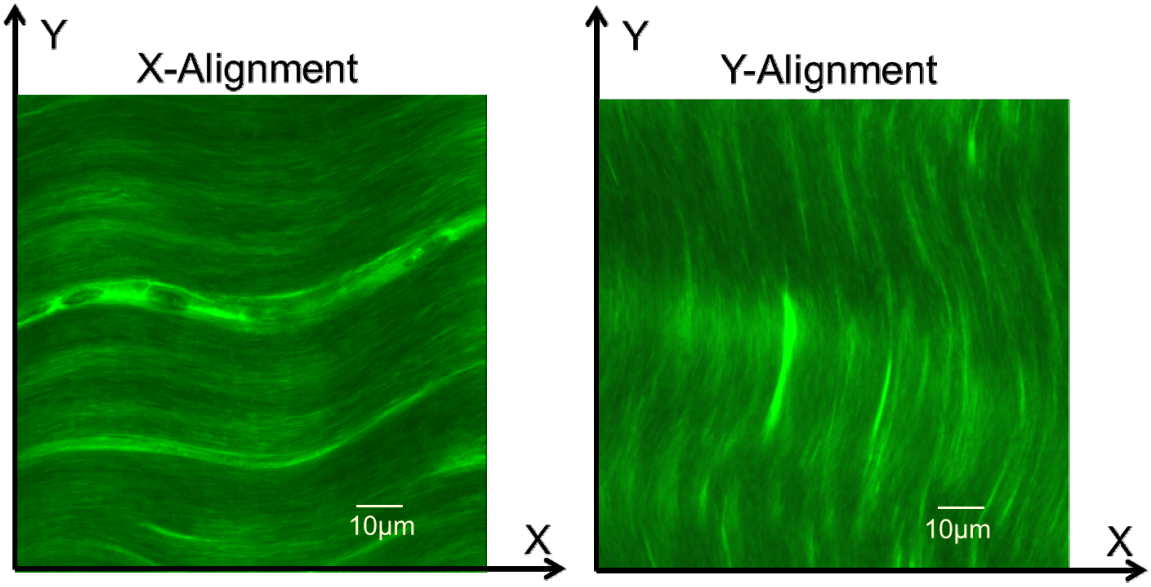

(a) (b)

Figure 6.4 The schematic of two types of observation protocol for fluorescent solute diffusion measurements in the porcine ligament tissues.
X-Y coordinates represent the microscopy coordinates fixed on the microscope sample stage. The fluorescent images demonstrate the major orientations of collagen fibers in the porcine ligament tissues. (a) In the protocol of X-Alignment, the main fiber orientation is aligned with X-axis. (b) In the protocol of Y-Alignment, the main fiber orientation is aligned with Y-axis.

6.3.5 Images and Data Processing

For both computer simulated and experimental MP-FRAP tests, the image processing was completed utilizing custom written codes in MATLAB (MATLAB 7.0, The MathWorks Inc., Natick, MA). Based on equation (6.3), the codes performed 3D Fourier transform and nonlinear curve-fitting to yield solutions for $D(u,v,w)$ which was the diffusion coefficient in the frequency domain. Based on equation (6.5), tecplot software (Tecplot, Inc., Bellevue, WA) was used to average $D(u,v,w)$ on "Shell$_4$" over different angle ranges [see equations (6.7)~(6.12)] and generated $D_{0,\pi,0,\pi}$, $D_{0,\pi/2,0,\pi}$, $D_{0,\pi,0,\pi/2}$, $D_{0,\pi/2,0,\pi/2}$, $D_{0,\pi/4,0,\pi}$, and $D_{0,\pi,0,3\pi/4}$. The selection of "Shell$_4$" was suggested by the results from the simulation experiments. Finally, using equation (6.13), the MATLAB codes calculated all components of the diffusion tensor.

6.3.6 Statistical Analysis

One-way ANOVA and Tukey's *post hoc* tests were performed on the diagonal components (*i.e.*, D_{xx}, D_{yy}, and D_{zz}) of diffusion tensors to examine the extent of anisotropy of solute diffusion in both glycerol and tissue specimens. An independent t-test was performed on the traces of diffusion tensors for the FD70 and FD150 in the porcine ligament tissue experiments to examine the size effect of solute diffusion in the tissue samples. The SPSS 16.0 software (SPSS Inc., Chicago, IL) was used for all statistical analysis and significant differences were reported at p-values < 0.05.

6.4 Results

6.4.1 Validation by Computer Simulated MP-FRAP Experiments

3D MP-FRAP experiments were simulated by pre-defining components of the anisotropic diffusion tensors. Numerically simulated FRAP digital image stack series were transformed into the frequency domain using SFA. All the components of diffusion tensors were determined based on our proposed method. The accuracy of the new method was assessed by the relative error (ε) which has been defined in the previous studies.[7, 17]

The capability to yield the accurate diffusion tensor of our MP-FRAP technique was assessed by pre-defining five groups of diffusion tensor in the simulation experiments. The Figure 6.5(a) showed the values of relative errors for three principal diffusion components (*i.e.*, D_{0xx}, D_{0yy}, and D_{0zz}) in the each test group. Overall, the relative errors of D_{0xx} were less than 1.80%, and the relative errors of D_{0yy} were less than 1.65%, while the relative errors of D_{0zz} were less than 0.77% for all simulated cases. These results indicated that the accuracy of the new method was not significantly sensitive to the rotation angles *(i.e.*, η_1, η_2, and η_3).

A simulated image stack series was analyzed under the different selections of the shell level in the frequency domain to study the preference of MP-FRAP technique. The maximum relative errors of the diagonal diffusion components (*i.e.*, D_{xx}, D_{yy}, and D_{zz}) were used to compare the accuracies of our method on the different shell levels. The results shown in the Figure 6.5(b) demonstrated the maximum relative errors varied among different shells. High relative errors occurred on the low frequency Shell_1 and

$Shell_2$, while, the best accuracy was achieved on the $Shell_4$. Therefore, based on these results, all the analyses in other studies were completed on the frequency $Shell_4$.

The sampling effect on the accuracy of our MP-FRAP method was investigated and the results were shown in the Figure 6.5(c). The results from pure simulated image stacks without noise indicated that the accuracy decreased with the ratio increased. There was a tremendous increase of maximum relative error when the ratio changed from 0.22 to 0.35. The same trend existed when the different levels (σ=5 and σ=10) of imaging noise were superposed on the pure simulated image stack series. The effect of imaging noise (σ) on the accuracy of the new method was examined as well. [Figure 6.5(c)] The maximum relative error of the diagonal diffusivities increased with increasing σ. When the ratios were less than 0.22, the maximum relative errors were less than 4.4% at σ = 5, while the errors were less than 7% at σ = 10. [Figure 6.5(c)]

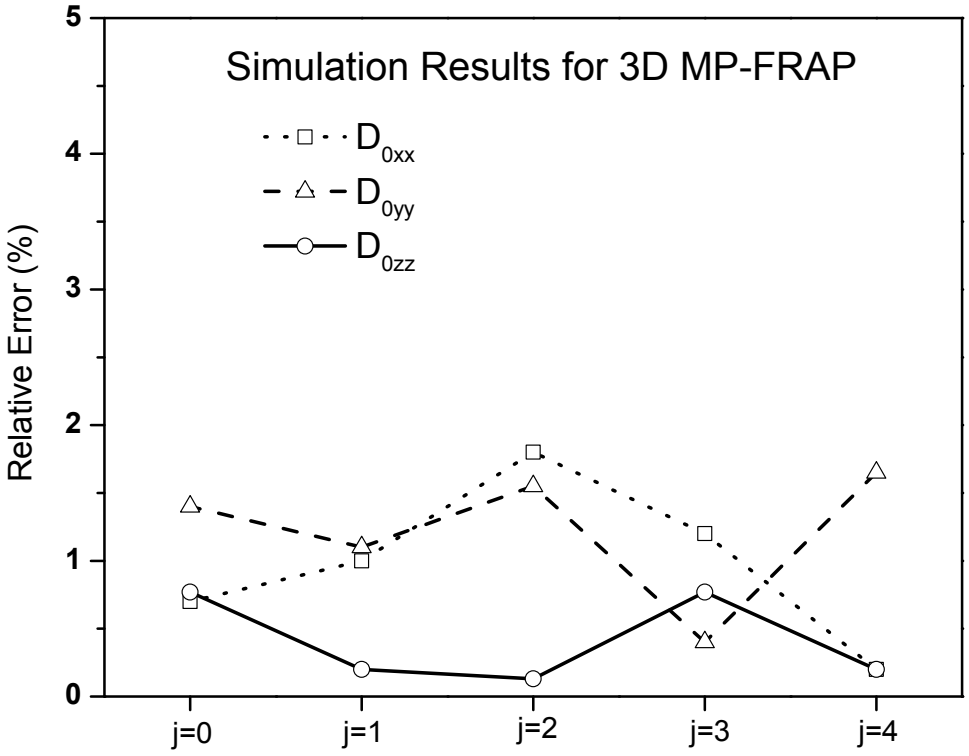
Simulation Results for 3D MP-FRAP
D0xx
D0yy
D0zz
Relative Error (%)
0
1
2
3
4
5
j=0
j=1
j=2
j=3
j=4

(a)

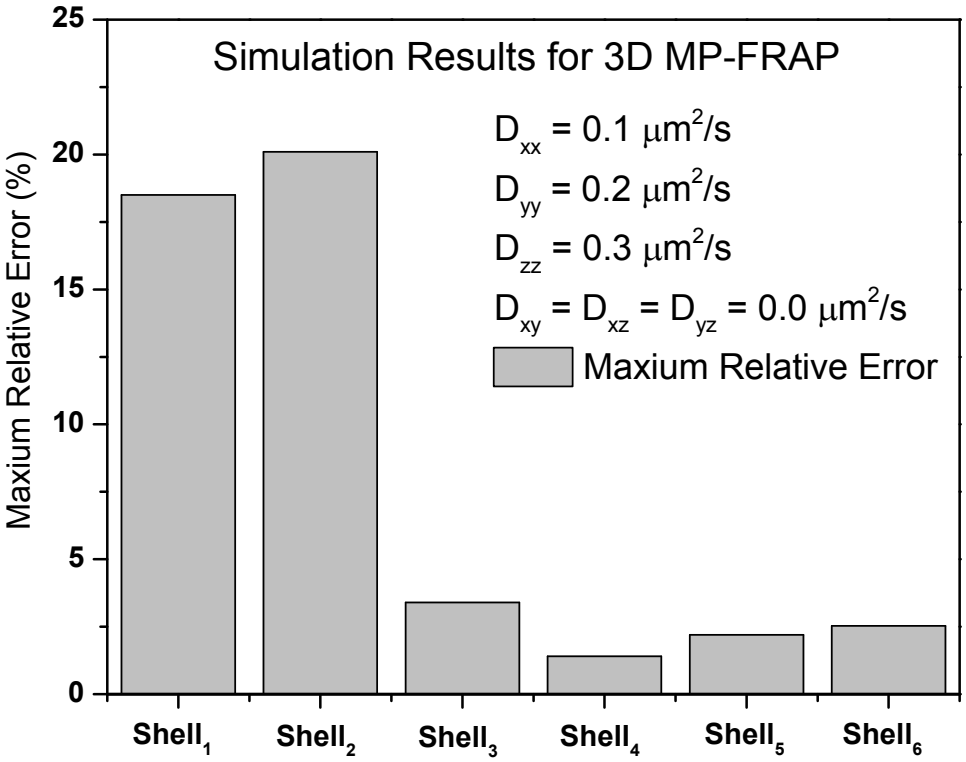
Simulation Results for 3D MP-FRAP
D_{xx} = 0.1 μm²/s
D_{yy} = 0.2 μm²/s
D_{zz} = 0.3 μm²/s
D_{xy} = D_{xz} = D_{yz} = 0.0 μm²/s
Maxium Relative Error
Maxium Relative Error (%)
25
20
15
10
5
0
Shell1
Shell2
Shell3
Shell4
Shell5
Shell6

(b)

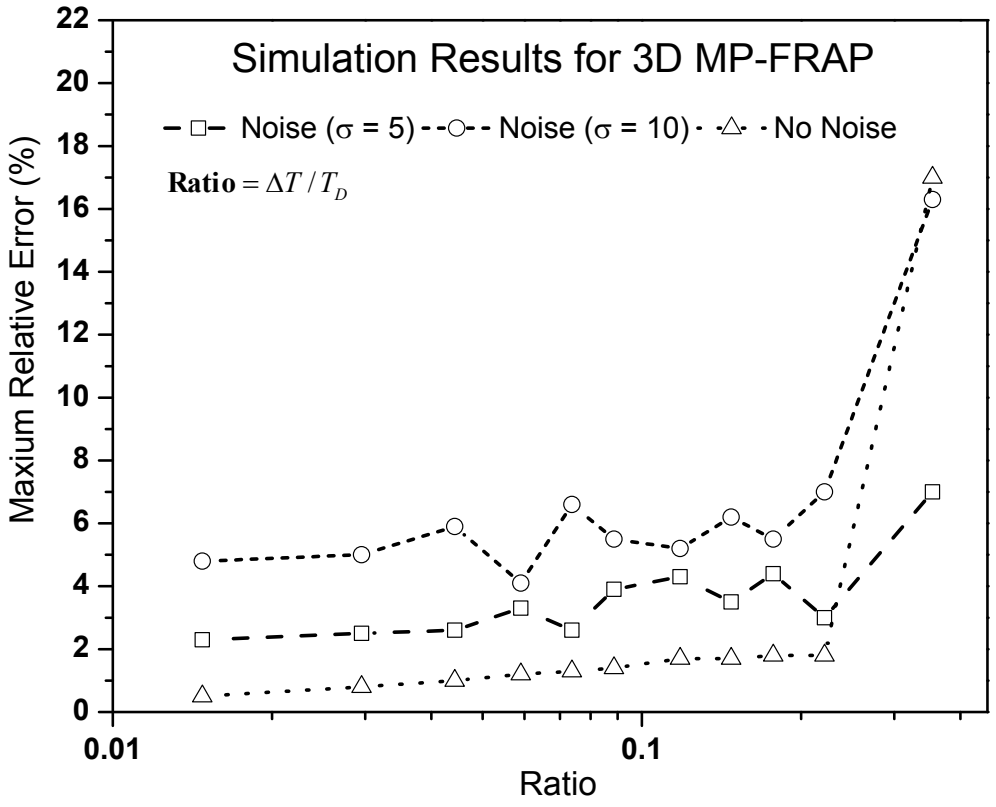

(c)

Figure 6.5 The results for the computer simulated 3D MP-FRAP experiments.
(a) The capability of new MP-FRAP technique is assessed by five groups of pre-defined diffusion tensors with different rotation angles. Overall, the relative errors of D_{0xx} are less than 1.80%, and the relative errors of D_{0yy} are less than 1.65%, while the relative errors of D_{0zz} are less than 0.77% for all simulated cases, which indicates that the accuracy of the new method was not significantly sensitive to the rotation angles. (b) The maximum relative errors of the diagonal diffusion components (*i.e.*, D_{xx}, D_{yy}, and D_{zz}) are used to study the effect of shell levels on the accuracies of new MP-FRAP method. The results indicate that the best accuracy was achieved on the $shell_4$. Therefore, all the analyses in other studies were completed on the $shell_4$. (c) The results of the sampling effect on the accuracy of new MP-FRAP method demonstrate that the accuracies decrease when the sampling rates decrease. The accuracies of new MP-FRAP method also decrease when the imaging noises increase.

6.4.2 Diffusion Measurements in Glycerol/PBS Solutions

The MP-FRAP technique was applied to determine the 3D diffusion measurements of FD500 molecules in the glycerol/PBS solutions with varying concentrations (from 75% v/v to 95% v/v). A typical MP-FRAP image stack series of FD500 in 95% glycerol/PBS solution was shown in the Figure 6.6(a). Three ortho-slices in the 3D molecular concentration profile were displayed and the dark region represented the multiphoton laser induced photobleaching geometry. This dark region gradually diminished during the recovery process over time due to the un-bleached fluorescent molecules diffused into this region.

The results of FD500 diffusion measurements were summarized in the Figure 6.7. In each concentration group, there were no significant differences between the diagonal diffusion components (*i.e.*, D_{xx}, D_{yy}, and D_{zz}), while the off-diagonal diffusion components were all close to zero. These results demonstrated the diffusion of FD500 molecules in the glycerol/PBS solutions is isotropic, which means the diffusivities are uniform in all orientations. The traces of diffusion tensor of FD500 molecules in each group were compared to study the concentration effect on the average diffusivities (Table 6.2). The significant differences (ANOVA, $p<0.0001$) of traces were found between each concentration group and the average diffusivities of FD500 decreased with the glycerol concentrations increased.

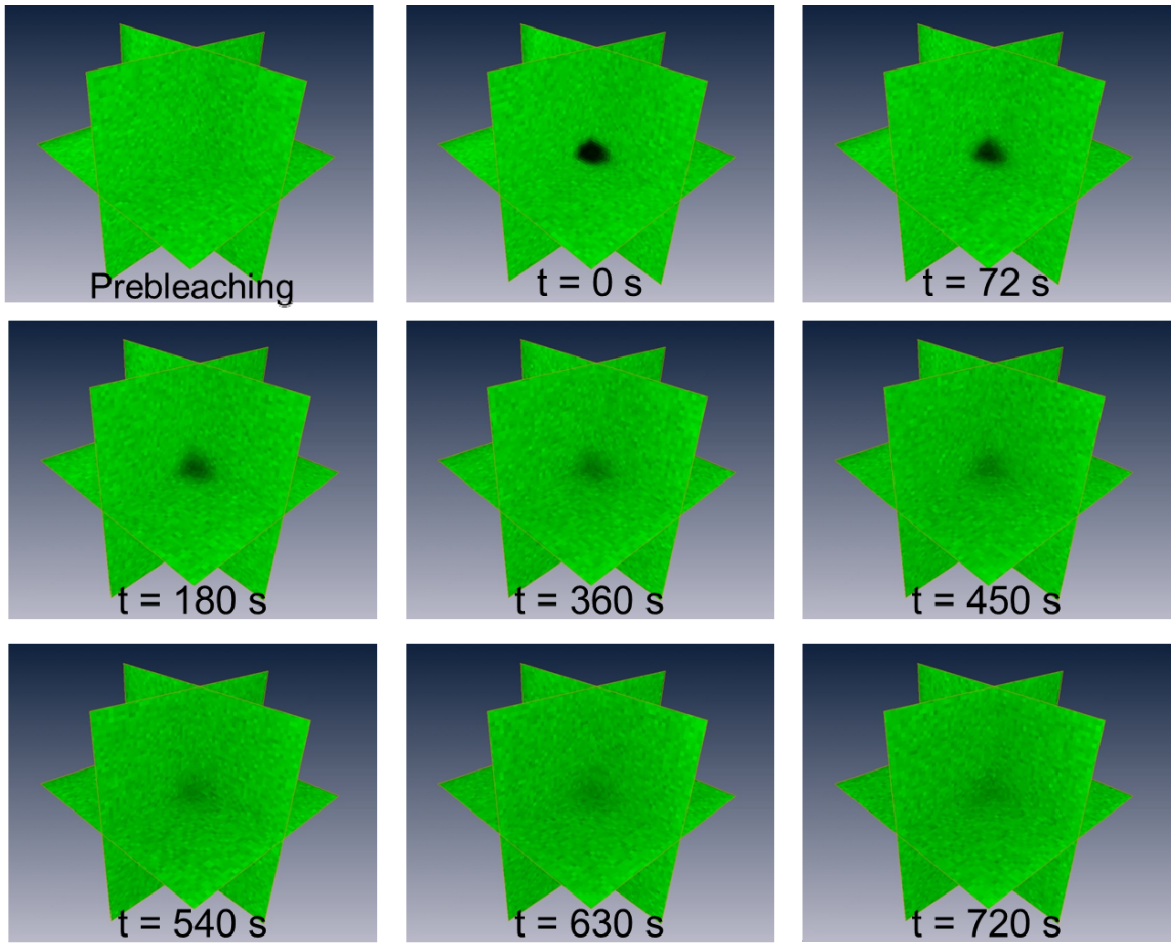

(a)

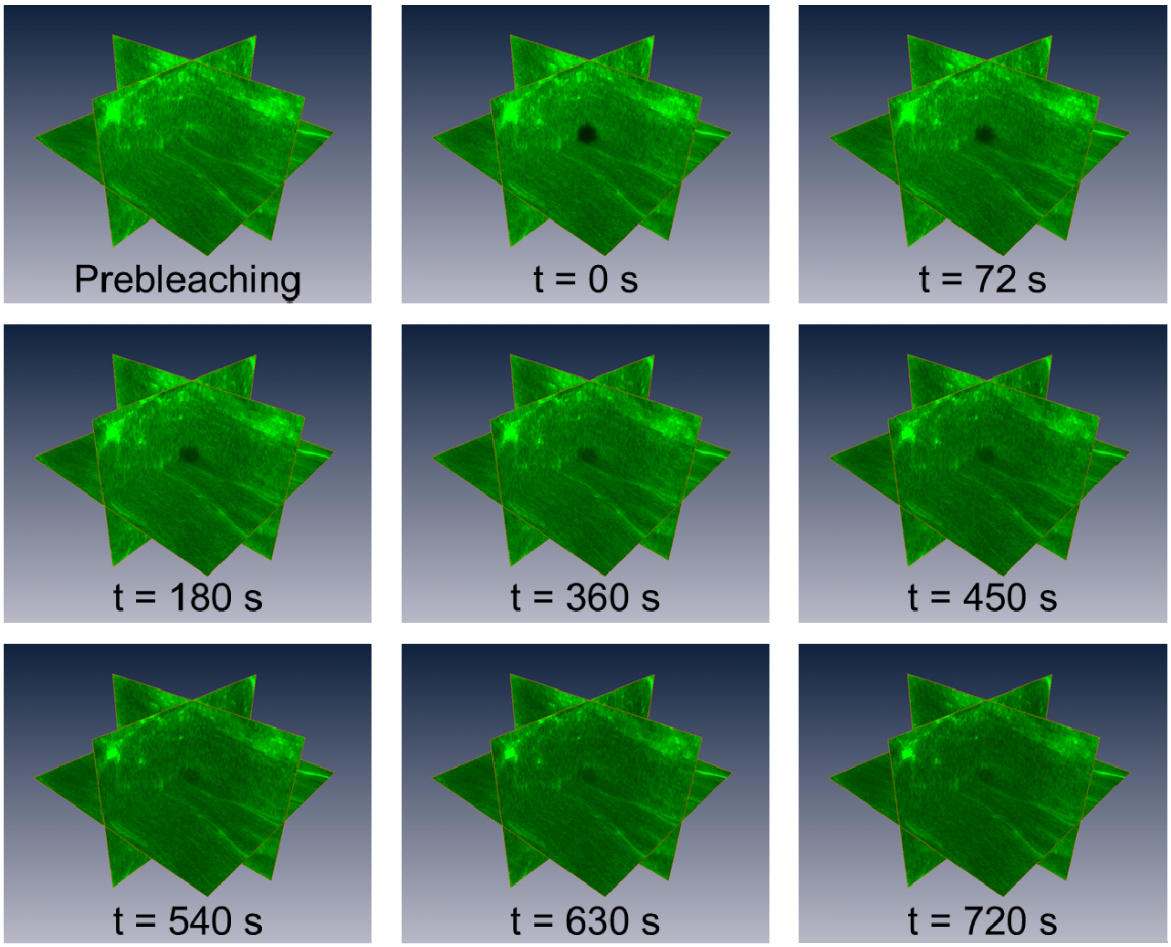

(b)

Figure 6.6 Typical 3D MP-FRAP Z-stack image series of fluorescent solutes for the experimental diffusion measurements in the glycerol/PBS solutions (a) and the porcine ligament tissues (b).
For each experiment, typically, 40 stacks of post-bleaching images, plus 1 stack prior to photobleaching, are acquired at an approximate rate of 18second/stack. Both (a) and (b) show only the central region of the observation volume is photobleached by the multiphoton laser and fluorescence recovers completely in the last Z-stack image series (t=720s).

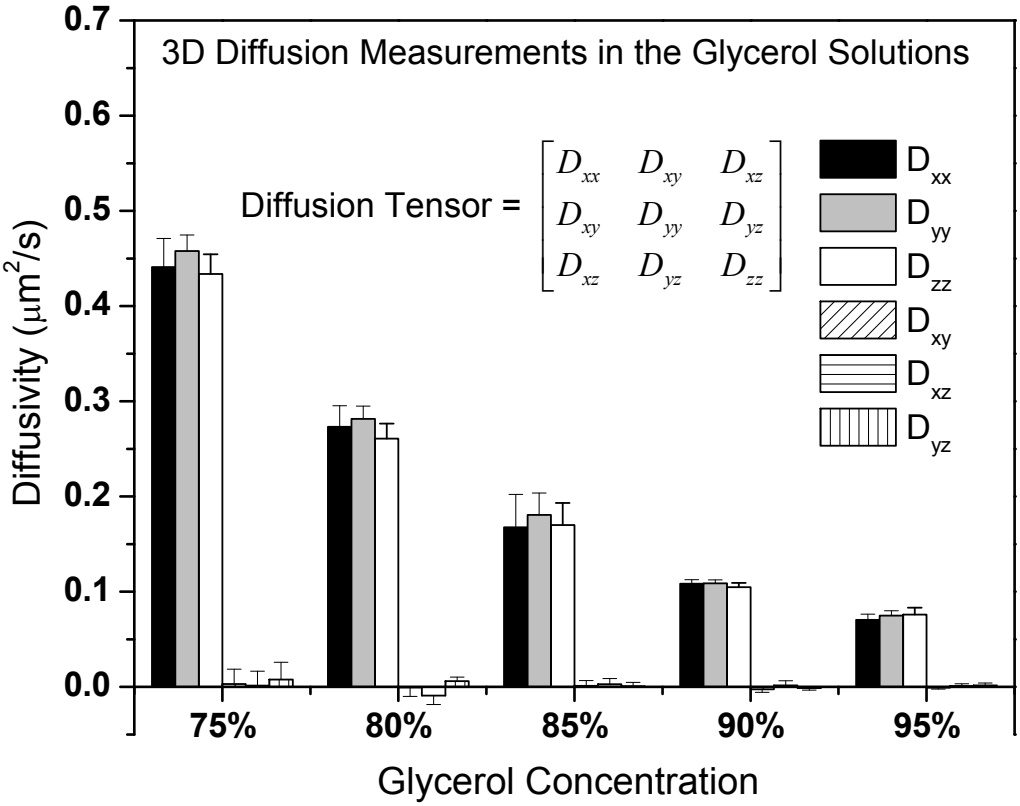

Figure 6.7 The results for the diffusion measurements in glycerol/PBS solutions indicate the diffusion of FD500 molecules is isotropic in these samples.
In each concentration group, there were no significant differences (ANOVA, $p>0.05$) between the diagonal diffusion components (i.e., D_{xx}, D_{yy}, and D_{zz}), while the off-diagonal diffusion components are all close to zero. Additionally, the average diffusivities of FD500 significantly decrease (ANOVA, $p<0.0001$) with the glycerol concentrations increase.

Table 6.2 The results (Mean ± Standard Deviation) of average diffusivity of FD500 in glycerol/PBS solutions with different concentrations.

	75%	**80%**	**85%**	**90%**	**95%**
$(D_{xx}+D_{yy}+D_{zz})/3$ ($\mu m^2/s$)	0.444±0.015*	0.272±0.012*	0.173±0.026*	0.107±0.002*	0.074±0.003*

(* means the average diffusivities are significantly different between each concentration group)

6.4.3 MP-FRAP Experiments on Porcine Ligament Tissues

The 3D anisotropic diffusion properties of FD70 and FD150 solutes in the porcine ligament tissues with optical clearing agent (*e.g.*, glycerol) application were experimentally determined by the new MP-FRAP method. The Figure 6.6(b) showed a typical process of MP-FRAP experiment in the tissue specimen (*e.g.*, FD70 and 60% glycerol). The collagen fiber distribution can be observed in the ortho-slices.

Six components of diffusion tensors of FD70 and FD150 in the ligament tissues were calculated by the proposed method and the results were shown in the Figure 6.8(a) The first two groups of diffusivities were the results of the FD70 diffusion in tissue specimens with two different observation protocols (*i.e.*, X-Alignment and Y-Alignment). In the X-Alignment group, the collagen fiber was mainly aligned with X-axis. The results indicated that the D_{xx} was significantly higher (ANOVA, $p < 0.0001$) than D_{yy} and D_{zz} in this group and there was no significant difference (ANOVA, $p = 0.884$) between D_{yy} and D_{zz}, while the values of all off-diagonal diffusion components were close to zero. In the Y-Alignment group, the FOV was rotated by 90 degree and the fiber orientation was primarily aligned along Y-axis. The results showed that the diffusion along the Y-axis was significantly faster (ANOVA, $p < 0.01$) than the other two directions in the Y-Alignment group and all off-diagonal diffusion components were close to zero as well. Furthermore, the third and fourth groups of diffusivities [Figure 6.8(a)] demonstrated that the exactly same trends existed in the results of FD150 diffusion in the tissue specimens. Thus, the 3D diffusion properties of these two types of FD solutes in the ligament tissue slices are anisotropic and the diffusion along the fiber orientation is always the fastest one.

The effect of solute size on the diffusion properties of FD in the ligament tissue slices was investigated and the results were shown in the Figure 6.8(b). The FD70 ($0.117\pm0.023\mu m^2/s$, Stokes radius: 6nm) had about 1.4 times higher (t-test, $p = 0.002$) average diffusivity than FD150 ($0.081\pm0.016\mu m^2/s$, Stokes radius: 8.5nm) in the ligament tissue specimens.

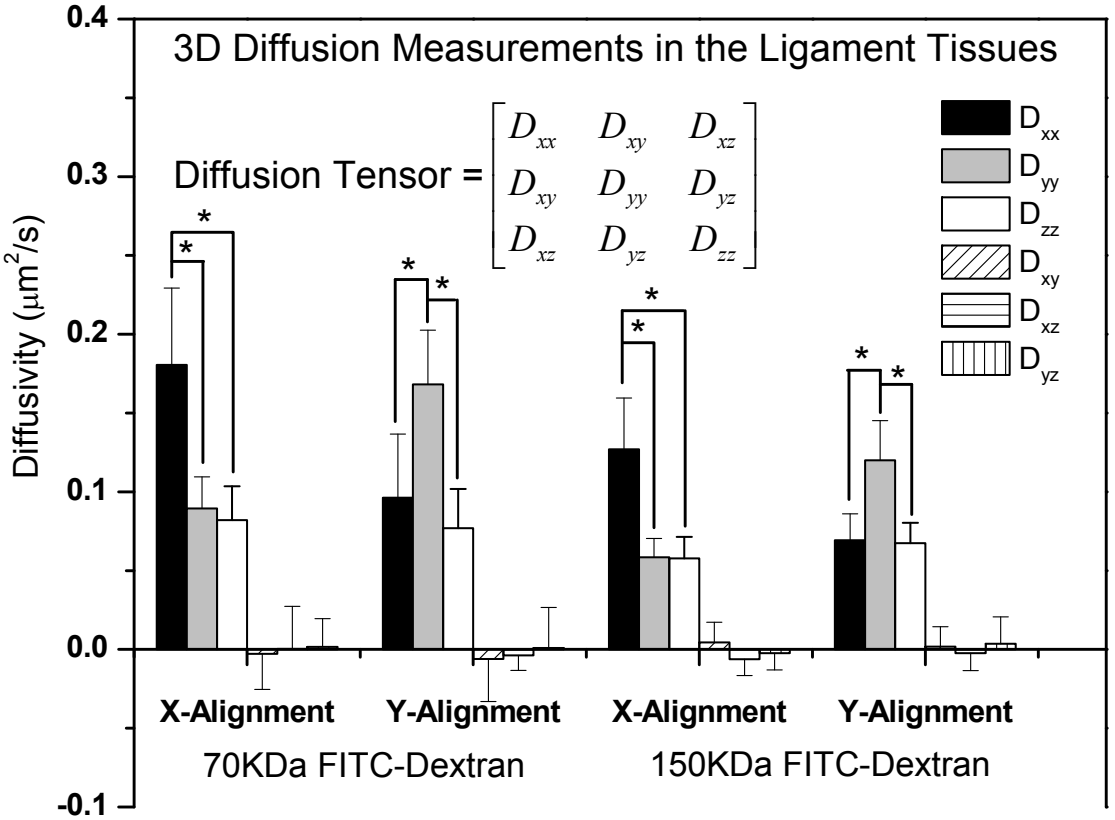
3D Diffusion Measurements in the Ligament Tissues
Diffusion Tensor =
$\begin{bmatrix} D_{xx} & D_{xy} & D_{xz} \\ D_{xy} & D_{yy} & D_{yz} \\ D_{xz} & D_{yz} & D_{zz} \end{bmatrix}$
Diffusivity (μm²/s)
0.4
0.3
0.2
0.1
0.0
-0.1
D_xx
D_yy
D_zz
D_xy
D_xz
D_yz
X-Alignment
Y-Alignment
X-Alignment
Y-Alignment
70KDa FITC-Dextran
150KDa FITC-Dextran

(a)

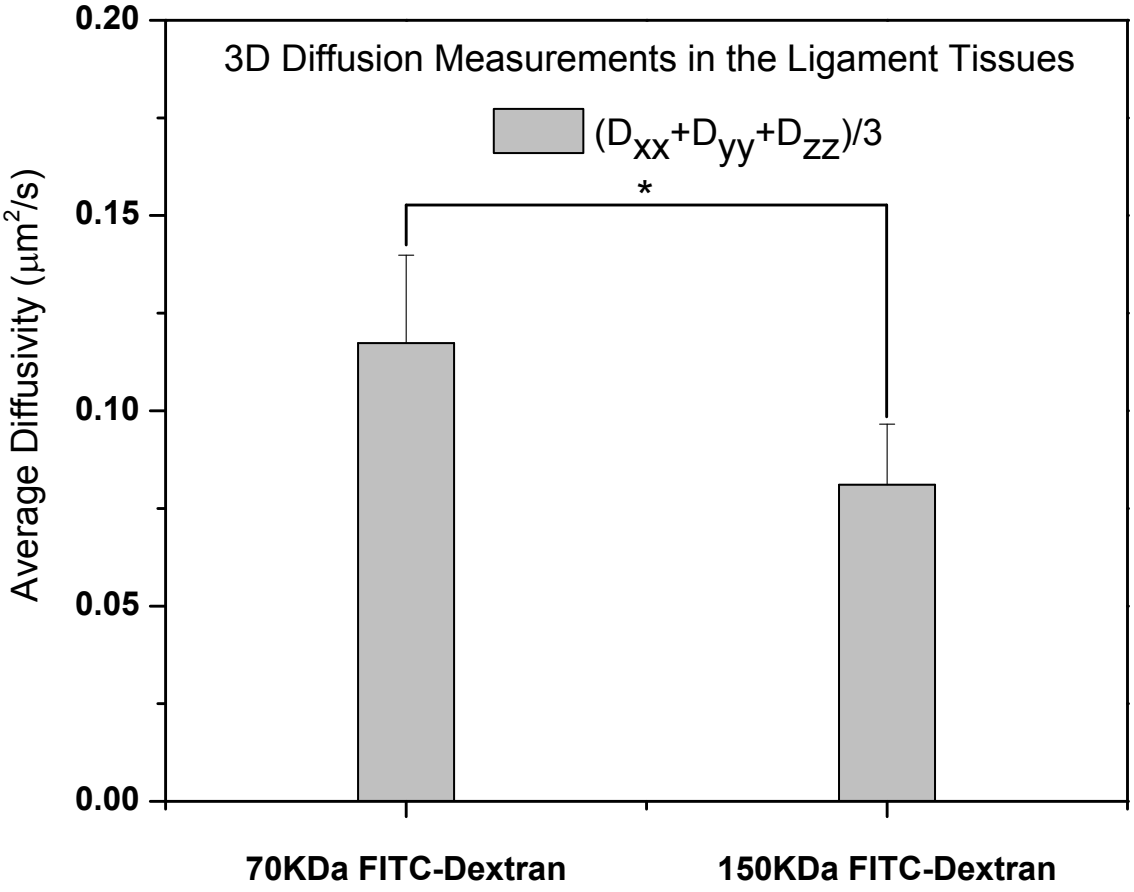

(b)

Figure 6.8 The results for the diffusion measurements in the porcine ligament tissues with optical clearing agent application indicate the diffusions of FD70 and FD150 molecules are anisotropic in the tissue specimens.
(a) The diffusion of FD70 and FD150 along the major fiber orientation is faster than the other two diffusions transversely to the fiber direction in both X and Y-Alignment observation protocols. (b) The average diffusivity of FD70 in the ligament tissue is significantly higher than FD150 due to the solute size effect.

6.5 Discussion

MP-FRAP technique has been well-established to measure the diffusion of macromolecules within biological systems. However, most of MP-FRAP models are based on the isotropic diffusion assumption and spatial domain analysis, the 3D anisotropic diffusion and frequency domain analysis for MP-FRAP methods are rarely studied. In this study, we have derived a new MP-FRAP model and technique for analyzing 3D anisotropic diffusion data by SFA. We have evaluated this new model by using computer-simulated MP-FRAP experiments with 3D anisotropic diffusion and experimental diffusion measurements on FD molecules in the glycerol/PBS solutions. We have also presented the new MP-FRAP technique in the determination of diffusion tensors of FD molecules within the porcine ligament tissues.

6.5.1 Influence of the Shell Radius and Recovery Data Sampling

As we mentioned in the theory, the diffusivity $D(u,v,w)$ can be averaged over the shells with different radii in the frequency domain. Theoretically, the average diffusivities on each frequency shell could yield the accurate components of diffusion tensors. However, in the practical implementation of our MP-FRAP technique, the 3D continuous fluorescence concentration profiles were digitalized into 3D image stacks with discrete intensity grayscales. The numerical errors occurred when those digital image stacks were transformed into frequency domain by SFA. The extent of these errors varied among different frequency shells. Typically, the higher frequency shells suffered more. Therefore, the use of higher frequency shells (*e.g.*, shell_5 and shell_6) may

not necessarily improve the accuracy of the results for ideal images.[Figure 6.5(b)] On the other hand, the lower frequency shells (*e.g.*, $shell_1$, $shell_2$ and $shell_3$) could have large errors due to the less effective data points which could enhance the accuracies of the average diffusivities. Based on our results, it was found that the $shell_4$ was the optimal frequency shell. The similar findings were reported in the previous studies on 2D FRAP analysis.[7, 17]

The initial microscopy systems were designed to image 2D specimens in X-Y plane, since the development of confocal and multiphoton scanning microscopy, the 3D fluorescence concentration distributions have become more convenient to be acquired. Nevertheless, the sampling rate of 3D fluorescence image stacks is still limited because the moving speed of scanner in the Z direction is relatively slower than the X-Y directions. For instance, in our experimental MP-FRAP tests, the typical scanning time for each 3D image stack was about 18s. So the fastest diffusion process that can be measured is limited by the sampling rate. The Figure 6.5(c) showed the sampling effect on the accuracy of MP-FRAP method. The ratio of ΔT to T_D represented the effective sampling rate for a certain diffusion process and the smaller ratio meant the faster sampling rate. The bottom dot plus triangle curve showing the results from pure simulated image stacks without noise indicated that the accuracy decreased with the ratio increased or sampling rate decreased. There was a tremendous increase of maximum relative error when the ratio changed from 0.22 to 0.35. According to these results, diffusion coefficient up to $0.5\mu m^2/s$ can be accessible by our method due to the limited 3D sampling rate. One might also notice from the Figure 6.5(c) that the same trend for

the sampling effect existed in the simulated image stack series with different noises (σ=5 and σ=10).

6.5.2 Simulated and Experimental Validation of Model

The accuracy and robustness of the new method was firstly assessed by the computer simulated MP-FRAP experiments. As shown in the Figure 6.5(a), the new model yielded accurate values for the principal components of diffusion tensors. Overall, the relative errors were less than 1.8% when the pre-defined diffusion tensors were rotated at different angles across the 3D space. It's worth mentioning that our method demonstrated the robustness against the image noises according to the results in the Figure 6.5(c). The dashed square and dashed circle curves in that figure showed the maximum relative errors under the image noise conditions. With the appropriate sampling rate, the maximum relative errors were less than 4.4% at σ = 5 level, while the errors were less than 7% at σ = 10 level.

Furthermore, in order to examine the effect of different bleaching geometries (initial conditions) on our method, additional simulation MP-FRAP experiments (results not shown) have been completed via creating different shapes (e.g., cylinder and sphere) of bleaching volumes. The components of diffusion tensors in all these simulations were calculated correctly, which indicated the bleaching geometry is not necessary to be exact cubic. This is another advantage to implement MP-FRAP technique in the real experiments.

The diffusion measurements on FD molecules in the glycerol/PBS solutions were used to validate the MP-FRAP model experimentally. The results in the Figure 6.7

showed the isotropic diffusion of FD500 molecules in the glycerol/PBS solutions with varying viscosities. The average diffusivities (0.44μm^2/s and 0.27μm^2/s) of FD500 in the two types of glycerol solutions (75% v/v and 80% v/v) were comparable to the diffusivities (0.60μm^2/s and 0.36μm^2/s) of the same solute in the glycerol solutions (80% w/w and 85% w/w) measured by other MP-FRAP technique.[145] The minor differences were probably caused by the different sample preparation procedures and observational volumes. The trend (Table 6.2) of decreasing the average diffusivities with increasing the glycerol concentrations was in agreement with the relationship between diffusivity and viscosity, which is defined in the Stokes-Einstein equation.

6.5.3 Application Example on Solute Diffusion in Ligament Tissue

The measurements of the 3D diffusion of FD molecules in the porcine ligament tissues were shown in the Figure 6.8(a) as an example of our MP-FRAP technique. We have applied this new technique to demonstrate the presence of 3D diffusional anisotropy of FD molecules in porcine ligament tissues. Diffusion coefficients of FD70 and FD 150 were significantly higher in a direction parallel to the collagen fibers in both X-Alignment and Y-Alignment testing protocols. Diffusional anisotropy could commonly be represented by the ratio of diffusivity along the fiber orientation to the diffusivity perpendicular to the fiber orientation. We found the anisotropic value of 2.1 for FD70 in the porcine ligament tissue with 60% glycerol application and value of 2.2 for FD150 under the same testing condition. In the previous study [85] using Fluorescence Imaging of Continuous Point Photobleaching (FICOPP), an anisotropic value of 2.2 was found for FD500 in the porcine ligament tissue without glycerol solutions. Other techniques have

been also utilized to investigate the diffusional anisotropy of different solutes in other types of tissues [e.g., mouse spinal cord [84], porcine knee cartilage [85], bovine annulus fibrosus in the IVD [14], and bovine meniscus [17]]. A brief summary and comparison of those studies was shown in the. It was found that the diffusional anisotropy is very strong in the mouse spinal cord and bovine meniscus tissues probably due to the existence of highly aligned fibers.

A 63×/1.3NA water immersion objective was used to observe the fluorescence intensity in the spatial volume of 102×102×102μm3. Due to the strong light scattering in the ligament tissue slices, the depth of multiphoton imaging with good contrast and signal to noise ratio (SNR) is limited. Therefore, one type of optical clearing agents (OCAs), glycerol, was applied to reduce the scattering and significantly enhance the light penetration depth and SNR of deep-tissue imaging [187, 188]. Additionally, the use of glycerol in the testing model also slowed down the diffusion of FD molecules, which allowed the multiphoton microscopy system to fully capture the 3D fluorescence recovery processes by a limited sampling rate (18s/stack). Even though the application of glycerol may change the biochemical properties of ECM in the ligament tissues, the diffusion of FD molecules is not likely to be effected by the binding reactions due to their uncharged and biologically inert nature. The results shown in the Figure 6.8(b) demonstrated the size effect on the solute diffusion properties. The ratio (1.44) of two average diffusivities was in agreement with the ratio (1.42) of two stocks radii, indicating the Stocks-Einstein equation is satisfied in our testing model and further verifying the solute diffusion properties could still be characterized by Fick's laws of diffusion.

Table 6.3 The comparison of diffusional anisotropies of fluorescent solutes in the varying types of biological tissues.

Reference	Solute	Tissue	Anisotropy
84	FD70	Mouse spinal cord	5
85	FD3	Porcine ligament tissue	1.3
85	FD3	Porcine knee cartilage	1
85	FD500	Porcine ligament tissue	2.2
85	FD500	Porcine knee cartilage (surface)	1.5
14	Fluorescein(332Da)	Bovine annulus fibrosus in the IVD	1.5
17	Fluorescein(332Da)	Bovine meniscus	3
Chapter 6	FD70	Porcine ligament tissue with glycerol	2.1
Chapter 6	FD150	Porcine ligament tissue with glycerol	2.2

6.6 Conclusion

To our knowledge here, we have proposed a new MP-FRAP technique for determining 3D anisotropic diffusion at the tissue level. A closed-form solution for 3D anisotropic diffusion equation was derived by using SFA. The new method was validated by analyzing computer simulated MP-FRAP data and qualifying the diffusion properties of FD500 in the glycerol solutions. Quantitative analysis of 3D MP-FRAP experiments in the ligament tissues was demonstrated as an in-vitro application of our technique. The features of SFA-based FRAP techniques have been discussed in the previous 2D studies [15, 16] and they all persist in the new 3D method. For instance, first, the boundary and initial conditions for this analysis are flexible, so bleaching volume could be any 3D geometries and the real first recovery image stack right after photobleaching is not required for the calculation. Second, the diffusion tensor can be calculated without measuring the point spread function or optical transfer function of the microscope.[16] Due to these features, our technique can be conveniently carried out on a commercial MPLSM for the diffusion measurements.

On the other hand, the current 3D sampling rate of MPLSM limits the capability of our technique to a slow diffusion measurement. However, a few studies [189, 190] have been done to show the development of various high-speed multiphoton imaging techniques which may acquire 3D images in real time (30 frames/s). By incorporating these techniques, the capabilities and applications of our method could be significantly

enhanced and broadened. Therefore, the development of 3D MP-FRAPa technique with high-speed fluorescence imaging technique could be the next step of our study.

CHAPTER 7 GENERAL CONCLUSIONS AND FUTURE DIRECTIONS

7.1 Conclusions

Cartilaginous tissue is a connective tissue composed of specialized cells (*e.g.,* chondrocytes and fibroblasts) that produce a large amount of extracellular matrix (ECM), which is comprised mostly of collagen fibers, abundant ground substance rich in proteoglycan, and elastic fibers. It is characterized by its avascular structures within the tissue, implying that nutrition for normal tissue cells and maintaining a healthy ECM, is mainly supplied through diffusion from nearby vascularized tissues and synovial fluid. Poor nutritional supply to the cartilaginous tissue is believed to be an important factor leading to tissue degeneration. Moreover, due to the complex collagen fiber structures, the solute diffusion properties in the cartilaginous tissues are mainly anisotropic (*i.e.*, orientation dependent). Therefore, the determination of nutrient solute anisotropic diffusion properties is crucial for understanding the mechanism of nutrient transport in the cartilaginous tissues. Furthermore, characterization of the solute diffusive transport properties in cartilaginous tissues will delineate the relationship between solute diffusion and tissue morphology for further understanding the pathophysiology and etiology of tissue dysfunction and degeneration.

Fluorescence recovery after photobleaching (FRAP) is a versatile and widely used tool for the determination of local diffusion properties within solutions, cells, and tissues. Due to its high spatial resolution, FRAP techniques offer the possibility to microscopically examine a specific region of a sample. However, there is a lack of

techniques which can determine the two-dimensional (2D) and three-dimensional (3D) anisotropic solute diffusion properties in the cartilaginous tissues.

Based on the above requirements, this dissertation was focused on (1) the development of a novel 2D FRAP technique to determine the anisotropic solute diffusion tensors in porcine temporomandibular joint (TMJ) disc, (2) the investigation on the relationship between solute anisotropic diffusion properties and tissue morphology in the TMJ disc, and (3) the development of a novel 3D FRAP technique with multiphoton photobleaching and spatial Fourier analysis (SFA) to characterize the local 3D anisotropic solute diffusion properties in the tissue samples. To achieve those research aims, three major studies were performed in this dissertation, including (1) the development and validation of new 2D FRAP technique as well as the application of this new diffusion technique in cartilaginous tissues (Chapter 4), (2) the determination of solute anisotropic diffusion properties by using new FRAP technique and the examination of tissue morphology by using scanning electron microscopy (SEM) in cartilaginous tissues (Chapter 5), and (3) the development and validation of new 3D multiphoton based FRAP (MP-FRAP) technique as well as the application of this new 3D diffusion technique in collagenous tissues (Chapter 6). Computer simulated diffusion experiments with finite element method (FEM) and solute diffusion studies in the glycerol/PBS solutions were used to validate the new 2D and 3D FRAP techniques. The research interest was mainly focused on the TMJ disc. The most important findings of each study are summarized below.

7.1.1 Development of 2D FRAP technique solely based on SFA

In this study, a new FRAP method solely based on the SFA of post-bleaching (recovery) images was developed to completely determine the 2D anisotropic diffusion tensor in hydrated soft tissues. This method was used to determine the region-dependent and anisotropic diffusion tensors in porcine TMJ discs.

$$\begin{cases} D_{xx} = D_{0,\pi} + \dfrac{\pi(D_{0,\frac{\pi}{4}} - D_{0,\frac{\pi}{2}})}{2} \\ D_{yy} = D_{0,\pi} - \dfrac{\pi(D_{0,\frac{\pi}{4}} - D_{0,\frac{\pi}{2}})}{2} \\ D_{xy} = \dfrac{\pi}{2}(D_{0,\frac{\pi}{2}} - D_{0,\pi}) \end{cases} \tag{7.1}$$

The major innovations of this study included the derivation of a close-form solution for the 2D diffusion equation by solely using Fourier transform and the determination of three independent components of the 2D diffusion tensor by using equation (7.1). The new theory was implemented by writing codes in MATLAB and validated by computer simulated FRAP experiments indicating the high accuracy and robustness of our new technique. For instance, the relative errors of $D_{\text{Eig\_Min}}$ were less than 1.5% and the relative errors of $D_{\text{Eig\_Max}}$ were less than 1% for all simulation cases. It was shown that this technique also had more robustness against the imaging noise when compared with other similar techniques. The new method was applied to determine the 2D diffusion tensor of 4kDa FITC-Dextran (FD) in porcine TMJ discs. The average characteristic diffusivity of 4kDa FD across the disc was 26.05 ± 4.32 $\mu m^2/s$ which is about 16% of its diffusivity in water. In the anteroposterior direction, the anterior region

(30.99 ± 5.93 $\mu m^2/s$) had significantly higher characteristic diffusivity than the intermediate region (20.49 ± 5.38 $\mu m^2/s$) and posterior region (20.97 ± 2.46 $\mu m^2/s$). The ratio of the two principal diffusivities represented the anisotropy of the diffusion and ranged between 0.45 and 0.51 (1.0 = isotropic). It was found that the diffusion of this solute in TMJ discs was inhomogeneous and anisotropic. These findings suggested that diffusive transport in TMJ disc is dependent upon tissue composition (*e.g.*, water content) and structure *(e.g.*, collagen orientation).

This study provided a new method to quantitatively investigate the relationship between transport properties and tissue composition and structure. The obtained transport properties are crucial for future development of numerical models studying nutritional supply within the TMJ disc.

7.1.2 Investigation on anisotropic solute diffusion and tissue morphology

In this study, TMJ discs from eleven pigs aged 6-8 months were divided into five regions: anterior, intermediate, posterior, lateral, and medial. The transport properties and tissue morphology were investigated in three orthogonal orientations: anteroposterior, mediolateral, and superoinferior. The anisotropic diffusivity of fluorescein (Molecular weight: 332 Da) in the right discs was determined by the FRAP protocols. The tissue morphology in the left discs was quantified by the scanning electron microscopy.

The tissue morphology study demonstrated that the collagen fibers in the TMJ disc aligned anteroposteriorly in the medial, intermediate and lateral regions while aligning mediolaterally in the posterior region. Interestingly, fibers aligned in both anteroposterior and mediolateral directions were found in the anterior region of the TMJ

disc. (Figure 7.1) The diffusivities of fluorescein in the TMJ disc were significantly anisotropic, except the anterior region. In the medial, intermediate, and lateral regions, the diffusion along the fiber orientation (*i.e.*, anteroposterior direction) was significantly faster than the diffusion in mediolateral and superoinferior directions. In the posterior regions, the diffusion along the fiber orientation (*i.e.*, mediolateral direction) was significantly faster than the diffusion in anteroposterior and superoinferior directions. The diffusion in the anterior was mostly isotropic, likely due to the multi-directional fiber arrangements. (Figure 7.1) Furthermore, the degree of diffusional anisotropy was correlated to the degree of collagen fiber alignment. The anterior region had the highest mean diffusivity [65.6 (49.3-81.8) $\mu m^2/s$] in the disc due to its high water content. The overall average diffusivity of fluorescein cross the TMJ disc was 57.0 (43.0-71.0) $\mu m^2/s$.

This study has provided a baseline investigation in the relationship between solute transport properties and tissue morphology. Both FRAP and SEM techniques were utilized to determine the 3D solute diffusion properties and collagen fiber orientations, respectively. It was found that the diffusion of fluorescein in the TMJ disc was anisotropic and inhomogeneous, which suggested that tissue structures (*i.e.*, the collagen fiber alignment) and composition (*e.g.*, water content) could be key factors that affect the solute diffusion properties within TMJ discs.

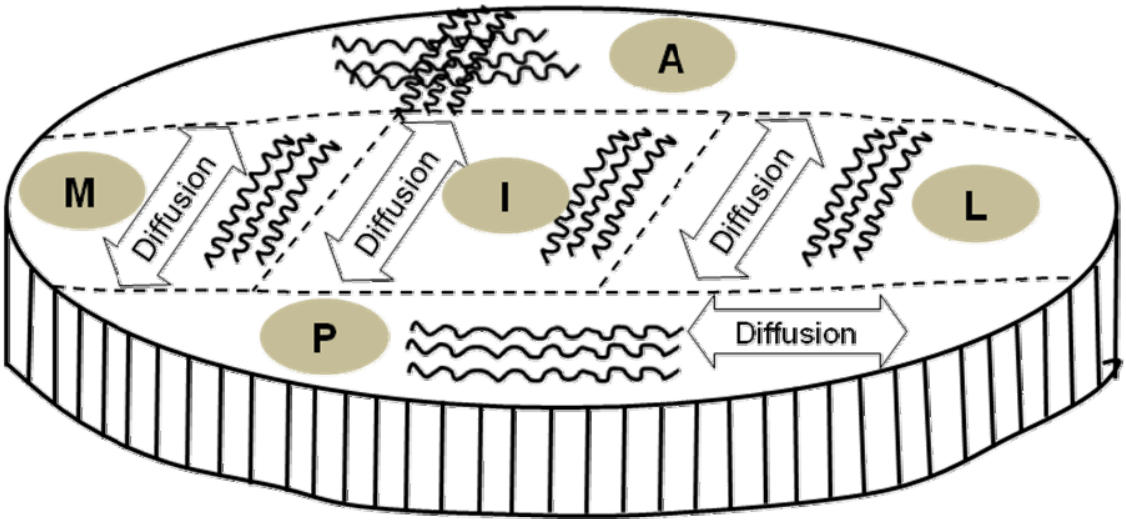

Figure 7.1 Schematic of the relationship between solute diffusion orientations and tissue morphology in the TMJ discs.
In the medial, intermediate, lateral and posterior regions, the diffusion is anisotropic and the main diffusion directions are aligned with the fiber orientations, but in the anterior region, the diffusion is mostly isotropic due to the multi-directional fiber arrangement.

7.1.3 Development of 3D anisotropic diffusion by MP-FRAP technique

Due to the complex 3D ECM structures found in chapter 5, it's believed that the solute diffusion is 3D anisotropic in most cartilaginous tissues. However, there is no FRAP technique available to characterize the 3D anisotropic diffusion properties. Therefore, we have proposed a new MP-FRAP technique for determining 3D anisotropic diffusion in cartilaginous tissues. A closed-form solution for the 3D anisotropic diffusion equation was derived by using SFA as shown in the equation (7.2).

$$\begin{cases} D_{xy} = \dfrac{3\pi}{4}(D_{0,\pi/2,0,\pi} - D_{0,\pi,0,\pi}) \\ D_{yz} = \dfrac{3\pi}{4}(D_{0,\pi,0,\pi/2} - D_{0,\pi,0,\pi}) \\ D_{xz} = \dfrac{3\pi}{4}(D_{0,\pi/2,0,\pi/2} + D_{0,\pi,0,\pi} - D_{0,\pi/2,0,\pi} - D_{0,\pi,0,\pi/2}) \\ D_{xx} = (2\sqrt{2}+2)D_{0,\pi,0,3\pi/4} - 2\sqrt{2}D_{0,\pi,0,\pi} - D_{0,\pi,0,\pi/2} + \dfrac{3\pi}{4}(D_{0,\pi/4,0,\pi} - D_{0,\pi/2,0,\pi}) \\ D_{yy} = (2\sqrt{2}+2)D_{0,\pi,0,3\pi/4} - 2\sqrt{2}D_{0,\pi,0,\pi} - D_{0,\pi,0,\pi/2} - \dfrac{3\pi}{4}(D_{0,\pi/4,0,\pi} - D_{0,\pi/2,0,\pi}) \\ D_{zz} = (4\sqrt{2}+3)D_{0,\pi,0,\pi} + 2D_{0,\pi,0,\pi/2} - (4\sqrt{2}+4)D_{0,\pi,0,3\pi/4} \end{cases} \tag{7.2}$$

All the components of 3D diffusion tensor were obtained by averaging the diffusivities over a shell of a spherical surface in the frequency domain.

The new method was well validated by analyzing computer simulated MP-FRAP data, the relative errors of D_{0xx} were less than 1.80%, and the relative errors of D_{0yy} were less than 1.65%, while the relative errors of D_{0zz} were less than 0.77% for all simulated cases. These results indicated that the new 3D diffusion measurement technique had a high accuracy which was not significantly sensitive to the rotation angles *(i.e.*, η_1, η_2, and η_3).

The diffusion measurements on FD molecules in the glycerol/PBS solutions were used to validate the new MP-FRAP method experimentally. The results showed the isotropic diffusion of FD with molecular weight of 500kDa (FD500) molecules in the glycerol/PBS solutions with varying viscosities. The average diffusivities ($0.44\mu m^2/s$ and $0.27\mu m^2/s$) of FD500 in the two types of glycerol solutions (75% v/v and 80% v/v) were comparable to the diffusivities ($0.60\mu m^2/s$ and $0.36\mu m^2/s$) of the same solute in the glycerol solutions (80% w/w and 85% w/w) measured by other MP-FRAP technique. The trend of decreasing the average diffusivities with increasing the glycerol concentrations was in agreement with the relationship between diffusivity and viscosity, which is defined in the Stokes-Einstein equation.

Quantitative analysis of 3D MP-FRAP experiments in the ligament tissues was demonstrated as an *in vitro* application of our technique. The results demonstrated that the 3D diffusion properties of two types of FD solutes (FD70 and FD150) in the ligament tissue slices were anisotropic and the diffusion along the fiber orientation was always faster than the other two directions. The effect of solute size on the diffusion properties of FD in the ligament tissue slices was also found. The FD70 ($0.117\pm0.023\mu m^2/s$, Stokes radius: 6nm) had about 1.4 times higher (t-test, $p = 0.002$) average diffusivity than FD150 ($0.081\pm0.016\mu m^2/s$, Stokes radius: 8.5nm) in the ligament tissue specimens.

The advantages of this new MP-FRAP technique also have been discussed in this study. For instance, first, the boundary and initial conditions for this analysis are flexible, so bleaching volume could be any 3D geometry. Next, the real first recovery image stack right after photobleaching is not required for the diffusion tensor calculation. Moreover,

the diffusion tensor can be calculated without measuring the point spread function or optical transfer function of the microscope. Due to these features, our technique can be conveniently carried out on a commercial multiphoton laser scanning microscope (MPLSM) for the 3D anisotropic diffusion measurements.

7.2 Future directions

The ultimate research goals of this project were to elucidate the pathophysiology and etiology of human cartilaginous tissues dysfunction and degeneration as well as to develop new strategies for effective diagnostic procedures of cartilaginous tissue degeneration and new treatments for restoring tissue function or retarding further tissue degeneration. Although the cartilaginous tissues from porcine specimens have been tested to study diffusion properties, the determination of the solute diffusivity on human cartilaginous tissues is also needed in the future study of this project. Other future directions of this project are discussed in the following sections.

7.2.1 Incorporating high-speed fluorescence imaging techniques into MP-FRAP

The current 3D fluorescence imaging acquisition speed (*i.e.*, sampling rate) of MPLSM limits the capability of our technique to a slow diffusion measurement. According to the results, only diffusion coefficient up to 0.5$\mu m^2/s$ can be accessible by our method due to this limitation. However, a few studies [189-196] have been done recently to show the development of various high-speed fluorescence (confocal/multiphoton) imaging techniques which have significantly improved the acquisition speed of 3D Z-stack image series in fluorescence imaging system. For example, instead of using single focal plane, Ram S. *et al.* developed high-speed 3D

fluorescence imaging modality by using multifocal plane microscopy. In the future, by incorporating these advanced high-speed fluorescence imaging techniques into our 3D MP-FRAP method, the capabilities and applications of our method could be significantly enhanced and broadened.

7.2.2 Investigating diffusion in cartilaginous tissues by using other imaging modalities

Currently, magnetic resonance imaging (MRI) and computed tomography (CT) are the dominantly routine clinical imaging modalities diagnosing the cartilaginous tissue degeneration (*e.g.,* TMJ disc and lumbar IVD degeneration).[197, 198] However, most current diagnostic strategies mainly focus on the evaluation of tissue morphology (*e.g.*, tissue height), which are not effective to diagnose the tissue degeneration in the early stage. Recently, a few studies have started to investigate the changes of diffusion properties during the tissue degeneration process by using diffusion tensor imaging (DTI) and aimed to develop new diagnostic tools which are sensitive to the early-stage detection for IVD tissue degeneration. [167, 199, 200] Interestingly, a pilot study has been conducted in our lab to determine the diffusion properties of sodium iodide (NaI) in the hydrogel and IVD tissue samples by using micro-CT (μCT) imaging system and more importantly the 3D diffusion tensors of NaI in these samples can be calculated by using our mathematical theory for 3D MP-FRAP technique. Therefore, studying the solute diffusion properties in cartilaginous tissues *in vivo* by using DTI or CT related modalities may lead to translational applications for the FRAP techniques developed in this dissertation.

REFERENCES

1.Nicholson, C., *Diffusion and related transport mechanisms in brain tissue.* Reports on Progress in Physics, 2001. **64**: p. 815-884.

2.Magzoub, M., S. Jin, and A.S. Verkman, *Enhanced macromolecule diffusion deep in tumors after enzymatic digestion of extracellular matrix collagen and its associated proteoglycan decorin.* FASEB J, 2008. **22**(1): p. 276-84.

3.Verkman, A.S., *Solute and macromolecule diffusion in cellular aqueous compartments.* Trends Biochem Sci, 2002. **27**(1): p. 27-33.

4.Filler, A., *Magnetic resonance neurography and diffusion tensor imaging: origins, history, and clinical impact of the first 50,000 cases with an assessment of efficacy and utility in a prospective 5000-patient study group.* Neurosurgery, 2009. **65**(4 Suppl): p. A29-43.

5.Leddy, H.A. and F. Guilak, *Site-specific molecular diffusion in articular cartilage measured using fluorescence recovery after photobleaching.* Ann Biomed Eng, 2003. **31**(7): p. 753-60.

6.Travascio, F., et al., *Relationship between solute transport properties and tissue morphology in human annulus fibrosus.* J Orthop Res, 2009. **27**(12): p. 1625-30.

7.Shi, C., et al., *Anisotropic solute diffusion tensor in porcine TMJ discs measured by FRAP with spatial Fourier analysis.* Ann Biomed Eng, 2010. **38**(11): p. 3398-408.

8.Urban, J.P., S. Smith, and J.C. Fairbank, *Nutrition of the intervertebral disc.* Spine (Phila Pa 1976), 2004. **29**(23): p. 2700-9.

9.Raya, J.G., et al., *Change of diffusion tensor imaging parameters in articular cartilage with progressive proteoglycan extraction.* Invest Radiol, 2011. **46**(6): p. 401-9.

10.Meyvis, T.K., et al., *Fluorescence recovery after photobleaching: a versatile tool for mobility and interaction measurements in pharmaceutical research.* Pharm Res, 1999. **16**(8): p. 1153-62.

11.J.C.G. Blonk, A.D., H. Van Aalst and J.J. Birmingham, *Fluorescence photobleaching recovery in the confocal scanning light microscope.* Journal of Microscopy, 1993. **169**: p. 363-374.

12.Brown, E.B., et al., *Measurement of molecular diffusion in solution by multiphoton fluorescence photobleaching recovery.* Biophys J, 1999. **77**(5): p. 2837-49.

13.Axelrod, D., et al., *Mobility measurement by analysis of fluorescence photobleaching recovery kinetics.* Biophys J, 1976. **16**(9): p. 1055-69.

14.Travascio, F. and W.Y. Gu, *Anisotropic diffusive transport in annulus fibrosus: experimental determination of the diffusion tensor by FRAP technique.* Ann Biomed Eng, 2007. **35**(10): p. 1739-48.

15.Tsay, T.T. and K.A. Jacobson, *Spatial Fourier analysis of video photobleaching measurements. Principles and optimization.* Biophys J, 1991. **60**(2): p. 360-8.

16.Berk, D.A., et al., *Fluorescence photobleaching with spatial Fourier analysis: measurement of diffusion in light-scattering media.* Biophys J, 1993. **65**(6): p. 2428-36.

17.Travascio, F., W. Zhao, and W.Y. Gu, *Characterization of anisotropic diffusion tensor of solute in tissue by video-FRAP imaging technique.* Ann Biomed Eng, 2009. **37**(4): p. 813-23.

18.Mehrer, H., *Diffusion in Solids: Fundamentals, Methods, Materials, Diffusion-Controlled Processes*. Springer series in solid state science ; 1552007, New York: Springer. 2-3pp.

19.Crank, J., *The mathematics of diffusion*. Second ed. Oxford science publications1975, New York: Oxford University Press, USA. 5pp.

20.Torzilli, P.A., T.C. Adams, and R.J. Mis, *Transient solute diffusion in articular cartilage.* J Biomech, 1987. **20**(2): p. 203-14.

21.Urban, J.P., S. Holm, and A. Maroudas, *Diffusion of small solutes into the intervertebral disc: as in vivo study.* Biorheology, 1978. **15**(3-4): p. 203-21.

22.Owicki, J.C. and H.M. McConnell, *Lateral diffusion in inhomogeneous membranes. Model membranes containing cholesterol.* Biophys J, 1980. **30**(3): p. 383-97.

23.Braeckmans, K., et al., *Three-dimensional fluorescence recovery after photobleaching with the confocal scanning laser microscope.* Biophys J, 2003. **85**(4): p. 2240-52.

24.Calvert, P.D., W.E. Schiesser, and E.N. Pugh, Jr., *Diffusion of a soluble protein, photoactivatable GFP, through a sensory cilium.* J Gen Physiol, 2010. **135**(3): p. 173-96.

25.Singer, S.J. and G.L. Nicolson, *The fluid mosaic model of the structure of cell membranes.* Science, 1972. **175**(23): p. 720-31.

26.Wey, C.L., R.A. Cone, and M.A. Edidin, *Lateral diffusion of rhodopsin in photoreceptor cells measured by fluorescence photobleaching and recovery.* Biophys J, 1981. **33**(2): p. 225-32.

27.Zlatanov, I.V., et al., *Developmental changes in the lateral diffusion of Leydig cell membranes measured by the FRAP method.* FEBS Lett, 1987. **222**(1): p. 47-50.

28.Georgiou, G., et al., *Measurement of the lateral diffusion of human MHC class I molecules on HeLa cells by fluorescence recovery after photobleaching using a phycoerythrin probe.* Biophys J, 2002. **82**(4): p. 1828-34.

29.Maiti, S., U. Haupts, and W.W. Webb, *Fluorescence correlation spectroscopy: diagnostics for sparse molecules.* Proc Natl Acad Sci U S A, 1997. **94**(22): p. 11753-7.

30.Fushimi, K. and A.S. Verkman, *Low viscosity in the aqueous domain of cell cytoplasm measured by picosecond polarization microfluorimetry.* J Cell Biol, 1991. **112**(4): p. 719-25.

31.Mastro, A.M., et al., *Diffusion of a small molecule in the cytoplasm of mammalian cells.* Proc Natl Acad Sci U S A, 1984. **81**(11): p. 3414-8.

32.Nicholson, C., et al., *Diffusion of molecules in brain extracellular space: theory and experiment.* Prog Brain Res, 2000. **125**: p. 129-54.

33.Fischer, A.E., et al., *Visualisation of mass transport of small organic molecules and metal ions through articular cartilage by magnetic resonance imaging.* Magn Reson Imaging, 1995. **13**(6): p. 819-26.

34.Hsu, E.W. and L.A. Setton, *Diffusion tensor microscopy of the intervertebral disc anulus fibrosus.* Magn Reson Med, 1999. **41**(5): p. 992-9.

35.Torzilli, P.A., et al., *Effect of proteoglycan removal on solute mobility in articular cartilage.* J Biomech, 1997. **30**(9): p. 895-902.

36.Quinn, T.M., V. Morel, and J.J. Meister, *Static compression of articular cartilage can reduce solute diffusivity and partitioning: implications for the chondrocyte biological response.* J Biomech, 2001. **34**(11): p. 1463-9.

37.Maroudas, A., *Distribution and diffusion of solutes in articular cartilage.* Biophys J, 1970. **10**(5): p. 365-79.

38.Maroudas, A., *Biophysical chemistry of cartilaginous tissues with special reference to solute and fluid transport.* Biorheology, 1975. **12**(3-4): p. 233-48.

39.Nachemson, A., et al., *In vitro diffusion of dye through the end-plates and the annulus fibrosus of human lumbar inter-vertebral discs.* Acta Orthop Scand, 1970. **41**(6): p. 589-607.

40.Maroudas, A., et al., *Factors involved in the nutrition of the human lumbar intervertebral disc: cellularity and diffusion of glucose in vitro.* J Anat, 1975. **120**(Pt 1): p. 113-30.

41.Jackson, A.R., et al., *Effect of compression and anisotropy on the diffusion of glucose in annulus fibrosus.* Spine (Phila Pa 1976), 2008. **33**(1): p. 1-7.

42.Barak, L.S. and W.W. Webb, *Diffusion of low density lipoprotein-receptor complex on human fibroblasts.* J Cell Biol, 1982. **95**(3): p. 846-52.

43.Qian, H., M.P. Sheetz, and E.L. Elson, *Single particle tracking. Analysis of diffusion and flow in two-dimensional systems.* Biophys J, 1991. **60**(4): p. 910-21.

44.Schmidt, T., et al., *Imaging of single molecule diffusion.* Proc Natl Acad Sci U S A, 1996. **93**(7): p. 2926-9.

45.Saxton, M.J., *Single-particle tracking: the distribution of diffusion coefficients.* Biophys J, 1997. **72**(4): p. 1744-53.

46.Saxton, M.J. and K. Jacobson, *Single-particle tracking: applications to membrane dynamics.* Annu Rev Biophys Biomol Struct, 1997. **26**: p. 373-99.

47.Hall, D., *Analysis and interpretation of two-dimensional single-particle tracking microscopy measurements: effect of local surface roughness.* Anal Biochem, 2008. **377**(1): p. 24-32.

48.Saxton, M.J., *Single-particle tracking: connecting the dots.* Nat Methods, 2008. **5**(8): p. 671-2.

49.Douglas Magde, E.E., and W.W. Webb, *Thermodynamic Fluctuations in a Reacting System-Measurement by Fluorescence Correlation Spectroscopy.* Phys. Rev. Lett, 1972. **29**(11): p. 705-708

50.Elson, E.L. and D. Magde, *Fluorescence correlation spectroscopy. I. Conceptual Basis and Theory.* Biopolymers, 1974. **13**(1): p. 1-27.

51.Magde, D., E.L. Elson, and W.W. Webb, *Fluorescence correlation spectroscopy. II. An experimental realization.* Biopolymers, 1974. **13**(1): p. 29-61.

52.Koppel, D.E., et al., *Dynamics of fluorescence marker concentration as a probe of mobility.* Biophys J, 1976. **16**(11): p. 1315-29.

53.Fahey, P.F., et al., *Lateral diffusion in planar lipid bilayers.* Science, 1977. **195**(4275): p. 305-6.

54.Hess, S.T., et al., *Biological and chemical applications of fluorescence correlation spectroscopy: a review.* Biochemistry, 2002. **41**(3): p. 697-705.

55.Thompson, N.L., A.M. Lieto, and N.W. Allen, *Recent advances in fluorescence correlation spectroscopy.* Curr Opin Struct Biol, 2002. **12**(5): p. 634-41.

56.Alexandrakis, G., et al., *Two-photon fluorescence correlation microscopy reveals the two-phase nature of transport in tumors.* Nat Med, 2004. **10**(2): p. 203-7.

57.Bulseco, D.A. and D.E. Wolf, *Fluorescence correlation spectroscopy: molecular complexing in solution and in living cells.* Methods Cell Biol, 2007. **81**: p. 525-59.

58.Houtsmuller, A.B. and W. Vermeulen, *Macromolecular dynamics in living cell nuclei revealed by fluorescence redistribution after photobleaching.* Histochem Cell Biol, 2001. **115**(1): p. 13-21.

59.Lippincott-Schwartz, J., E. Snapp, and A. Kenworthy, *Studying protein dynamics in living cells.* Nat Rev Mol Cell Biol, 2001. **2**(6): p. 444-56.

60.Houtsmuller, A.B., *Fluorescence recovery after photobleaching: application to nuclear proteins.* Adv Biochem Eng Biotechnol, 2005. **95**: p. 177-99.

61.Loren, N., M. Nyden, and A.M. Hermansson, *Determination of local diffusion properties in heterogeneous biomaterials.* Adv Colloid Interface Sci, 2009. **150**(1): p. 5-15.

62.Smith, B.A. and H.M. McConnell, *Determination of molecular motion in membranes using periodic pattern photobleaching.* Proc Natl Acad Sci U S A, 1978. **75**(6): p. 2759-63.

63.Jacobson, K., F. Zhang, and T.T. Tsay, *Fluorescence recovery after photobleaching techniques to measure translational mobility in microscopic samples.* Scanning Microsc, 1991. **5**(2): p. 357-61; discussion 361-2.

64.Lippincott-Schwartz, J., N. Altan-Bonnet, and G.H. Patterson, *Photobleaching and photoactivation: following protein dynamics in living cells.* Nat Cell Biol, 2003. **Suppl**: p. S7-14.

65.Nicholson, C. and L. Tao, *Hindered diffusion of high molecular weight compounds in brain extracellular microenvironment measured with integrative optical imaging.* Biophys J, 1993. **65**(6): p. 2277-90.

66.Xiao, F., et al., *Diffusion of flexible random-coil dextran polymers measured in anisotropic brain extracellular space by integrative optical imaging.* Biophys J, 2008. **95**(3): p. 1382-92.

67.Sykova, E. and C. Nicholson, *Diffusion in brain extracellular space.* Physiol Rev, 2008. **88**(4): p. 1277-340.

68.Maroudas, A., *Physicochemical properties of cartilage in the light of ion exchange theory.* Biophys J, 1968. **8**(5): p. 575-95.

69.Gu, W.Y. and M.A. Justiz, *Apparatus for measuring the swelling dependent electrical conductivity of charged hydrated soft tissues.* J Biomech Eng, 2002. **124**(6): p. 790-3.

70.Gu, W.Y., M.A. Justiz, and H. Yao, *Electrical conductivity of lumbar anulus fibrosis: effects of porosity and fixed charge density.* Spine (Phila Pa 1976), 2002. **27**(21): p. 2390-5.

71.Jackson, A., et al., *Anisotropic ion diffusivity in intervertebral disc: an electrical conductivity approach.* Spine (Phila Pa 1976), 2006. **31**(24): p. 2783-9.

72.Sadleir, R.J., et al., *A controllably anisotropic conductivity or diffusion phantom constructed from isotropic layers.* Ann Biomed Eng, 2009. **37**(12): p. 2522-31.

73.Kuo, J., et al., *Effect of mechanical loading on electrical conductivity in porcine TMJ discs.* J Dent Res, 2011. **90**(10): p. 1216-20.

74.Torrey, H.C., *Bloch Equations with Diffusion Terms.* Phys. Rev., 1956. **104**: p. 563-565.

75.Carr, H.Y.a.P., E. M. , *Effects of Diffusion on Free Precession in Nuclear Magnetic Resonance Experiments.* Phys. Rev., 1954. **94**: p. 630-638.

76.Stejskal, E.O. and J.E. Tanner, *Spin Diffusion Measurements: Spin Echoes in the Presence of a Time-Dependent Field Gradient.* J. Chem. Phys., 1965. **42**: p. 288-292.

77.Warach, S., J.F. Dashe, and R.R. Edelman, *Clinical outcome in ischemic stroke predicted by early diffusion-weighted and perfusion magnetic resonance imaging: a preliminary analysis.* J Cereb Blood Flow Metab, 1996. **16**(1): p. 53-9.

78.Fisher, M. and G.W. Albers, *Applications of diffusion-perfusion magnetic resonance imaging in acute ischemic stroke.* Neurology, 1999. **52**(9): p. 1750-6.

79.Le Bihan, D., et al., *Diffusion tensor imaging: concepts and applications.* J Magn Reson Imaging, 2001. **13**(4): p. 534-46.

80.Jensen, J.H., et al., *Diffusional kurtosis imaging: the quantification of non-gaussian water diffusion by means of magnetic resonance imaging.* Magn Reson Med, 2005. **53**(6): p. 1432-40.

81.Jensen, J.H., et al., *Preliminary observations of increased diffusional kurtosis in human brain following recent cerebral infarction.* NMR Biomed, 2010.

82.Jensen, J.H. and J.A. Helpern, *MRI quantification of non-Gaussian water diffusion by kurtosis analysis.* NMR Biomed, 2010. **23**(7): p. 698-710.

83.Wedekind, P., et al., *Line-scanning microphotolysis for diffraction-limited measurements of lateral diffusion.* Biophys J, 1996. **71**(3): p. 1621-32.

84.Papadopoulos, M.C., J.K. Kim, and A.S. Verkman, *Extracellular space diffusion in central nervous system: anisotropic diffusion measured by elliptical surface photobleaching.* Biophys J, 2005. **89**(5): p. 3660-8.

85.Leddy, H.A., M.A. Haider, and F. Guilak, *Diffusional anisotropy in collagenous tissues: fluorescence imaging of continuous point photobleaching.* Biophys J, 2006. **91**(1): p. 311-6.

86.Kang, M., et al., *A generalization of theory for two-dimensional fluorescence recovery after photobleaching applicable to confocal laser scanning microscopes.* Biophys J, 2009. **97**(5): p. 1501-11.

87.Jacobson, K., et al., *Measurement of the lateral mobility of cell surface components in single, living cells by fluorescence recovery after photobleaching.* J Supramol Struct, 1976. **5**(4): p. 565(417)-576(428).

88.Barisas, B.G., *Criticality of beam alignment in fluorescence photobleaching recovery experiments.* Biophys J, 1980. **29**(3): p. 545-8.

89.Wolf, D.E., M. Edidin, and P.R. Dragsten, *Effect of bleaching light on measurements of lateral diffusion in cell membranes by the fluorescence photobleaching recovery method.* Proc Natl Acad Sci U S A, 1980. **77**(4): p. 2043-5.

90.Yguerabide, J., J.A. Schmidt, and E.E. Yguerabide, *Lateral mobility in membranes as detected by fluorescence recovery after photobleaching.* Biophys J, 1982. **40**(1): p. 69-75.

91.Soumpasis, D.M., *Theoretical analysis of fluorescence photobleaching recovery experiments.* Biophys J, 1983. **41**(1): p. 95-7.

92.van Zoelen, E.J., L.G. Tertoolen, and S.W. de Laat, *Simple computer method for evaluation of lateral diffusion coefficients from fluorescence photobleaching recovery kinetics.* Biophys J, 1983. **42**(1): p. 103-8.

93.Koppel, D.E., *Fluorescence redistribution after photobleaching. A new multipoint analysis of membrane translational dynamics.* Biophys J, 1979. **28**(2): p. 281-91.

94.Lopez, A., et al., *Fluorescence recovery after photobleaching (FRAP) experiments under conditions of uniform disk illumination. Critical comparison of analytical solutions, and a new mathematical method for calculation of diffusion coefficient D.* Biophys J, 1988. **53**(6): p. 963-70.

95.Wolf, D.E., A.H. Handyside, and M. Edidin, *Effect of microvilli on lateral diffusion measurements made by the fluorescence photobleaching recovery technique.* Biophys J, 1982. **38**(3): p. 295-7.

96.Wolf, D.E., *Theory of fluorescence recovery after photobleaching measurements on cylindrical surfaces.* Biophys J, 1992. **61**(2): p. 487-93.

97.Sbalzarini, I.F., et al., *Simulations of (an)isotropic diffusion on curved biological surfaces.* Biophys J, 2006. **90**(3): p. 878-85.

98.Periasamy, N. and A.S. Verkman, *Analysis of fluorophore diffusion by continuous distributions of diffusion coefficients: application to photobleaching measurements of multicomponent and anomalous diffusion.* Biophys J, 1998. **75**(1): p. 557-67.

99.Saxton, M.J., *Anomalous diffusion due to obstacles: a Monte Carlo study.* Biophys J, 1994. **66**(2 Pt 1): p. 394-401.

100.Saxton, M.J., *Anomalous subdiffusion in fluorescence photobleaching recovery: a Monte Carlo study.* Biophys J, 2001. **81**(4): p. 2226-40.

101.Smith, B.A., W.R. Clark, and H.M. McConnell, *Anisotropic molecular motion on cell surfaces.* Proc Natl Acad Sci U S A, 1979. **76**(11): p. 5641-4.

102.Wirth, M.J., *Frequency Domain Analysis for Fluorescence Recovery After Photobleaching.* Applied Spectroscopy, 2006. **60**(1): p. 89-94.

103.Travascio, F. and W.Y. Gu, *Simultaneous measurement of anisotropic solute diffusivity and binding reaction rates in biological tissues by FRAP.* Ann Biomed Eng, 2011. **39**(1): p. 53-65.

104.Jacobson, K., E. Wu, and G. Poste, *Measurement of the translational mobility of concanavalin A in glycerol-saline solutions and on the cell surface by fluorescence recovery after photobleaching.* Biochim Biophys Acta, 1976. **433**(1): p. 215-22.

105.Schlessinger, J., et al., *Mobility and distribution of a cell surface glycoprotein and its interaction with other membrane components.* Proc Natl Acad Sci U S A, 1977. **74**(7): p. 2909-13.

106.Golan, D.E. and W. Veatch, *Lateral mobility of band 3 in the human erythrocyte membrane studied by fluorescence photobleaching recovery: evidence for control by cytoskeletal interactions.* Proc Natl Acad Sci U S A, 1980. **77**(5): p. 2537-41.

107.Sheetz, M.P., M. Schindler, and D.E. Koppel, *Lateral mobility of integral membrane proteins is increased in spherocytic erythrocytes.* Nature, 1980. **285**(5765): p. 510-1.

108.Criado, M., et al., *Translational diffusion of acetylcholine receptor (monomeric and dimeric forms) of Torpedo marmorata reconstituted into phospholipid bilayers studied by fluorescence recovery after photobleaching.* Biochemistry, 1982. **21**(23): p. 5750-5.

109.Vaz, W.L., et al., *Size dependence of the translational diffusion of large integral membrane proteins in liquid-crystalline phase lipid bilayers. A study using fluorescence recovery after photobleaching.* Biochemistry, 1982. **21**(22): p. 5608-12.

110.Gaub, H., et al., *Lateral diffusion and phase separation in two-dimensional solutions of polymerized butadiene lipid in dimyristoylphosphatidylcholine bilayers. A photobleaching and freeze fracture study.* Biophys J, 1984. **45**(4): p. 725-31.

111.Vaz, W.L., E.C. Melo, and T.E. Thompson, *Translational diffusion and fluid domain connectivity in a two-component, two-phase phospholipid bilayer.* Biophys J, 1989. **56**(5): p. 869-76.

112.Ladha, S., et al., *Lateral diffusion in planar lipid bilayers: a fluorescence recovery after photobleaching investigation of its modulation by lipid composition, cholesterol, or alamethicin content and divalent cations.* Biophys J, 1996. **71**(3): p. 1364-73.

113.Ratto, T.V. and M.L. Longo, *Obstructed diffusion in phase-separated supported lipid bilayers: a combined atomic force microscopy and fluorescence recovery after photobleaching approach.* Biophys J, 2002. **83**(6): p. 3380-92.

114.Wu, E.S., K. Jacobson, and D. Papahadjopoulos, *Lateral diffusion in phospholipid multibilayers measured by fluorescence recovery after photobleaching.* Biochemistry, 1977. **16**(17): p. 3836-41.

115.Giffard, C.J., et al., *Interaction of nisin with planar lipid bilayers monitored by fluorescence recovery after photobleaching.* J Membr Biol, 1996. **151**(3): p. 293-300.

116.Guo, L., et al., *Molecular diffusion measurement in lipid bilayers over wide concentration ranges: a comparative study.* Chemphyschem, 2008. **9**(5): p. 721-8.

117.Storrie, B., et al., *The intracellular mobility of a viral membrane glycoprotein measured by confocal microscope fluorescence recovery after photobleaching.* J Cell Sci, 1994. **107 (Pt 5)**: p. 1309-19.

118.Hochman, J.H., et al., *Lateral mobility of cytochrome c on intact mitochondrial membranes as determined by fluorescence redistribution after photobleaching.* Proc Natl Acad Sci U S A, 1982. **79**(22): p. 6866-70.

119.Kreis, T.E., B. Geiger, and J. Schlessinger, *Mobility of microinjected rhodamine actin within living chicken gizzard cells determined by fluorescence photobleaching recovery.* Cell, 1982. **29**(3): p. 835-45.

120.Salmon, E.D., et al., *Diffusion coefficient of fluorescein-labeled tubulin in the cytoplasm of embryonic cells of a sea urchin: video image analysis of fluorescence redistribution after photobleaching.* J Cell Biol, 1984. **99**(6): p. 2157-64.

121.White, J. and E. Stelzer, *Photobleaching GFP reveals protein dynamics inside live cells.* Trends Cell Biol, 1999. **9**(2): p. 61-5.

122.Reits, E.A. and J.J. Neefjes, *From fixed to FRAP: measuring protein mobility and activity in living cells.* Nat Cell Biol, 2001. **3**(6): p. E145-7.

123.Seksek, O., J. Biwersi, and A.S. Verkman, *Translational diffusion of macromolecule-sized solutes in cytoplasm and nucleus.* J Cell Biol, 1997. **138**(1): p. 131-42.

124.Youn, B.S., et al., *In vivo resolution of oligomers with fluorescence photobleaching recovery histograms.* Cell Stress Chaperones, 2006. **11**(2): p. 170-9.

125.Nandi, P. and P. Wahl, *Diffusion properties of clathrin on the surface of isolated mouse liver nuclei by the fluorescence recovery after photobleaching technique.* Biochim Biophys Acta, 1988. **943**(2): p. 367-70.

126.Phair, R.D. and T. Misteli, *High mobility of proteins in the mammalian cell nucleus.* Nature, 2000. **404**(6778): p. 604-9.

127.Nicholson, C. and E. Sykova, *Extracellular space structure revealed by diffusion analysis.* Trends Neurosci, 1998. **21**(5): p. 207-15.

128.Tao, L., *Effects of osmotic stress on dextran diffusion in rat neocortex studied with integrative optical imaging.* J Neurophysiol, 1999. **81**(5): p. 2501-7.

129.Berk, D.A., et al., *Direct in vivo measurement of targeted binding in a human tumor xenograft.* Proc Natl Acad Sci U S A, 1997. **94**(5): p. 1785-90.

130.Brown, E.B., et al., *Measurement of macromolecular diffusion coefficients in human tumors.* Microvasc Res, 2004. **67**(3): p. 231-6.

131.Stylianopoulos, T., et al., *Diffusion anisotropy in collagen gels and tumors: the effect of fiber network orientation.* Biophys J, 2010. **99**(10): p. 3119-28.

132.Fetter, N.L., et al., *Composition and transport properties of human ankle and knee cartilage.* J Orthop Res, 2006. **24**(2): p. 211-9.

133.Su, M., et al., *Knee-loading modality drives molecular transport in mouse femur.* Ann Biomed Eng, 2006. **34**(10): p. 1600-6.

134.Frey, S., R.P. Richter, and D. Gorlich, *FG-rich repeats of nuclear pore proteins form a three-dimensional meshwork with hydrogel-like properties.* Science, 2006. **314**(5800): p. 815-7.

135.Kubitscheck, U., et al., *Two-photon scanning microphotolysis for three-dimensional data storage and biological transport measurements.* J Microsc, 1996. **182**(Pt 3): p. 225-33.

136.U. KUBITSCHECK, P.W.R.P., *Three-dimensional diffusion measurements by scanning microphotolysis.* Journal of Microscopy, 1998. **192**: p. 126-138.

137.Braeckmans, K., et al., *Line FRAP with the confocal laser scanning microscope for diffusion measurements in small regions of 3-D samples.* Biophys J, 2007. **92**(6): p. 2172-83.

138.Leddy, H.A., S.E. Christensen, and F. Guilak, *Microscale diffusion properties of the cartilage pericellular matrix measured using 3D scanning microphotolysis.* J Biomech Eng, 2008. **130**(6): p. 061002.

139.Braga, J., J.M. Desterro, and M. Carmo-Fonseca, *Intracellular macromolecular mobility measured by fluorescence recovery after photobleaching with confocal laser scanning microscopes.* Mol Biol Cell, 2004. **15**(10): p. 4749-60.

140.Seiffert, S. and W. Oppermann, *Systematic evaluation of FRAP experiments performed in a confocal laser scanning microscope.* J Microsc, 2005. **220**(Pt 1): p. 20-30.

141.Waharte, F., et al., *A two-photon FRAP analysis of the cytoskeleton dynamics in the microvilli of intestinal cells.* Biophys J, 2005. **88**(2): p. 1467-78.

142.Stroh, M., et al., *Diffusion of nerve growth factor in rat striatum as determined by multiphoton microscopy.* Biophys J, 2003. **85**(1): p. 581-8.

143.Schnell, E.A., et al., *Diffusion measured by fluorescence recovery after photobleaching based on multiphoton excitation laser scanning microscopy.* J Biomed Opt, 2008. **13**(6): p. 064037.

144.Mazza, D., et al., *Role of three-dimensional bleach distribution in confocal and two-photon fluorescence recovery after photobleaching experiments.* Appl Opt, 2007. **46**(30): p. 7401-11.

145.Mazza, D., et al., *A new FRAP/FRAPa method for three-dimensional diffusion measurements based on multiphoton excitation microscopy.* Biophys J, 2008. **95**(7): p. 3457-69.

146.Werner, J.A., B. Tillmann, and A. Schleicher, *Functional anatomy of the temporomandibular joint. A morphologic study on human autopsy material.* Anat.Embryol.(Berl), 1991. **183**(1): p. 89-95.

147.Nickel, J.C. and K.R. McLachlan, *In vitro measurement of the stress-distribution properties of the pig temporomandibular joint disc.* Arch Oral Biol, 1994. **39**(5): p. 439-48.

148.Nickel, J.C. and K.R. McLachlan, *In vitro measurement of the frictional properties of the temporomandibular joint disc.* Arch Oral Biol, 1994. **39**(4): p. 323-31.

149.Dworkin, S.F., et al., *Epidemiology of signs and symptoms in temporomandibular disorders: clinical signs in cases and controls.* J Am Dent Assoc, 1990. **120**(3): p. 273-81.

150.Gatchel, R.J., et al., *Efficacy of an early intervention for patients with acute temporomandibular disorder-related pain: a one-year outcome study.* J Am Dent Assoc, 2006. **137**(3): p. 339-47.

151.Stegenga, B., *Osteoarthritis of the temporomandibular joint organ and its relationship to disc displacement.* J Orofac Pain, 2001. **15**(3): p. 193-205.

152.Stegenga, B., L.G. de Bont, and G. Boering, *Osteoarthrosis as the cause of craniomandibular pain and dysfunction: a unifying concept.* J Oral Maxillofac Surg, 1989. **47**(3): p. 249-56.

153.Berkovitz, B.K. and H. Robertshaw, *Ultrastructural quantification of collagen in the articular disc of the temporomandibular joint of the rabbit.* Arch Oral Biol, 1993. **38**(1): p. 91-5.

154.Gage, J.P., et al., *Presence of type III collagen in disc attachments of human temporomandibular joints.* Arch Oral Biol, 1990. **35**(4): p. 283-8.

155.Nakano, T. and P.G. Scott, *A quantitative chemical study of glycosaminoglycans in the articular disc of the bovine temporomandibular joint.* Arch Oral Biol, 1989. **34**(9): p. 749-57.

156.Nakano, T. and P.G. Scott, *Changes in the chemical composition of the bovine temporomandibular joint disc with age.* Arch Oral Biol, 1996. **41**(8-9): p. 845-53.

157.Sindelar, B.J., et al., *Effects of intraoral splint wear on proteoglycans in the temporomandibular joint disc.* Arch Biochem Biophys, 2000. **379**(1): p. 64-70.

158.Rees, L.A., *The structure and function of the mandibular joint.* British Dental Journal, 1954. **96**: p. 125-133.

159.Detamore, M.S. and K.A. Athanasiou, *Structure and function of the temporomandibular joint disc: implications for tissue engineering.* J Oral Maxillofac Surg, 2003. **61**(4): p. 494-506.

160.Torzilli, P.A., *Effects of temperature, concentration and articular surface removal on transient solute diffusion in articular cartilage.* Med Biol Eng Comput, 1993. **31 Suppl**: p. S93-8.

161.Minarelli, A.M., M. Del Santo Junior, and E.A. Liberti, *The structure of the human temporomandibular joint disc: a scanning electron microscopy study.* J Orofac Pain, 1997. **11**(2): p. 95-100.

162.Kuo, J., et al., *The region-dependent biphasic viscoelastic properties of human temporomandibular joint discs under confined compression.* J Biomech. **43**(7): p. 1316-21.

163.Peters, R., et al., *A microfluorimetric study of translational diffusion in erythrocyte membranes.* Biochim Biophys Acta, 1974. **367**(3): p. 282-94.

164.Pluen, A., et al., *Diffusion of macromolecules in agarose gels: comparison of linear and globular configurations.* Biophys J, 1999. **77**(1): p. 542-52.

165.Wirth, M.J., *Frequency domain analysis for fluorescence recovery after photobleaching.* Appl Spectrosc, 2006. **60**(1): p. 89-94.

166.Bevington, P.R., *Data reduction and error analysis for the physical sciences*1969, New York: McGraw-Hill. 36pp.

167.Benavides, E., et al., *High-resolution magnetic resonance imaging and diffusion tensor imaging of the porcine temporomandibular joint disc.* Dentomaxillofac Radiol, 2009. **38**(3): p. 148-55.

168.Detamore, M.S., et al., *Quantitative analysis and comparative regional investigation of the extracellular matrix of the porcine temporomandibular joint disc.* Matrix Biol, 2005. **24**(1): p. 45-57.

169.Rees, L.A., *The structure and function of the mandibular joint.* Br.Dent.J., 1954. **96**: p. 125-133.

170.Leonardi, R., et al., *Expression of vascular endothelial growth factor in human dysfunctional temporomandibular joint discs.* Arch.Oral Biol., 2003. **48**(3): p. 185-192.

171.Yamaguchi, A., et al., *Role of hypoxia and interleukin-1beta in gene expressions of matrix metalloproteinases in temporomandibular joint disc cells.* Arch.Oral Biol., 2005. **50**(1): p. 81-87.

172.Tojyo, I., et al., *Effect of hypoxia and interleukin-1beta on expression of tenascin-C in temporomandibular joint.* Oral Dis., 2008. **14**(1): p. 45-50.

173.O'Hara, B.P., J.P. Urban, and A. Maroudas, *Influence of cyclic loading on the nutrition of articular cartilage.* Ann Rheum Dis, 1990. **49**(7): p. 536-539.

174.Garcia, A.M., et al., *Contributions of fluid convection and electrical migration to transport in cartilage: relevance to loading.* Arch.Biochem.Biophys., 1996. **333**(2): p. 317-325.

175.Evans, R.C. and T.M. Quinn, *Solute convection in dynamically compressed cartilage.* J Biomech, 2006. **39**(6): p. 1048-55.

176.Yao, H. and W.Y. Gu, *Convection and diffusion in charged hydrated soft tissues: a mixture theory approach.* Biomechan Model Mechanobiol, 2006. **6**: p. 63-72.

177.Jackson, A. and W. Gu, *Transport Properties of Cartilaginous Tissues.* Curr Rheumatol Rev, 2009. **5**(1): p. 40-50.

178.Basser, P.J. and C. Pierpaoli, *Microstructural and physiological features of tissues elucidated by quantitative-diffusion-tensor MRI.* J Magn Reson B, 1996. **111**(3): p. 209-19.

179.Fonck, E., et al., *Effect of aging on elastin functionality in human cerebral arteries.* Stroke, 2009. **40**(7): p. 2552-6.

180.Rezakhaniha, R., et al., *Experimental investigation of collagen waviness and orientation in the arterial adventitia using confocal laser scanning microscopy.* Biomech Model Mechanobiol, 2012. **11**(3-4): p. 461-73.

181.Shengyi, T. and Y. Xu, *Biomechanical properties and collagen fiber orientation of TMJ discs in dogs: Part 1. Gross anatomy and collagen fiber orientation of the discs.* J Craniomandib Disord, 1991. **5**(1): p. 28-34.

182.Mills, D.K., D.J. Fiandaca, and R.P. Scapino, *Morphologic, microscopic, and immunohistochemical investigations into the function of the primate TMJ disc.* J Orofac Pain, 1994. **8**(2): p. 136-54.

183.Scapino, R.P., et al., *The behaviour of collagen fibres in stress relaxation and stress distribution in the jaw-joint disc of rabbits.* Arch Oral Biol, 1996. **41**(11): p. 1039-52.

184.Dieteren, C.E., et al., *Solute diffusion is hindered in the mitochondrial matrix.* Proc Natl Acad Sci U S A, 2011. **108**(21): p. 8657-62.

185.Helmchen, F. and W. Denk, *Deep tissue two-photon microscopy.* Nat Methods, 2005. **2**(12): p. 932-40.

186.Sullivan, K.D., et al., *Improved model of fluorescence recovery expands the application of multiphoton fluorescence recovery after photobleaching in vivo.* Biophys J, 2009. **96**(12): p. 5082-94.

187.Cicchi, R., et al., *Contrast and depth enhancement in two-photon microscopy of human skin ex vivo by use of optical clearing agents.* Opt Express, 2005. **13**(7): p. 2337-44.

188.Genina, E.A., A.N. Bashkatov, and V.V. Tuchin, *Tissue optical immersion clearing.* Expert Rev Med Devices, 2010. **7**(6): p. 825-42.

189.Niesner, R., et al., *The power of single and multibeam two-photon microscopy for high-resolution and high-speed deep tissue and intravital imaging.* Biophys J, 2007. **93**(7): p. 2519-29.

190.Carriles, R., et al., *Invited review article: Imaging techniques for harmonic and multiphoton absorption fluorescence microscopy.* Rev Sci Instrum, 2009. **80**(8): p. 081101.

191.Nielsen, T., et al., *High efficiency beam splitter for multifocal multiphoton microscopy.* J Microsc, 2001. **201**(Pt 3): p. 368-76.

192.Fricke, M. and T. Nielsen, *Two-dimensional imaging without scanning by multifocal multiphoton microscopy.* Appl Opt, 2005. **44**(15): p. 2984-8.

193.Ram, S., et al., *High accuracy 3D quantum dot tracking with multifocal plane microscopy for the study of fast intracellular dynamics in live cells.* Biophys J, 2008. **95**(12): p. 6025-43.

194.Ram, S., et al., *3D single molecule tracking of quantum-dot labeled antibody molecules using multifocal plane microscopy.* Proc SPIE, 2010. **7575**.

195.Zhang, R., et al., *Two-photon 3D FIONA of individual quantum dots in an aqueous environment.* Nano Lett, 2011. **11**(10): p. 4074-8.

196.Ram, S., et al., *3D Single Molecule Tracking with Multifocal Plane Microscopy Reveals Rapid Intercellular Transferrin Transport at Epithelial Cell Barriers.* Biophys J, 2012. **103**(7): p. 1594-603.

197.Haughton, V., *Imaging intervertebral disc degeneration.* J Bone Joint Surg Am, 2006. **88 Suppl 2**: p. 15-20.

198.Scrivani, S.J., D.A. Keith, and L.B. Kaban, *Temporomandibular disorders.* N Engl J Med, 2008. **359**(25): p. 2693-705.

199.Beattie, P.F., P.S. Morgan, and D. Peters, *Diffusion-weighted magnetic resonance imaging of normal and degenerative lumbar intervertebral discs: a new method to potentially quantify the physiologic effect of physical therapy intervention.* J Orthop Sports Phys Ther, 2008. **38**(2): p. 42-9.

200.Zhang, Z., et al., *Age-related diffusion patterns in human lumbar intervertebral discs: a pilot study in asymptomatic subjects.* Magn Reson Imaging, 2012. **30**(2): p. 181-8.